CHALMERS

# Fibre reinforced polymer bridge decks

## A feasibility study on upgrading existing concrete-steel bridges

*Master of Science Thesis in the Master's Programme Structural Engineering and Building Performance Design*


VALBONA MARA

Department of Civil and Environmental Engineering
*Division of Structural Engineering*
*Steel and Timber Structures*
CHALMERS UNIVERSITY OF TECHNOLOGY
Göteborg, Sweden 2011


Master's Thesis 2011:76

MASTER'S THESIS 2011:76

# Fibre reinforced polymer bridge decks

A feasibility study on upgrading existing concrete-steel bridges

*Master of Science Thesis in the Master's Programme Structural Engineering and Building Performance Design*

VALBONA MARA

Department of Civil and Environmental Engineering
*Division of Structural Engineering*
*Steel and Timber Structures*
CHALMERS UNIVERSITY OF TECHNOLOGY
Göteborg, Sweden 2011

Fibre reinforced polymer bridge decks
A feasibility study on upgrading existing concrete-steel bridges

*Master of Science Thesis in the Master's Programme Structural Engineering and Building Performance Design*
VALBONA MARA



Examensarbete/Institutionen för bygg- och miljöteknik,
Chalmers tekniska högskola 2011:76

Department of Civil and Environmental Engineering
Division of Structural Engineering
Steel and Timber Structures
Chalmers University of Technology
SE-412 96 Göteborg
Sweden
Telephone: + 46 (0)31-772 1000

Cover:
Construction of Friedberg bridge in Germany consisting of FRP deck on steel girders. Courtesy of Fiberline Inc.

Chalmers reproservice
Göteborg, Sweden 2011

Fibre reinforced polymer bridge decks
A feasibility study on upgrading existing concrete-steel bridges

*Master of Science Thesis in the Master's*

VALBONA MARA
Department of Civil and Environmental Engineering
Division of Structural Engineering
Steel and Timber Structures
Chalmers University of Technology

ABSTRACT

In recent years, the growing number of deteriorated concrete and steel bridge decks has highlighted the need for research on new high-performance construction material for the rehabilitation of transportation infrastructures. The relatively old age of most existing bridges and the increasing traffic demands have also risen the needs for upgrading methods with focus on minimizing traffic disruption. Fibre reinforced polymer decks have a great potential in refurbishment and replacement of concrete and steel decks in existing bridges. These decks offer superior properties such as high strength and stiffness-to-weight-ratio, superior fatigue and corrosion resistance and enhanced durability. In addition, FRP decks can be prefabricated leading to fast and easy erection and thus minimizing traffic disruption. The topic of using FRP decks for bridge upgrading is relatively new. Nevertheless, several research projects have been conducted and some highway bridges have been constructed or upgraded using this method. In most cases, the concept has been to combine FRP decks with steel girders. Despite the research effort, there is still a lack of knowledge regarding how to design and construct FRP-steel bridges. To date, no design guidelines exist, a factor which has limited the widespread of application of FRP decks. Another question that needs research in more detail is the connection between FRP deck and steel girders. Practical and economically feasible solutions need to be developed in order to ensure good composite action between FRP deck and steel girders.

This thesis will firstly present a thorough literature study done on the use of FRP decks both for new construction and upgrading of existing bridges. The efficiency of FRP decks for replacing concrete decks is examined through a detailed finite element study. The analysis is done on an old concrete-steel bridge which is in need for upgrading and deck widening. The bridge had an inadequate structural capacity to bear the current traffic loads. Two scenarios are considered: FRP decks working non-compositely with the girders, as well as two methods of achieving composite action between the deck and the girders. Different connection techniques are examined. Finite element analysis is utilized to assess the overall structural behaviour of the bridge under different load effects. The results show that a considerable reduction in stresses due to the light weight of the deck and composite action between FRP decks and steel girders can be obtained. This allows for increase in traffic loads. The stress reduction is higher when concrete is incorporated in the connection between FRP deck and steel girders. Bolts and shear stud connections as well as bonding between FRP deck and steel girders are shown to be feasible for adoption in bridge engineering.

Key words: FRP decks, composite bridge, fiber reinforced polymers, bridge decks, connections

# Contents

# Preface

This thesis deals with a feasibility study for upgrading existing concrete-steel bridges with FRP decks. The project is carried out at the Department of Structural Engineering, Division of Steel and Timber Structures, Chalmers University of Technology, Sweden.

Firstly, I would like to thank my supervisor Assoc. Prof. Mohammad Al-Emrani who supported and gave me confidence to finish this thesis during the whole academic year. His contributions were vital and the completion of this thesis would not have been possible without his valuable assistance.

I am also thankful to Mustafa Aygul and Reza Haghani for the guidance, advices and encouragements to accomplish this master thesis.

Last but not least, I want to thank my family and my dearest friend Anisa for being supportive and helpful and who always believed in my success.

Göteborg 2011

Valbona Mara

# Notations

### Roman upper case letters

A Area

DL Deal load

E Modulus of elasticity

G Modulus of shear

LL Live load

$Q_{ik}$ Magnitude of characteristic axle load on notional lane number (*i*=1, 2, 3…) of a road bridge

$Q_{hk}$ Magnitude of characteristic longitudinal forces (braking loads) on a road bridge

$Q_{trk}$ Characteristic transverse braking force on road bridges

### Roman lower case letters

$f_u$ Ultimate limit strength

$f_y$ Yield strength

$q_{ik}$ Magnitude of characteristic vertical distributed load on notional lane number (*i*=1, 2, 3…) of a road bridge

### Greek lower case letters

$\alpha_{Qi}$ Adjustment factor for characteristic axle load on notional lane number (*i*=1, 2, 3…) of a road bridge

$\alpha_{qi}$ Adjustment factor for characteristic vertical distributed load on notional lane number (*i*=1, 2, 3…) of a road bridge

$\nu$ Poisson's ratio

$\sigma$ Normal stress

$\gamma_F$ Partial load safety factor

### Abbreviations

CFRP Carbon fibre reinforced polymers

FEM Finite element model

FRP Fibre reinforced polymers

GFRP Glass fibre reinforced polymers

SLS Serviceability limit state

ULS Ultimate limit state

# 1 Introduction

## 1.1 Background

The application of fibre reinforced polymers in bridge construction has firstly started for strengthening of existing concrete bridges (carbon fibre reinforced polymer lamellas). Subsequently, FRP reinforcing bars were employed in production of 'steel-free' concrete decks in order to avoid corrosion problems. The next move was to produce bridge decks made entirely of fibre reinforced polymer composites. The primary reason of FRP materials being convenient for use in bridge decks is the characteristics of light weight and high strength in combination with resistance to corrosion.

A big number of pedestrian bridges have been built as 'all-composite' bridges where all the bridge components are made of FRP materials. While the most likely use of FRP materials in road bridges is FRP decks over mainly steel girders.

Nowadays, numerous road bridges are classified as structurally deficient or functionally obsolete due to deteriorated structural components or low load carrying capacity. In general, the main load-carrying members of these bridges are in good condition while the deck system is deteriorated. Deterioration of bridge decks, which often are made of reinforced concrete, is mainly caused by corrosion of the reinforcement steel due to de-icing salts. In most cases, deterioration of concrete bridges occurs before these bridges reach their design service life. The current practice when rehabilitating these bridge decks is to demolish the old deteriorated concrete deck and replace it by a new concrete deck which might be either precast or cast in place. This ascends a problem of time, especially in urban areas, where a crucial request for rehabilitation of these bridges is fast erection in order to minimize traffic disruption. Another demand is to limit the environmental impact at the construction site.

Fibre reinforced composites (FRP) have high strength-to-weight, high stiffness-to-weight ratios as well as high corrosion and fatigue resistance. These qualities make FRP a well-suited material to be used in bridge decks for rehabilitation of existing bridges while maintaining the original steel or concrete girders. The self-weight of FRP decks is approximately 20% of the concrete decks (the weight of a concrete deck is 5300 $N/m^2$, while the weight of a FRP deck varies from 480-1440 $N/m^2$). They offer therefore an attractive and competitive solution for upgrading the load-carrying capacity of existing bridges, without the need of strengthening the supporting girders. Furthermore, FRP-s exhibit a superior resistance to environmental degradation compared to traditional building materials which leads to a longer service life of the entire bridge superstructure. FRP decks offer the benefit of prefabricated panels. The short installation time of the prefabricated panels makes FRP decks appealing for urban bridges with high traffic volumes where the construction time should be minimized as much as possible.

Fibre-reinforced polymer composite decks hold also a great promise as a means of deck replacement for deficient historic bridges while maintaining the original primary structure or in movable bridges where low self-weight is very advantageous. In addition, these decks are being used in the construction of new bridges when light weight, corrosion resistance and rapid installation are demanded.

## 1.2 Project motivation and aim

The driving force of this thesis is the advantageous characteristics that FRP decks offer. The most significant ones are low-weight, corrosion resistant, rapid construction which makes them particularly useful in replacement, rehabilitation and upgrading of existing traditional bridges. A crucial feature is that they are prefabricated and fast installation is possible compared to traditional reinforced concrete decks. This minimizes the traffic interruption which is a big concern especially in big urban areas.

Being motivated by these qualities, it was decided to study these decks to get a good overview and understanding of this innovative building technology. Hence, the aim is to investigate the feasibility and efficiency of FRP decks used for replacing and upgrading conventional decks.

## 1.3 Objectives

To reach the main aim, the questions that need an answer by the work presented in this thesis are:

1. Is it important to have a composite action between the FRP deck and underlying girders? What are the benefits and drawbacks of having non-composite and composite action?
2. How can this composite action be achieved?
3. What type of connections can be used in different cases and what is the capacity?
4. How should the connections be detailed to achieve effective and rapid on-site assembly?

The answers of these questions are the objectives of this thesis which are realized by the investigation of upgrading an existing concrete-steel bridge with FRP deck.

## 1.4 Method

The method to realize the objectives is based on outcome of the literature study and analysis of upgrading a concrete deck with FRP deck in an old bridge. Numerical analyses by means of finite element modelling were utilized to assess the overall structural behaviour and load carrying capacity of the bridge under different load effects. Some simple analytical analyses were done mostly to design the mechanical connections between the FRP deck and the steel decks. The general organization of the study is illustrated below.

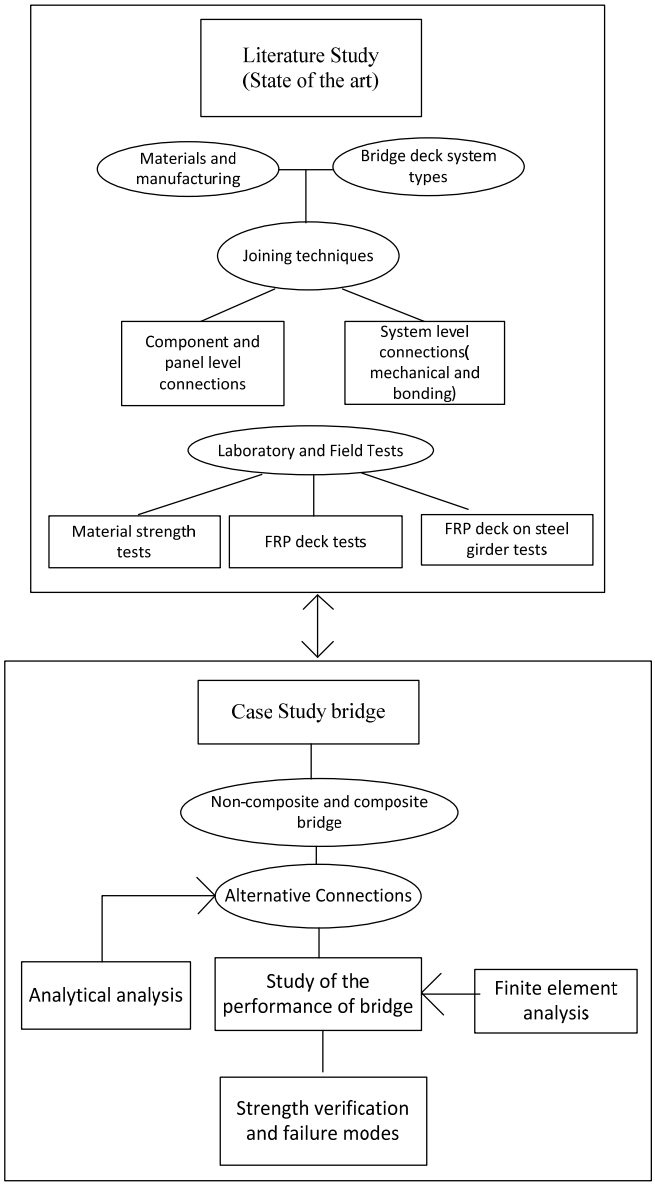


*Figure 1.1 The organization and method of the study*

## 1.5 Limitations

The limitations that apply on this thesis are:

- In the analysis of the bridge just ASSET deck system was considered. The selection of ASSET deck was mainly because of the collaboration of Chalmers University of Technology with the company Fiberline manufacturing these decks. The material data of the deck was provided by the company.

## 1.6 Outline of thesis

After the introduction part the thesis continues with a detailed literature review and the feasibility study on upgrading existing concrete-steel bridges.

Chapter two presents the thorough literature study concerning FRP decks in bridge construction. It starts with the presentation of the constituent materials of FRP decks and different manufacturing methods of these decks. Several bridge deck types manufactured by different manufacturing companies are presented. Joining techniques between deck components, deck panels and deck to girders developed up to now are introduced. Laboratory and field tests done on FRP decks and hybrid girders made of steel girders and FRP decks are studied and the results are presented. Some other different deck types made of FRP materials combined with traditional materials are studied. The installation and construction of FRP decks on steel girders and the performance of FRP decks reported by monitoring several cases of FRP-steel bridges are presented.

Chapter three presents the feasibility study of upgrading an old concrete-steel bridge with FRP deck. This chapter covers the consideration of different scenarios of upgrading this bridge such as non-composite and composite bridge. Several connections between the deck and the girders are presented. Strength evaluation of these different connections referring also to the literature review was performed. Consequently, the detailing of these connections focusing on the ease of installation and rapid on-site assembly are studied.

Conclusions are discussed in Chapter four and the need for further research is proposed in the last chapter.

# 2 Literature Study

## 2.1 Constituent materials of FRP composites

Fibre-reinforced polymer composites combine the strength of fibres with the stability of resin. The strength comes largely from the fibres which in most cases are glass, carbon or aramid fibres. Fillers can be added to the matrix resin to alter or enhance the material characteristics. In civil engineering and infrastructure applications the most common fibres are glass or carbon. Thermosetting polymers are used for the resins which are usually brittle in nature.

The most common resins used today are presented below in the order of increasing material properties and cost:

1. Orthophthalic polyester
2. Isophthalic polyester
3. Vinyl esters
4. Epoxies

Iso-polyesters are the most preferred material for bridge decks due to their low cost and better structural and environmental properties compared to ortho-polyesters. Vinyl esters exhibit higher material strength and environmental resistance than the polyesters but their cost is higher(Park *et al.*, 2007). Therefore, vinyl esters are used when environmental conditions are severe. Epoxies are used when peak performance is needed and they are comparatively more expensive, thus they have not been used in any bridge deck systems until now. The mechanical properties of these four types of resins with and without fibreglass reinforcement (glass mat type in this case) are given in Table 2.1. As it can be noted the fibres are the components which contribute most to the stiffness and the strength of the composite material. Resin is used to transfer the loads to the fibres and protect the fibres.

In FRP bridge deck applications mainly E-glass fibres are used due to their low cost. In this context, when writing FRP composites usually it means that the fibres are glass. The fibre type is specified when speaking about carbon fibre reinforced polymer (CFRP) composites. The mechanical properties of some fibre reinforcement which are being used (mainly E-glass) and may see their way in the use of FRP decks in the future are given in Table 2.2.

*Table 2.1 The mechanical properties of different resins with and without fibreglass reinforcement(NCHRP)*

| Resin type | | Compressive strength[MPa] | Tensile Strength[MPa] | Tensile Modulus[GPa] | Heat deflection temperatures [$^{o}$C]* |
|---|---|---|---|---|---|
| Orthophtalic | Without reinforcement | NA | 49.6 – 58.6 | 3.1 – 4.55 | 79.4 |
| | With reinforcement | NA | 151.7 | 11.7 | |
| Isophthalic | Without reinforcement | 117.2 | 50 – 75 | 3.1 – 4.6 | 90.6 |
| | With reinforcement | 206.8 | 158.6 | 11.7 | |
| Vinyl ester | Without reinforcement | NA | 75.8 – 87.5 | 3.17 – 3.93 | 100 |
| | With reinforcement | 206.8 | 158.6 | 11 | |
| Epoxy | Without reinforcement | NA | 60 - 85 | 2.6 – 3.8 | 49 - 104 |
| | With reinforcement | 241.3 | 206.8 | 12.4 | |

*Heat deflection temperature is the temperature when the resins start to soften and lose the strength.

*Table 2.2 Mechanical properties of some fibre reinforcement*

| Material | Density (g/cm$^3$) | Tensile modulus E [GPa] | Tensile strength [MPa] |
|---|---|---|---|
| E-glass | 2.46-2.58 | 70 | 2000-3000 |
| S-glass | 2.46-2.58 | 85-90 | 3500-4800 |
| Carbon : high strength | 1.74-2.20 | 220-240 | 3500-4800 |
| Carbon: high modulus | 1.74-2.20 | 300-350 | 2700-4000 |
| Alumina/Boria/silica fibres | 3.0 | 186 | 2000 |

The typical forms of reinforcement fibres are as follows:

1. Continuous Roving

The fibres are bundled together to form large strands called roving. This is twisted around a spool which can be used directly for distribution for example in the pultrusion process (this process is described in Section 2.2). The creels of continuous fibre roving are illustrated in Figure 2.1.

*Figure 2.1 Creels of continuous glass fibre roving(NCHRP)*

2. Discontinuous Roving

Discontinuous roving is chopped in very small pieces (1.3 to 5 cm) and is used to fabricate parts using hand-spray method (see Figure 2.2). This type of roving is used mostly when reduced mechanical properties are acceptable.

*Figure 2.2 Chopped strand glass fibres(NCHRP)*

3. Woven Roving

Fibreglass roving is weaved in fabric to form a coarse reinforcement product which is used predominantly in hand lay-up moulding manufacturing process (Section 2.2). The weave can be made with different amounts and directions of the fibres to engineer the desired properties.

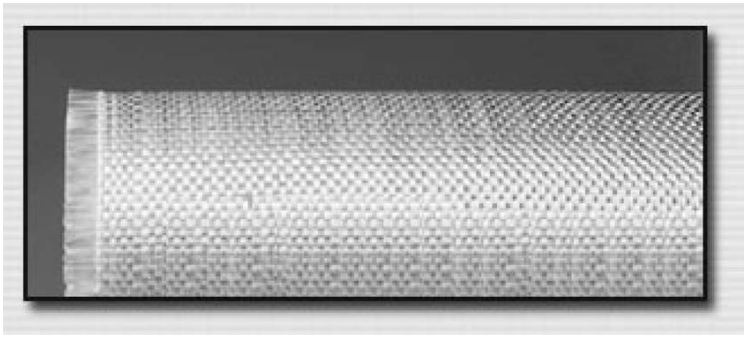

*Figure 2.3 Woven roving fabric(NCHRP)*

4. Mats

Mats are produced as continuous or chopped strand mats. They are produced by depositing strands and binding them to each other (see Figure 2.4). The continuous strand mat has better strength characteristics than a chopped mat.

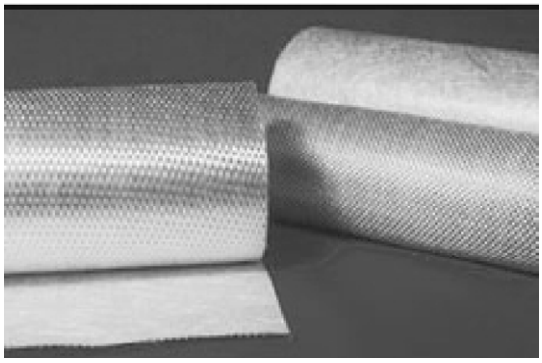

*Figure 2.4 Chopped strand mat fabrics(NCHRP)*

5. Non- crimp fabrics

Non-crimp fabrics are made by stitching or knitting fibre strands together in multi-orientations by combining the longitudinal ($0^o$), transverse ($90^o$), and double bias (+-$45^o$) to produce straight, non-crimped, layers of fibres(NCHRP). They have higher strength and stiffness than woven fabrics but the cost of manufacture is higher.

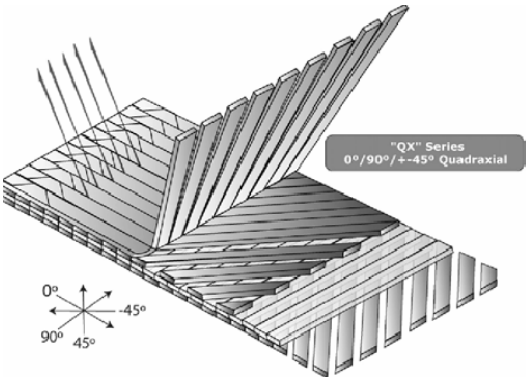


*Figure 2.5 Non-crimp fabrics*

Mechanical properties of FRP composites depend on the type, volume and orientation of the fibre reinforcement, which classifies the material as anisotropic. The most common forms of reinforcement fibres used in manufacturing of FRP decks are the continuous roving and mats.

## 2.2 Manufacturing of FRP decks

Fibre reinforced polymer bridge decks are prefabricated in a shop, then assembled and installed at a bridge site. The manufacturing method and the bonding materials used in the assembly of different deck parts affect the final properties of the deck. There exist three basic manufacturing methods of FRP decks:

- Pultrusion
- Vacuum-assisted-resin-transfer-moulding (VARTM)
- Open mould hand lay-up

Pultrusion process is described as a complex arrangement of glass fibre that are pulled through a resin bath and heated as it passes through a die to produce sections, which later are bonded together to form deck panels (see Figure 2.6). The reinforcement is pulled through the resin bath to completely saturate the fibres with resin. The resin bath contains apart from resin, pigments to add colour, fillers to enhance properties and catalyst to aid in curing of the material from liquid to solid. The saturated reinforcement is then pulled through the heated die to form the shape of the product and cure the resin. The pulling speed and temperature gradient within the die is dependent upon the time-temperature curing profile of the product. For example it can be cured in $60^{o}$ C for 8 hours or $160^{o}$ C for a couple of minutes. Then the product is cut into pre-programmed lengths by a cut off saw. The pultrusion process is a fully-automated manufacturing process, with high production ratio. However, the pultrusion process has some limitations. The pultrusion speed, for example, has to be controlled in order to ensure adequate resin wet-out and avoid air voids in the final product. If the resin wet-out and cure is not done properly a premature failure will initiate leading to low mechanical properties of the composite part. During pultrusion, the creels of continuous roving provide longitudinal tensile strength whistle the rolls of woven roving, mats or non-crimp fabrics provide strength according to the orientations of fibres in the profile.

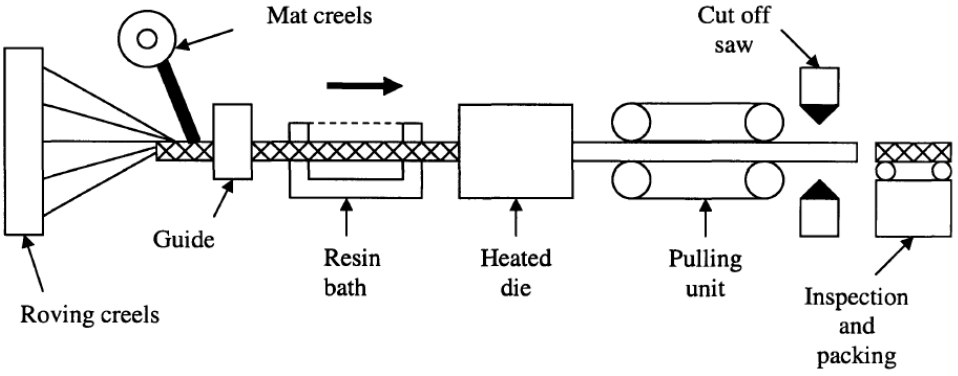


*Figure 2.6 Different steps in pultrusion process(Tuakta, 2005)*

Sandwich systems are produced by VARTM or hand lay-up procedures, where a core is bonded between top and bottom face sheets. In Figure 2.7, the core of a sandwich deck is depicted which will be sandwiched by bonding adhesively a top and a bottom face sheet. Sandwich deck systems are fabricated with pultruded cellular modules that are bonded together in orthogonal direction. VARTM uses a vacuum to infuse resin into reinforcement fibres that are placed in an evacuated mould. The mixture is allowed to cure under vacuum (see Figure 2.8).

*Figure 2.7 The core of an open mould sandwich deck(Jerome S. O'CONNOR)*

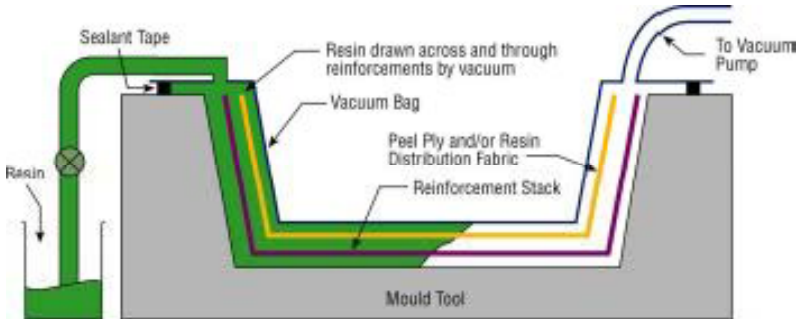


*Figure 2.8 Schematic of vacuum resin transfer moulding(Tuakta, 2005)*

Hand lay-up process is a labour intensive method and one of the oldest composite manufacturing technologies. Liquid resin is applied to the mould and fibre reinforcement is placed manually on top (see Figure 2.9). In order to impregnate the fibre with resin and remove any trapped air metal laminating roller is used. Some limitations of hand lay-up include low fibre volume fraction, inconsistency in quality of produced parts, environmental and health concern of styrene emission.

**Dry filament placement** **Fabric saturation**

*Figure 2.9 Hand lay-up process(NCHRP)*

VARTM or hand lay-up processes can accommodate connector parts, such as steel inserts into the deck, with ease compared to pultrusion process. However, comparing all the manufacturing processes, it can be concluded that the overall quality of the pultrusion method is higher than the other methods since it is done under controlled conditions.

## 2.3 FRP bridge deck systems

In principal, two construction forms of FRP composite decks can be discerned: deck elements from pultruded shapes adhesively bonded together and large-sized sandwich slabs with different core structures.

The majority of the decks are composed of pultruded members that are glued together (see Figure 2.10). These decks have constant depth. The decks usually span between two or more adjacent girders, oriented with the direction of pultrusion perpendicular to the girders (see Figure 2.11). The maximum span of the deck between the girders has been limited to approximately 2.7 meters. It is, in general, the stiffness of the deck (i.e. deflection between the girders) which imposes this limitation. Therefore, in wide highway bridges several longitudinal girders are usually used to overcome this problem. In principal, the decks can be considered as load carrying in the direction of the pultrusion only. Furthermore, it is difficult to form slopes in the transverse direction of the bridge due to constant depth of the deck panels. In order to achieve the transverse slope, haunches of varying thicknesses over different girders are employed. The haunches are usually made of non-shrink grout. In some other applications, the thickness of the overlay (wearing surface) is varied to give the necessary slope to the deck. Pultruded FRP-decks have been produced with various shapes and dimensions. Some of the commercial products available in the market today are listed below:

a) EZ-span system: has a constant depth of 216 mm and consists of pultruded triangular sections glued together and as well as to the top and bottom flanges. The EZ-span deck weighs about 0.96kN/m$^2$.

b) Superdeck system: has a constant depth of 203mm and consists of two separately pultruded members with hexagonal and half depth trapezoidal cross sections glued together. Its weight is approximately 1kN/m$^2$.

c) DuraSpan system: has slab depths of 127 mm (DuraSpan 500) or 195 mm (DuraSpan 766) and is composed of trapezoidal sections with alternating diagonals. It weighs in the order of 1.05kN/m$^2$.

d) Strongwell system: is composed of pultruded rectangular hollow section members and flat top and bottom plates. It has a constant depth of 170 mm.

e) ASSET system: has a constant depth of 225 mm and is composed of pultruded triangular shaped cells bonded together. It weighs about 1kN/m$^2$.

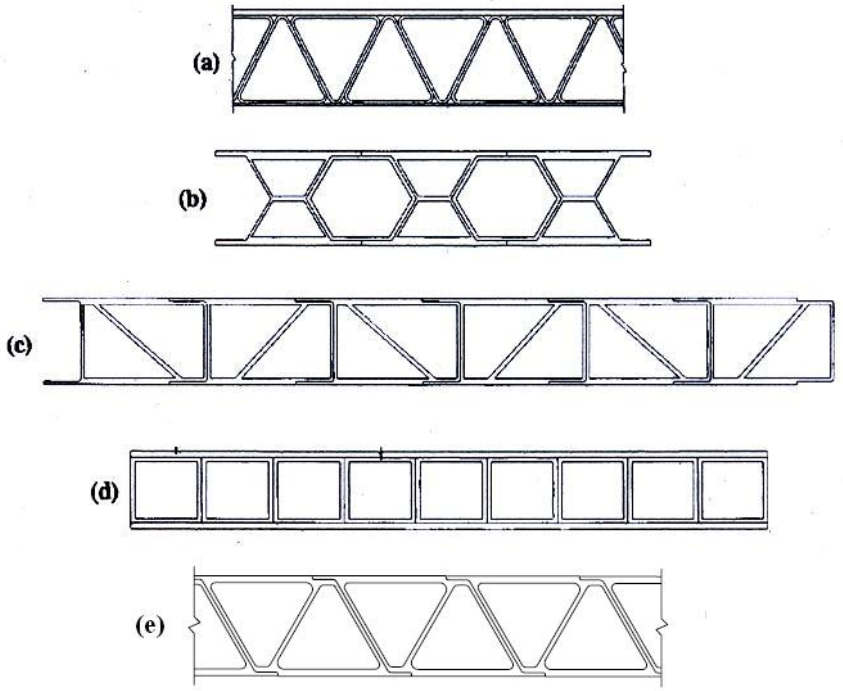


*Figure 2.10 Cross-sections of pultruded bridge decks: (a) EZ-span system; (b) Superdeck system; (c) DuraSpan system; (d) Strongwell system (e) ASSET system (based on (El-Qaleoby et al., Keller & Gürtler, 2005b))*

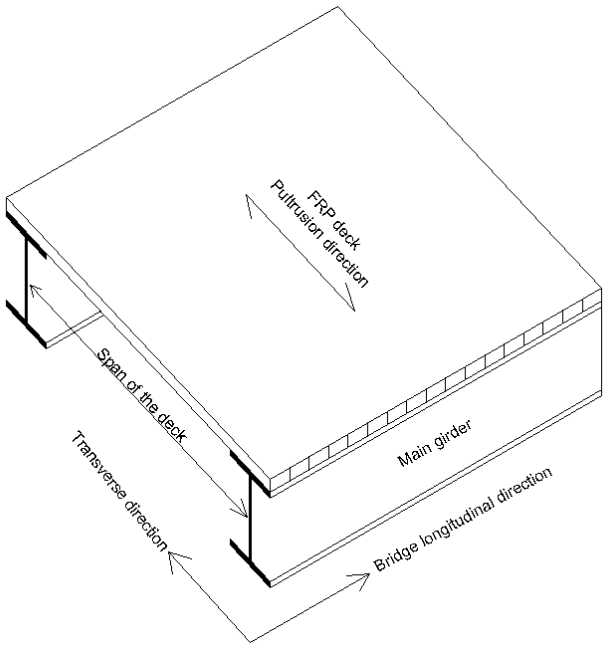


*Figure 2.11 A simple sketch of FRP deck on steel girders. The deck is oriented with the pultrusion direction perpendicular to the main girders*

FRP-decks manufactured by vacuum assisted resin transfer moulding (VARTM) or open mould hand lay-up can be made with varying depths which solves the problem of the transverse slope of the deck. Sandwich deck systems having different core structures such as thin walled cellular materials (honeycomb sandwich) or stiffened foams (solid core sandwich) are fabricated with using VARTM or hand lay-up

processes (see Figure 2.12). The biggest span length between two girders achieved up to now is approximately 10 meters. The load-carrying behaviour of these decks can be in principal considered as bi-directional.

The most common deck types with sandwich system are described below:

1. Hardcore system: is built from sandwich elements that are manufactured by VARTM process. The majority of the decks use vertical standing foam boxes as the core of the deck. The maximum span length to date is 9.75 m. Its weight is between 0.96-1.68kN/m$^2$.
2. Kansas system: is built from sandwich elements fabricated using hand lay-up procedure. Maximum span length achieved up to year 2000 is 7.1m. The deck self-weight is variable.

**Honeycomb sandwich configuration**

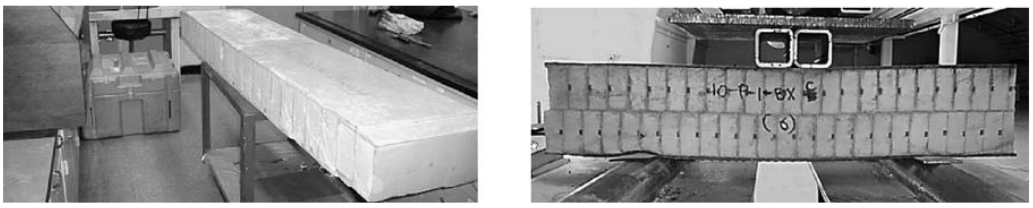

**Solid core sandwich configuration**

*Figure 2.12 FRP sandwich decks(NCHRP)*

## 2.4 Joining techniques

Different connection systems have been developed to join the deck plate elements to each other and to girders. These connections include:

- Component- component connections to form deck panels (component level connections CLC)
- Panel- panel connections to form deck systems (panel level connections PLC)
- FRP deck to support connections to form bridge superstructure (system level connections SLC)

In component level connections, adhesive bonding is the viable joining technique (see Figure 2.13). However, in some cases mechanical fastening is assisted. The principal objective of component level connection is to guarantee the integrity and load transfer efficiency of the formed deck panels. Laboratory test results have shown that failure occurs in the fibre-reinforced components near the bonded lines but not in the adhesive layer(Zhou & Keller, 2005).

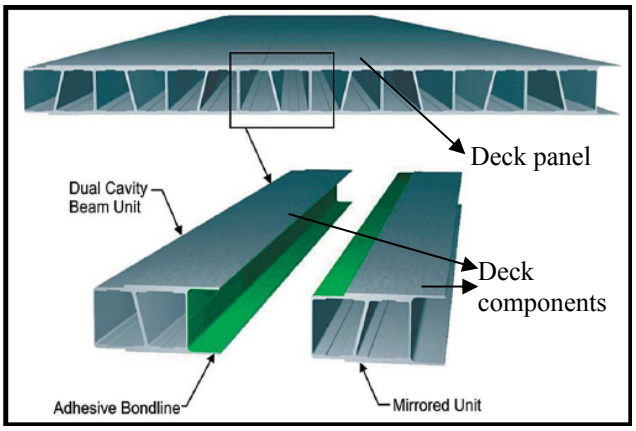


*Figure 2.13 Component level connection. Bonded pultruded shapes of DuraSpan deck components to form deck panel (Zhou & Keller, 2005)*

Panel level connections should ensure the transfer of bending moment and shear forces between joined panels. They should also guarantee deformation compatibility and ease of assembly in site. Mechanical fastening (clip-joint connection) or adhesive bonding (the splicing tongue-groove connection) can be used in panel level connections (see Figure 2.14). Results from constructed applications have shown that the mechanical connection is not reliable to resist dynamic loadings. Cracks have been appeared in the shear key connections a short period of time after exposure to traffic. (Zhou *et al.*)

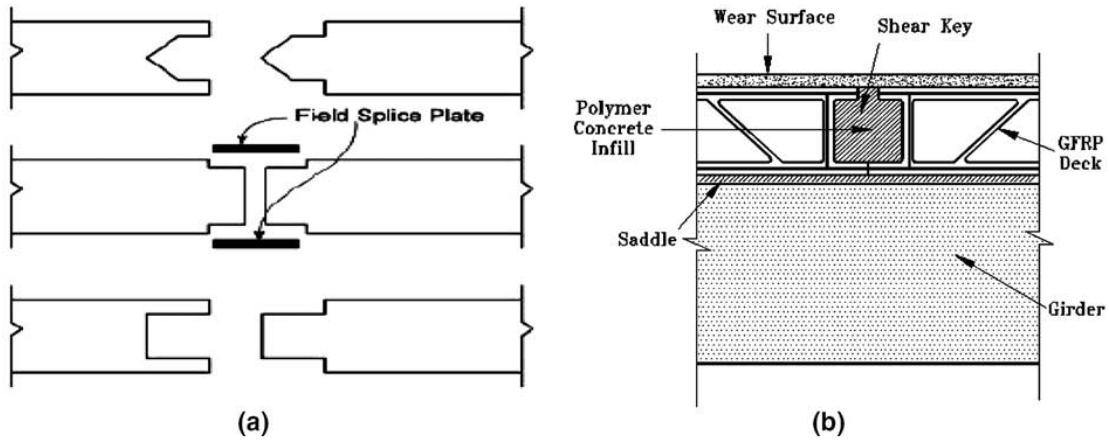


*Figure 2.14 Joining techniques of panel level connections (a) adhesive bonding (b) mechanical connection(Zhou & Keller, 2005)*

The most challenging connections are system level connections. The joints can be designed with or without composite action between the deck and the underlying girders. In case that no composite action is intended, the connection is often designed as a mechanical one which gives a flexibility and ease in assembling and possible disassembling in the future. When composite action is desired, the connections are made permanent by means of mechanical fasteners or through adhesive bonding. A combination of both types has also been used. In Figure 2.15, different types of system level connections are depicted.

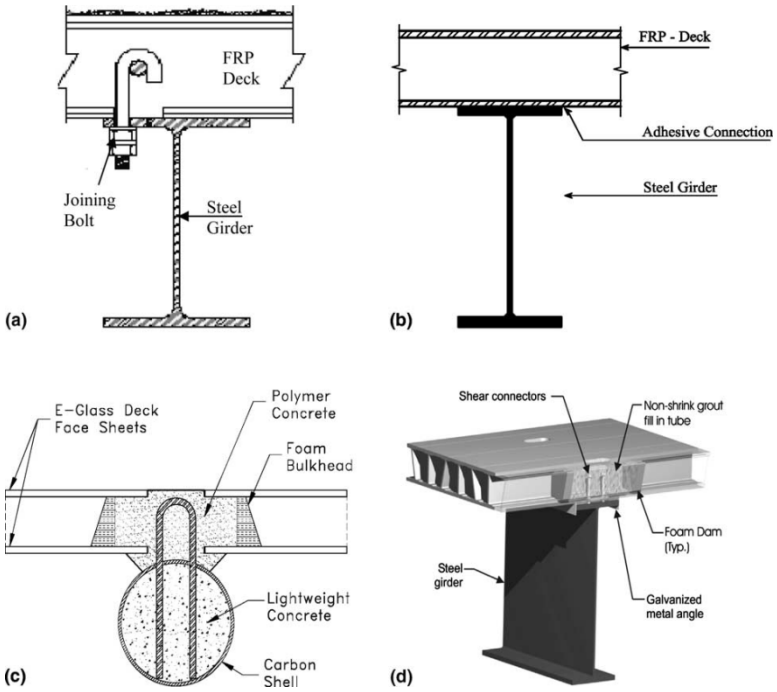


*Figure 2.15 Various types of joining techniques of deck-girder connections (a) bolted connection (b) adhesive bonding (c) hybrid connection (d) shear stud connection(Zhou & Keller, 2005)*

The bolted connection shown in Figure 2.15 (a) is not intended to provide composite action between the deck and the underlying girder. The bolts are anchored on steel rods as shown more in detail in Figure 2.16. FRP deck is composed of pultruded tube elements bonded together and a steel rod to apply a clamping force is employed. One obstacle of the bolted connections is that high stress concentrations appear in the composite matrix in the edges of the holes where FRP panels are drilled. This occurs for example when relative displacement takes place between the deck and the girder. Another type of bolted connection is one developed in Virginia Tech University, demonstrated in Figure 2.17. The first case is when the steel sleeves enclose the whole deck and in the second the bolt is fixing the lower deck panel.

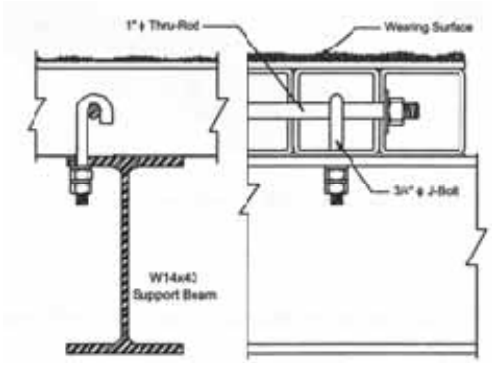


*Figure 2.16 FRP deck to girder connection by using bolts(Gurtler, 2004)*

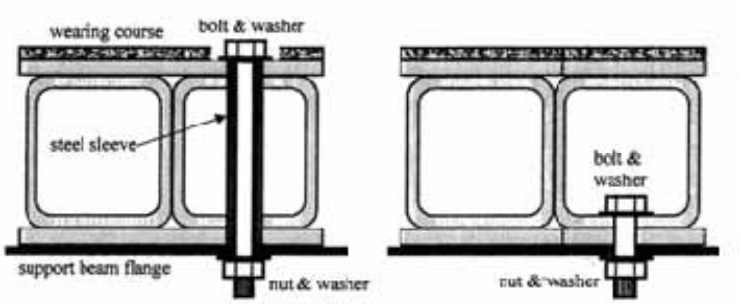


*Figure 2.17 Bolted connection between FRP deck and girders developed in Virginia Tech University (Gurtler, 2004)*

Adhesive connection is viable when the deck support (i.e. girder flange) is wide and flat (see Figure 2.15 (b). Adhesives have high shear force transferring capacity which leads to their application in bridge deck- girder connections. The first application of adhesively bonded bridge decks to girders is done in the late 60s in Germany. Prefabricated concrete bridge decks were bonded with steel girders and the motive of using adhesives was stated to be the time-saving aspect. These connections have revealed satisfactory performance and they are still in use and good condition (Gurtler, 2004). Mechanical connections providing composite action can be achieved with stirrups or shear studs as shown in Figure 2.15 (c) and (d). The connection of the FRP deck to carbon shell supports is depicted in Figure 2.15 (c). The carbon shell system was developed by F. Seible in 1995 which consists of thin carbon shell layers filled up with lightweight concrete in the site to prevent the carbon shell from buckling and to transfer the compression force.

Moreover, clamped connections have been implemented in some applications by Kansas Structural Composites Inc. These clamped connections are placed at panel-to-panel connections. They consist of a FRP tube where holes are drilled and bolts are used to lock the clamping device and the bottom flange of the steel girder against the FRP tube (see Figure 2.18).

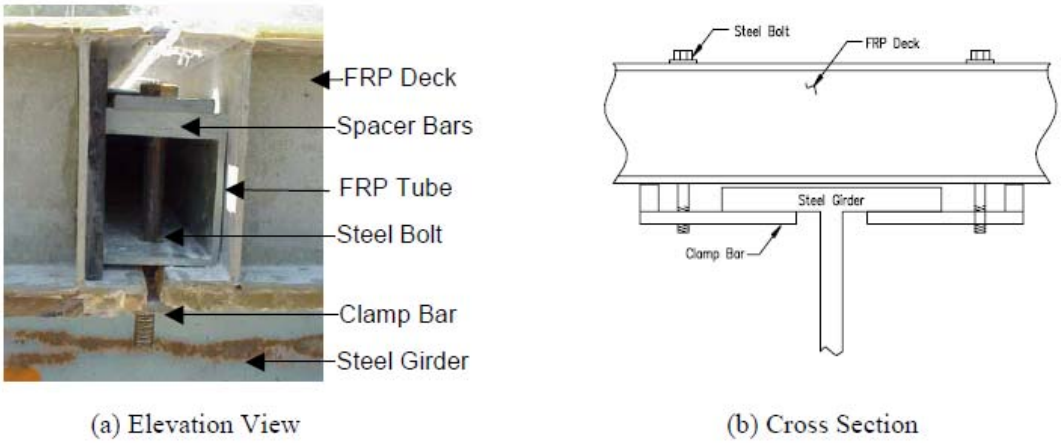


*Figure 2.18 Illustration of the clamped connections used by KSCI(Righman, 2002)*

This type of connection is not intended to provide composite action between the deck and the girder. It secures the deck in place and prevents it from uplifting. The bolts are installed from underneath of the bridge. The panel widths have to be manufactured in required widths fitting to the spacing of the connections. This type of connection might not be a good solution since they are quite labour intensive and have to be protected from the dirt and water leakage which might cause durability problems.

## 2.5 Laboratory tests and field investigations

Numerous tests have been performed to evaluate the material strength of fibre reinforced polymers, performance of FRP decks and hybrid girders made of FRP decks and steel girders. Most of the tests have been carried out in laboratory but some of them have been implemented in the field to provide valuable performance data. Several of the in-situ tests are being evaluated using long-term monitoring systems. The majority of the tests have been focused on the deck strength and stiffness and are performed on mainly pultruded FRP decks connected adhesively or mechanically to steel girders. Typical tests include static three or four point bending test with high or low cycle fatigue test under design truck loads (see Figure 2.19). In the following sections, the experience obtained from a number of tests is presented.

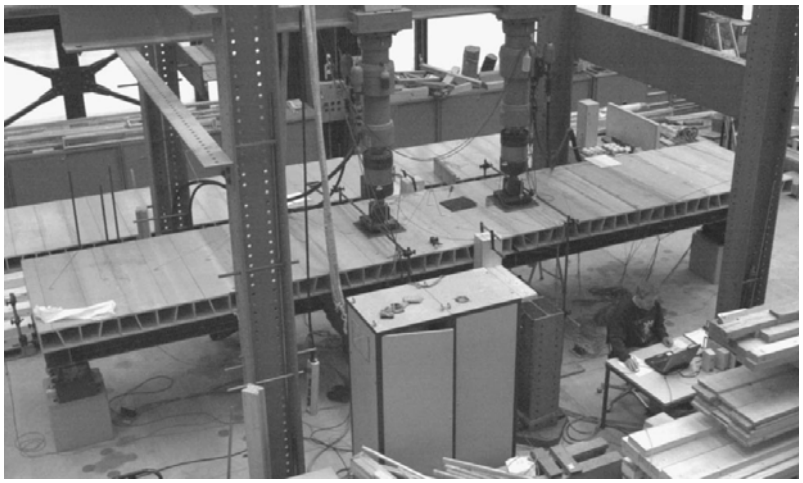

*Figure 2.19 Typical experimental set-up of a FRP deck connected to steel girders under four point loading(Keller & Gürtler, 2005a)*

### 2.5.1 Coupon level tests

Mechanical behaviour of FRP decks depends on the constituent materials of the composite material, the method of manufacture, direction of the fibres, and cross-sectional geometry and adhesives used for the deck component joints. In this section the tests done on coupon level basically to evaluate the strength of the material under different effects are presented.

A study was done by Park et al. to evaluate physical properties of flanges and webs made of different resins and fibre orientation that comprise FRP deck components. The physical properties are investigated in the direction of the fibres and in perpendicular direction to the fibres. Fibre architecture of the tested deck is given in Figure 2.20. In webs, +-45$^{o}$ woven mats were added to resist against in-plane shear deformation in the deck. Design fibreglass volume ratio constituting the flanges and webs was 65%. Two different types of resin that are polyester and vinyl ester were used in order to compare the properties. The thickness of the web was 11 mm and of the top and bottom flange was 18mm and 16 mm respectively.

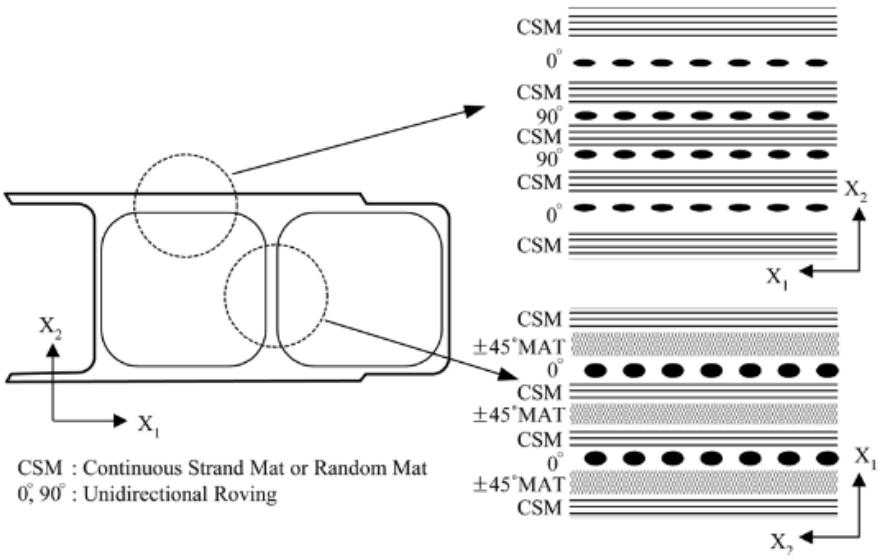


*Figure 2.20 Fibre architecture of flange and web panels(Park et al., 2007)*

Basic physical properties of the flanges and webs by resin type are given in the following table.

*Table 2.3 Basic physical properties of flanges and webs by resin type(Park et al., 2007)*

| Description | Vinyl ester | | Polyester | |
|---|---|---|---|---|
| | Flange | Web | Flange | Web |
| Tensile strength fibre direction [MPa] | 314 | 306 | 394 | 301 |
| Tensile strength transverse dir. [MPa] | 97 | 73.4 | 181.7 | 82.2 |
| E-modulus fibre direction [GPa] | 31.1 | 24.7 | 32.4 | 21 |
| E-modulus transverse direction [GPa] | 14.6 | 12.6 | 22 | 17.3 |
| Compression strength fibre direction [MPa] | 177 | 141 | 252 | 291 |
| Compression strength transverse dir. [MPa] | 90 | 89 | 80 | 183 |
| In-plane shear strength [MPa] | 64.2 | 95.9 | 65 | 48.4 |
| Poisson's ratio | 0.255 | | 0.255 | |

According to the results, tensile strengths are higher in polyester cases (except web in fibre direction). Moduli of elasticity in the fibre direction are close to each other, but in transverse direction polyester has higher modulus of elasticity. The compressive strength in the fibre direction is higher than the perpendicular direction and higher in case of polyester. Similar results in the cases of shear strength of flanges are shown, while in the case of web, vinyl ester showed approximately two times higher strength than polyester. It is noted as well that the properties in the perpendicular direction to the fibres are mainly less than half of those in the fibre direction for both cases. Therefore, it is quite obvious that the mechanical properties of FRP components depend on the constituent materials.

Durability tests were conducted as well considering thermal expansion tests, heat and cold resistance tests, chemical resistance tests and weathering tests.

Thermal expansion coefficients of steel and concrete are $12x10^{-6}$ and 10- $13x10^{-6}$, respectively. The average results of the thermal expansion coefficients of FRP are given in Table 2.4. The results show a diversity of the thermal expansion coefficients, thus the stresses induced by thermal expansion or contraction has to be considered when this material is used together with the conventional materials.

*Table 2.4 Thermal expansion coefficients results by (Park et al., 2007)*

| Description | Vinyl ester | | Polyester | |
|---|---|---|---|---|
| | Flange | Web | Flange | Web |
| Fibre direction [1/$^{o}$C] | $4.6*10^{-6}$ | $5.4*10^{-6}$ | $7.6*10^{-6}$ | $6.2*10^{-6}$ |
| Transverse dir. [1/$^{o}$C] | $10.5*10^{-6}$ | $10.9*10^{-6}$ | $7.9*10^{-6}$ | $6.5*10^{-6}$ |

Heat and cold resistance tests demonstrated that the strength and stiffness of deck specimens was rapidly decreased as the temperature was increased and almost no change in low temperatures. This decrease was detected more in specimens made of vinyl ester. Chemical and weathering resistance tests indicated that specimens made of vinyl ester exhibit higher resistance than polyester. This verifies the statement that vinyl esters have higher environmental resistance mentioned in Section 2.1.

The effect of moisture exposure on FRP pultruded material is studied by Smith(Smith, 2001a). The tests were run short-term in the lab and it was observed that there is impact of the moisture in the structural performance of the coupons. The strength and stiffness is reduced when the material is exposed to moisture.

The effect of the cross-section geometry of the deck to the properties of the deck was studied by (Motley *et al.*). Motley et. al. examined the effect of the orientation of the webs such as vertical and inclined in the response of FRP deck. It was found out that diagonal webs contribute to the response of the deck and lateral stability is increased significantly. The decks composed of only vertical webs show lateral instability under wheel loads and to overcome this problem, thick flanges are required which will increase the material cost. On the other hand, inclined webs help in transferring the wheel loads much better and hence, reduce the lateral instability problem. Accordingly, the use of inclined webs is found to be a better solution. The failure mode under high loads was usually buckling of the vertical web. Furthermore, the

effect of the angle of the webs to the global response was studied and the measured transverse deflection was observed to have not a significant change (see Figure 2.21). Thus, the angle of the webs does not influence the global stiffness of the deck.

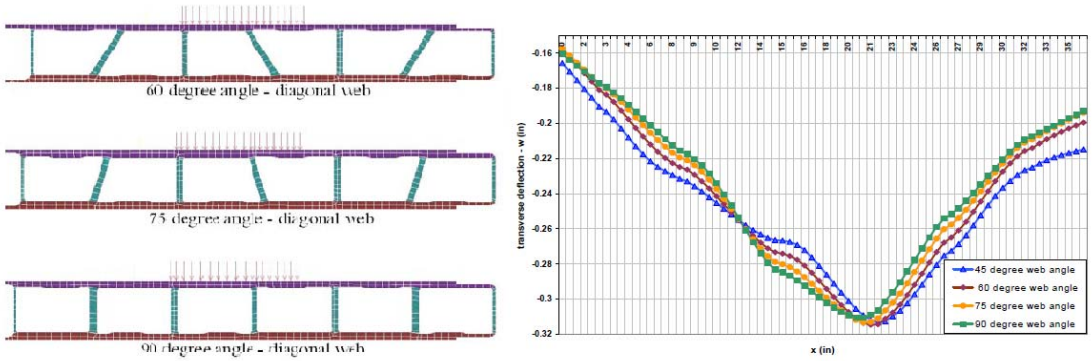


*Figure 2.21 Effect of angle of the webs on the transverse deflection (Smith, 2001a)*

## 2.5.2 Tests on FRP decks

Experimental tests conducted on the level of deck are presented in this section.

DuraSpan and Asset deck systems' properties were studied by (Keller & Gürtler, 2005b, Keller & Gürtler, 2006). Tests were performed to find out in-plane properties of these decks which might act as a top chord of bridge girders in case of composite action between the deck and the girders. The term 'in-plane' in this context means the properties in the deck plane and the tests are done transverse to the pultrusion direction. In-plane compression and in-plane shear tests were carried out on panels made of three adhesively bonded components (see Figure 2.22).

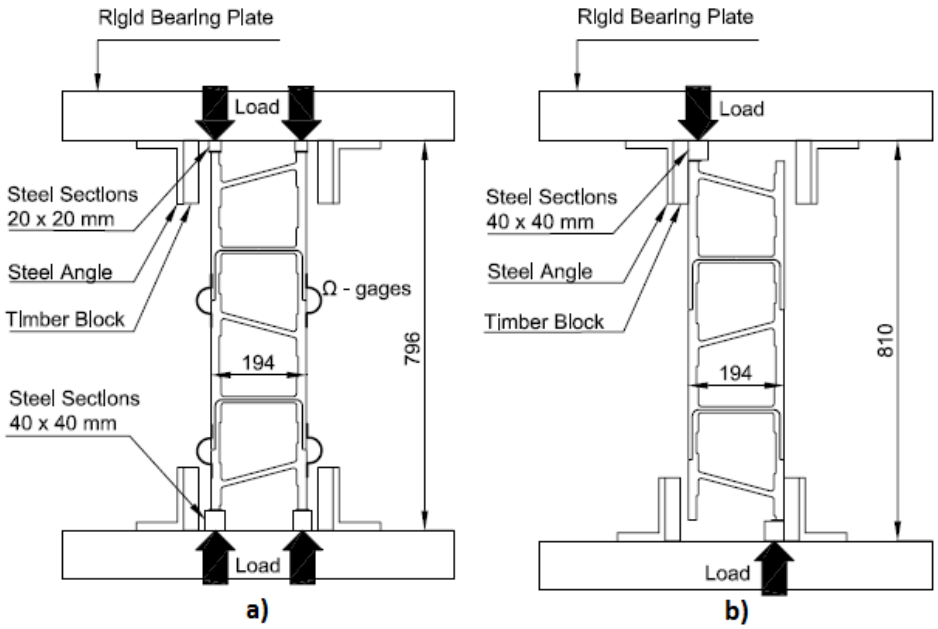


*Figure 2.22 Experimental set-up for a) in-plane compression; b) in-plane shear(Keller & Gürtler, 2006)*

In-plane properties of these two different deck systems are given in Table 2.5. The failure mode of ASSET deck was brittle and linear elastic up to failure, but DuraSpan deck exhibited some ductility. The so called 'elastic limits' mark the beginning of the local delamination failures. In tests of in-plane compression, DuraSpan deck was deformed laterally while loading and delamination in the flanges of the deck started propagating. In ASSET deck delamination in the stepped joint caused failure (see Figure 2.23).

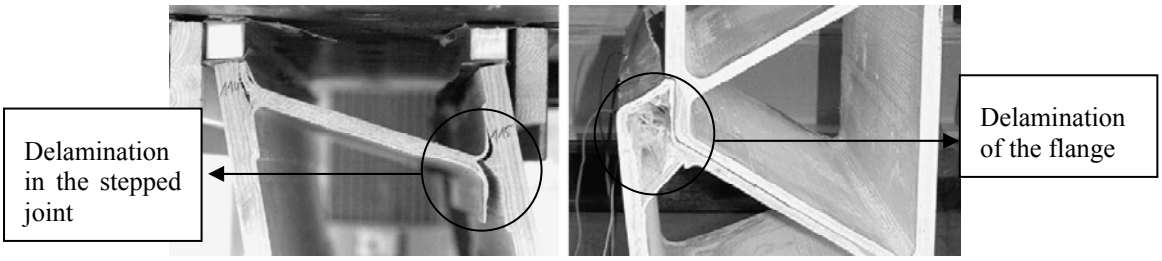


*Figure 2.23 Failure modes of DuraSpan in the left and Asset deck in the right for in-plane compression tests (Keller & Gürtler, 2006)*

Failure modes of in-plane shear tests were web delamination and joint failure for DuraSpan and failure in the stepped joint for Asset deck (see Figure 2.24).

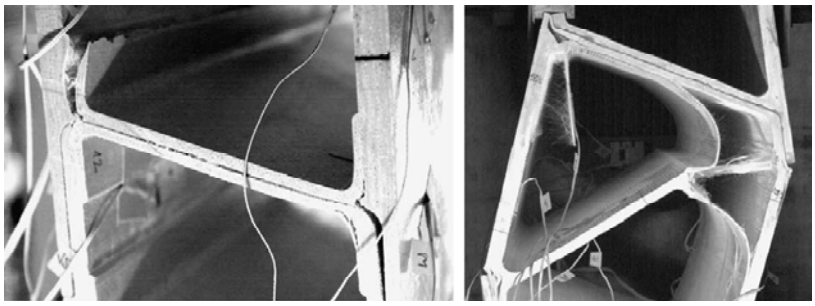

*Figure 2.24 Failure modes of DuraSpan in the left and Asset deck in the right for in-plane shear tests (Keller & Gürtler, 2006)*

In Table 2.5 it can be observed that the strength and stiffness of ASSET deck system are higher than DuraSpan deck system. The difference is more significant for in-plane shear stiffness and capacity. The configuration of ASSET deck is triangular compared to trapezoidal configuration of DuraSpan system, which makes possible the transfer of forces mostly by truss action. The transfer of forces in DuraSpan deck is mainly by Vierendeel action. Thus, ASSET deck has much higher in-plane shear stiffness and strength than DuraSpan deck.

*Table 2.5 In-plane properties of DuraSpan and ASSET deck systems(Keller & Gürtler, 2006)*

| Deck system | In-plane compression | | | In-plane tension | | | In-plane shear | | |
|---|---|---|---|---|---|---|---|---|---|
| | E-modulus [GPa] | Failure Stress [MPa] | Elastic limit stress [MPa] | Stiffness moduli [GPa] | Failure Stress [MPa] | Elastic limit stress [MPa] | G-modulus [GPa] | Failure Stress [MPa] | Elastic limit stress [MPa] |
| DuraSpan 766 | 11.7 | -34 | -29 | 9.6 | 18 | 8 | 0.005 | 0.13 | 0.09 |
| Asset | 16.2 | -41 | None | | | | 0.047 | 0.61 | None |

Furthermore, in-plane tension tests were executed on only DuraSpan deck system, to examine the in-plane tensile performance when the deck acts as a top chord in continuous bridges with negative moment regions (Keller & Schollmayer, 2006). The results are given in Table 2.5 under in-plane tension column. Failure mode in this case was failure in the stepped joints (see Figure 2.25).

*Figure 2.25 Failure in the joint for in-plane tension test in DuraSpan deck(Keller & Schollmayer, 2006)*

Tensile strength and stiffness of DuraSpan deck are lower than the compressive ones. It should be mentioned that the in-plane transverse stiffness is substantially reduced due to adhesive joints between the deck components.

Bending behaviour of DuraSpan deck system was further investigated by (Keller & Schollmayer, 2004). Static tests were performed on decks having varying span of 1.9 to 2.7 m (see Figure 2.26). The widths of the decks were varying as well from 1.016 to 1.626 m.

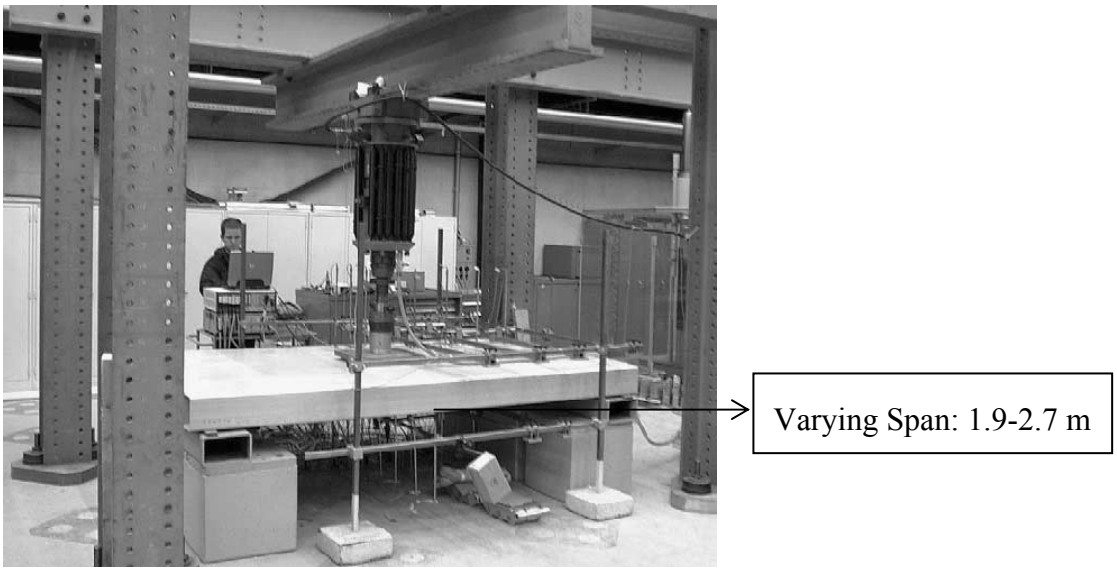


*Figure 2.26 Experimental set-up for static tests performed by (Keller & Schollmayer, 2004)*

The results showed that global load-deflection response was linear-elastic up to ultimate limit state loads. Failure of the deck occurred around the area of the patch load where buckling of the upper face sheet and the webs started (see Figure 2.27). Thereafter, delamination between the flanges and the webs were observed. The maximum resulting stress was 194 MPa at failure. Maximum spacing between the girders was determined as 2.7 m by putting deflection criteria limit as L/300.

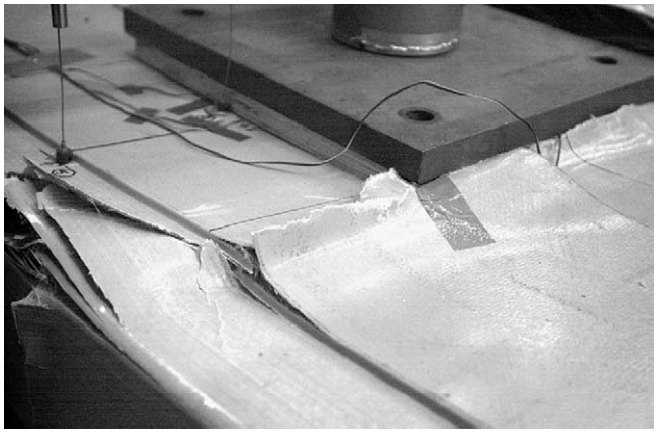

*Figure 2.27 Failure mode of DuraSpan deck: buckling and delamination(Keller & Schollmayer, 2004)*

Furthermore, a creep test of 14 hours loaded with SLS load was performed. It was observed that the creep deformation increased only 1 mm and after unloading the creep deformation went back to zero within 30 minutes. This test might not be sufficient but indicates that creep due to traffic loads might not be a decisive issue for the global deck design.

Another type of FRP deck system is Prodeck 4 which was developed by.(Prachasaree & Shekar, 2008). One component of Prodeck 4 deck system is depicted in Figure 2.28. To evaluate the static performance of this deck, static tests were performed in both pultrusion and transverse direction.

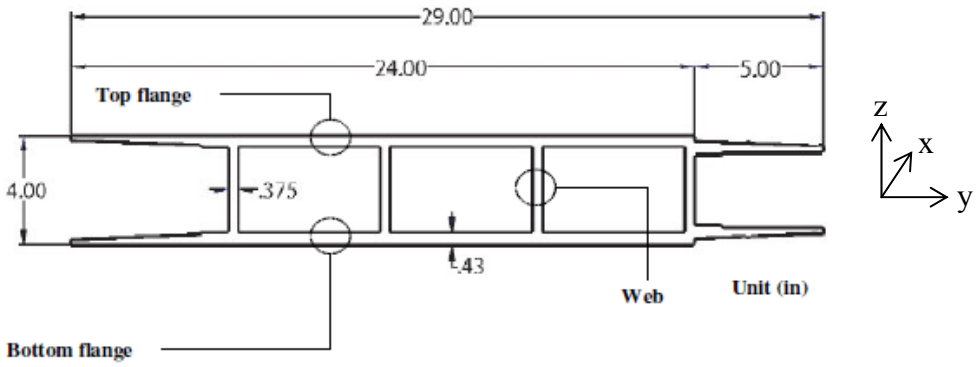


*Figure 2.28 Configuration and dimensions of one component of Prodeck 4 deck system (Prachasaree & Shekar, 2008)*

Three and four point bending tests in the longitudinal direction (pultrusion direction-x) were executed on one deck specimen having a span of 2.7 meters. The average ultimate bending strength was 220 MPa. The failure mode of the specimens varied. In some specimens the compression flanges buckled before webs leading to a separation of flanges and webs under the patch load. In other specimens separation of flanges and webs was observed in the ends of the specimens due to excessive shear stress. Another observed failure mode was delamination of the flanges followed by separation of flanges and webs. Transverse bending tests spanning 1.6 meters were performed to investigate transverse static performance of the deck. Deck components were bonded to each other with polyurethane based adhesive known as PLIOGRIP. Transverse bending modulus was found to be 2.7 times smaller than longitudinal bending modulus (see Table 2.6). The load versus deflection response was found to be linear up to failure for both cases. The maximum spacing between the girders was determined to be 1.2 m.

*Table 2.6 Longitudinal and transverse bending stiffness of Prodeck 4(Prachasaree & Shekar, 2008)*

| Description | Bending stiffness | |
|---|---|---|
| | $E_x$ [MPa] | $E_y$ [MPa] |
| Prodeck 4 | 26200 | 9650 |

Structural performance of another deck system which is Kansas sandwich deck was investigated by (Camata & Shing, 2005). The core of the deck had a sinusoidal shape and it was sandwiched by two stiff plates by hand lay-up process (see Figure 2.29).

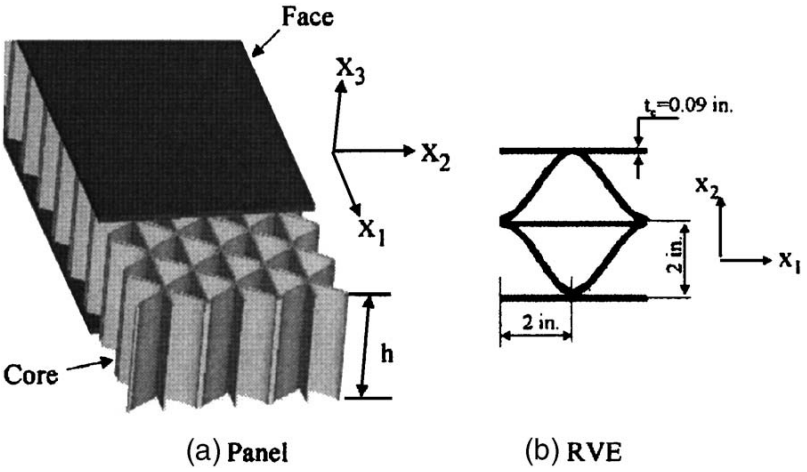


*Figure 2.29 Configuration of the Kansas deck system (Camata & Shing, 2005)*

Four beams of this deck system were tested with three-point loading test (see Figure 2.30). Crushing tests were performed as well on specimens to find out the ultimate crushing loads.

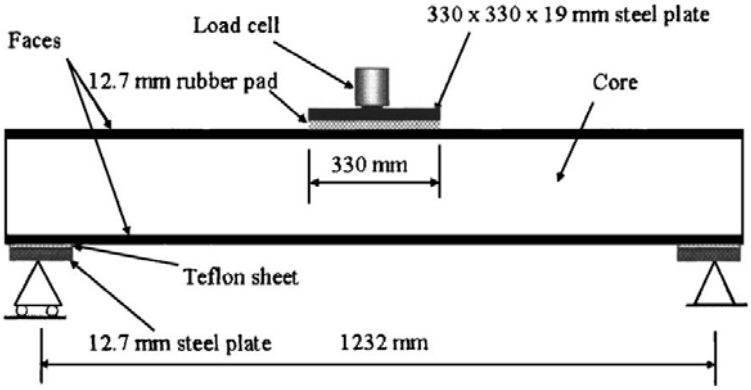


*Figure 2.30 Test set-up for Kansas beams performed by (Camata & Shing, 2005)*

Failure loads of the beams varied from 175 to 587 kN, and this scatter was due to adhesive bonding quality between the core and the plates. Load-deflection response of the four beams is shown in Figure 2.31.

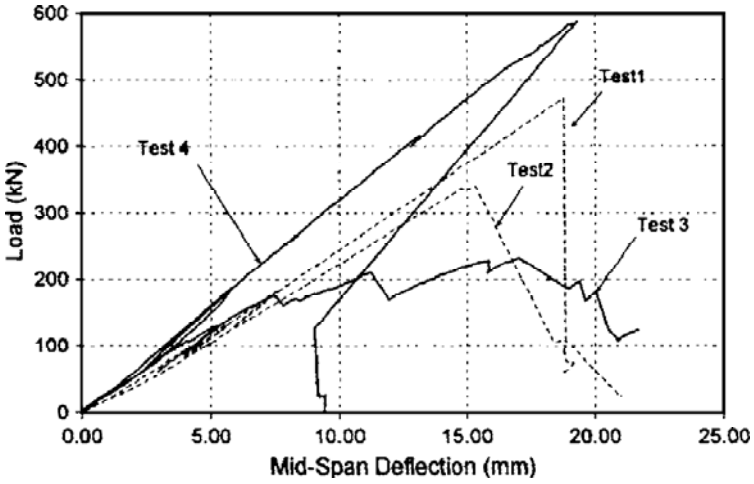


*Figure 2.31 Load-deflection curve of the beams (Camata & Shing, 2005)*

Failure mode of the beams was delamination of the flanges and debonding of the flanges from the webs. Failure modes were brittle. As observed in Figure 2.31, load-

deflection curves are linear up to failure except test 3. Failure mode of test 3 was pseudo-ductile different from the others. Delamination started in the top flange followed debonding non-uniformly and buckling of the core in the back side. This change and scatter in results is due to the manufacture process. These decks are manufactured by hand lay-up process which leads to imperfections and non-uniformities in the bonding. Ultimate crushing capacity of the specimens was approximately 721 kN. The average actual core stress was 64.7 MPa and the nominal stress when considering the whole loading area was computed as 7.1 MPa. The failure mode of the compressive crushing tests was buckling of the cores.

From the experience of these tests one can conclude that the properties of FRP deck systems vary considerably from system to system. In addition, hand lay-up manufacturing process is not a desirable manufacturing technique since it is not a controlled process and many imperfections result in the manufactured decks.

## 2.5.3 Tests on FRP-steel hybrid girders

Several tests have been performed on FRP-steel hybrid girders to evaluate mainly the strength and stiffness of these girders. Furthermore, composite action, effective widths, fatigue performance, creep performance has been assessed. The information gained by this literature study is presented in the following sections.

### 2.5.3.1 Composite action between the deck and the girders

Composite action between the deck and the girders refers to the degree that horizontal shear forces are transferred between the girder and the deck. In a section with full composite action 100% of the horizontal force is transferred between the girder and the web, on the contrary, no horizontal shear forces are transferred in a non-composite section. In addition, partial composite action occurs when a portion of this horizontal shear force is transferred between the deck and the girders. Full composite action is regarded as a plane strain distribution in the composite section, consequently fulfilling the hypothesis of Bernoulli (see Figure 2.32).

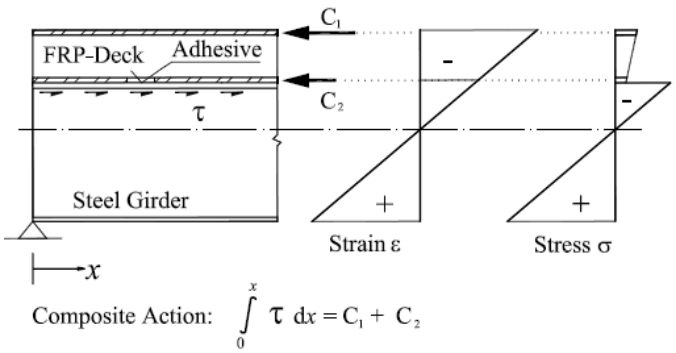


*Figure 2.32 Theory of the composite action in a composite section (Gurtler, 2004)*

The development of connections between FRP decks and girders is challenging in order to achieve full composite action. For bridges in general, composite action between bridge decks and the underlying girders gives a substantial increase in overall stiffness and load resistance of the system, which also leads to better economy. This holds for FRP decks as well. Moreover, composite action between a bridge deck made of brittle material such as an FRP deck and bridge girders with a more ductile behaviour will contribute to an enhanced ductility of the bridge structure.

The load transfer in deck-girder joints made of shear studs is complex and not yet precisely understood. Most of the constructed bridges consisting of FRP decks with steel girders up to now are done by using these types of connections. The design of the girders in these bridges is done without considering the contribution of the FRP deck and the FRP deck itself is assumed to have composite action. This design is conservative since the decks contribute to the load-carrying capacity of the girders. The major reason of considering this conservative design is due to lack of design methods and complex load-bearing behaviour.

In the case of replacing a concrete deck with an FRP composite deck, the FRP deck should offer the same functions provided by concrete deck in order to be a competitive option. In general, conventional concrete decks constructed during the last 3-4 decades have been designed to have full composite action with the girders. Therefore, when these decks are to be replaced with FRP decks, the latter may also be designed to act compositely with the girders. In this case, FRP decks must participate in the bridge's longitudinal direction as part of upper flange of the main girders in addition to providing transversal load-carrying action between the bridge girders. The degree of composite action between the girders and the FRP deck, apart from the connection between these two elements, depends also on the in-plane shear stiffness and in-plane axial stiffness of the FRP deck in the longitudinal bridge direction between the supports and in-plane tensile stiffness over the inner supports in case of continuous bridges (Keller & Gürtler, 2006).

The determination of the composite action between the deck and the girder can be determined by testing the hybrid girder. It can still not be determined by means of analytical solutions due to the lack of design methods.

Tests were performed by Keller and Gurtler on adhesively bonded hybrid FRP-steel girders. ASSET and DuraSpan deck systems were utilized. The test set-up is shown in Figure 2.33 for ASSET deck, which is the equivalent for DuraSpan deck system as well.

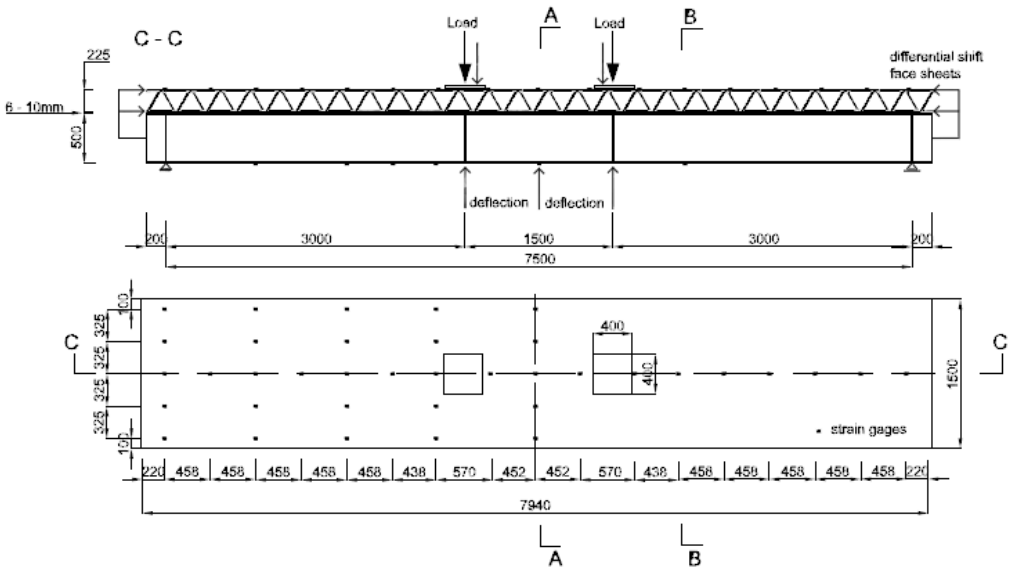


*Figure 2.33 Test set-up of adhesively bonded hybrid FRP-steel girders(Keller & Gürtler, 2006)*

The composite action of the deck itself was examined by comparing the strains and the differential shifts between the top and bottom deck panels.

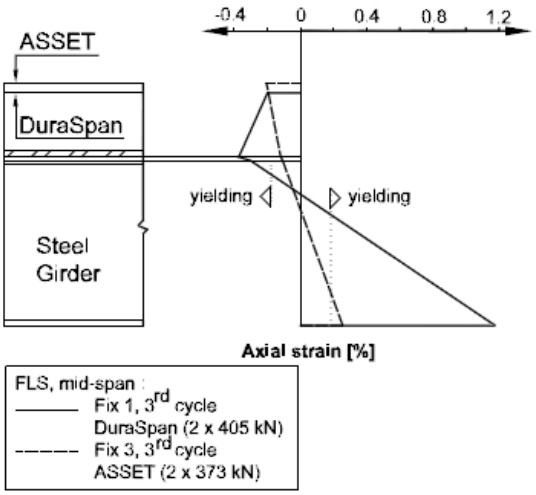


*Figure 2.34 Strain distribution in the mid-span of the Asset and DuraSpan hybrid girders*

As observed in Figure 2.34, the strains in the top flange are slightly reduced for Asset and significantly reduced for DuraSpan. Thus, it is concluded that ASSET deck has a slight reduction of participation of the top flange in the composite action of the deck and DuraSpan possesses a considerable reduction. This is verified by differential shifts between the panels as well, were the shifts of DuraSpan were approximately 40 times larger than those of ASSET deck. The participation of the upper deck panel was less pronounced for ASSET deck since it exhibits much higher in-plane shear stiffness as described in Section 2.5.2.

In sections where there are shear forces the strain distribution is different (see Figure 2.35). This change in strains is due to secondary moments in the deck itself caused by shear forces. This effect is more pronounced near the support where the global moment is small and the secondary moment of the deck caused by shear forces is high enough to cause tensile strains in top flange of the deck.

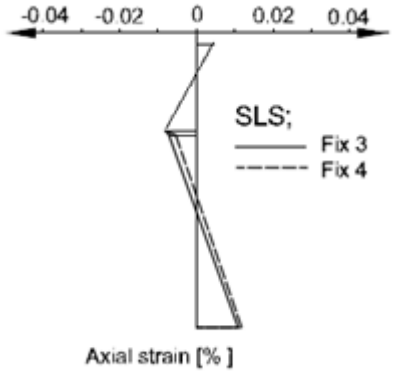


*Figure 2.35 Axial strain distribution between the support and the load(Gurtler, 2004)*

In Figure 2.35, Fix 3 and Fix 4 are the names of the composite beams tested under SLS loading.

In a composite deck-girder system, the portion of the deck assumed to contribute to the flexural capacity of the longitudinal girder is characterized by the effective width

of the deck. The effective deck width in the study performed by (Gurtler, 2004) was checked by measuring the strains on deck plates along the transverse direction. The strains are shown in Figure 2.36 for serviceability limit state (SLS) and failure limit state (FLS).

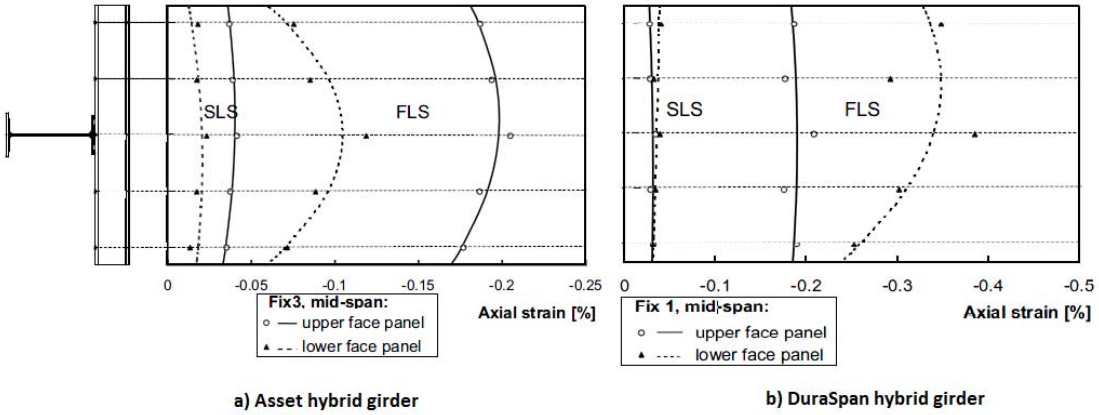


*Figure 2.36 The axial strains in transverse direction of the hybrid girders in mid-span to evaluate the effective widths(Gurtler, 2004)*

As it can be observed in the figure above, the strains in SLS for both decks are almost linear along the whole width of the deck. This indicates that the decks fully participate as top chords in the SLS state. In failure limit state this participation is reduced. The strains are not linear along the whole width but they decease in the ends of the deck width. This is more pronounced in the bottom panels.

The tests indicated that the deflections of the FRP-steel hybrid girders were decreased and the failure loads increased compared to just steel girders. The load-deflection curves for hybrid girders and steel girder are illustrated in Figure 2.37.

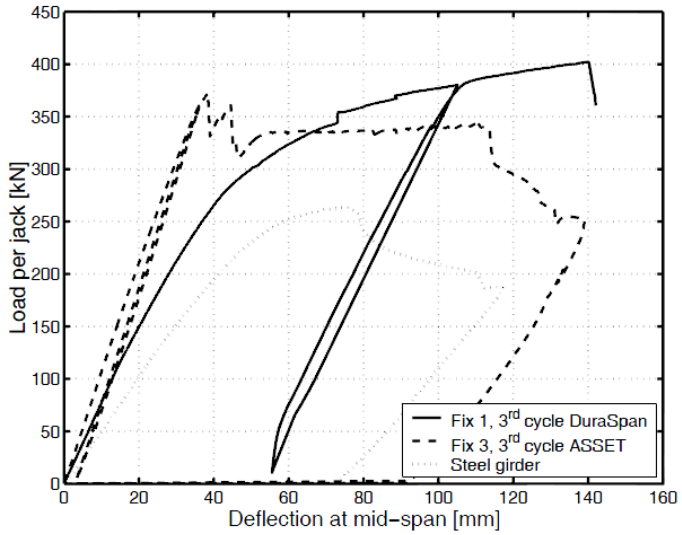


*Figure 2.37 Comparison of load-deflection curves for hybrid and steel girders(Gurtler, 2004)*

The failure in ASSET hybrid girder started on the stepped joint of the Asset deck close to patch load. Failure stresses of the hybrid girders were expected the same as the failure stresses of the decks obtained from in-plane compression tests (see Section 2.5.2). However, the failure stresses of the hybrid girders were different (see Table

2.7). The failure of ASSET hybrid girder was premature and in view of the fact that the failure was close to the patch load, the premature failure was believed to be due to the impact of the patch load. The failure on DuraSpan hybrid girders started in the transverse joint in the mid-span where there was maximum moment (see Figure 2.38). Thereafter, the bottom plate of DuraSpan deck detached from the steel girder flange and bucking of the deck between the loads occurred (see Figure 2.39 and Figure 2.40).

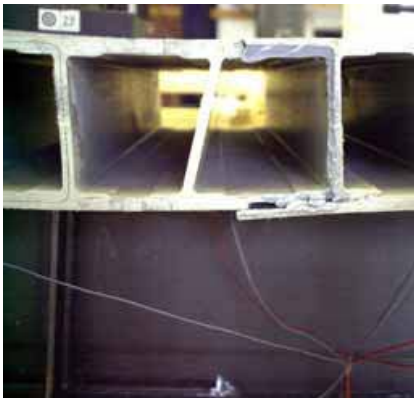

*Figure 2.38 Initial failure of DuraSpan hybrid girder in the joint in the mid-span(Gurtler, 2004)*

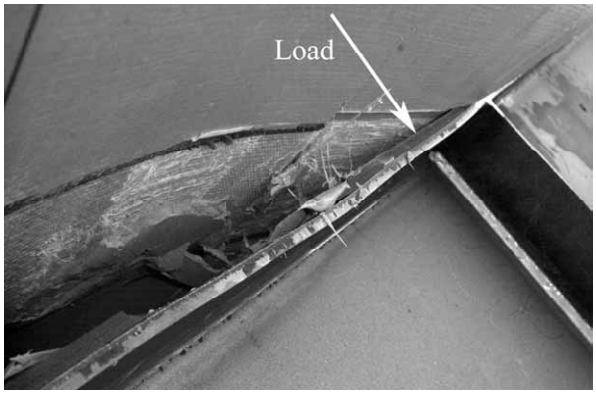


*Figure 2.39 Detachment of the FRP deck from the steel girder after initial failure(Gurtler, 2004)*

*Figure 2.40 Buckling of the DuraSpan deck between the loads after detachment (Gurtler, 2004)*

Failure stresses of DuraSpan girder are higher than the expected ones as depicted in Table 2.7. The failure of the deck during in-plane compression test was due to lateral buckling of the deck. When the deck is connected to the steel girders buckling of the deck is prevented, thus resulting in a higher failure stress of the hybrid DuraSpan girders.

*Table 2.7 Failure stresses of the FRP-steel hybrid girders(Gurtler, 2004)*

| Girder system | Expected Failure stress [MPa] | Failure stress [MPa] |
|---|---|---|
| DuraSpan | -34 | -45 |
| Asset | -41 | -33 |

The tests presented up to now for hybrid girders concerned when FRP decks were adhesively bonded to the steel girders. Other experimental investigations are performed for hybrid girders having shear stud connections. Some findings from these tests are reported in the following.

Assessment of effective widths of FRP decks connected by shear studs to steel girders in serviceability limit state was done by (Moses *et al.*, 2006). In-situ tests of three bridges composed of steel girders and DuraSpan deck systems were employed to assess the effective widths and the transverse distribution factors of forces. Shear stud connections between the deck and the girders are located in grouted pockets spaced 610 mm along the girders (see Figure 2.41). This discrete nature of shear stud connections rather than continuous (as it is in adhesive bonding) affects the efficiency of the decks to contribute as a top flange of the hybrid girder.

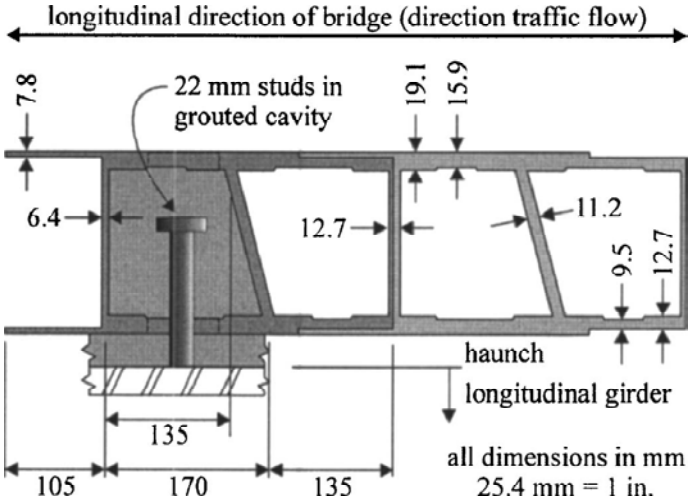


*Figure 2.41 Illustration of shear stud connections between DuraSpan deck and steel girders (Moses et al., 2006)*

The bridges were subjected to different loading cases and strain gages were placed to near mid-span of two shear stud connections to attain the strains. According to the strain records, neutral axes of the girders were determined and in all cases it was observed that the neutral axes were located higher than the girder mid depth.

Afterwards, the effective widths were computed taking into consideration the top and bottom flanges as if they contribute equally to the effective width. Thus, the transverse shear lag phenomenon was not considered in calculations even though not both top and bottom flanges might contribute the same to the effective width. In addition, the effective deck widths were calculated as indicated in AASHTO for a concrete deck having the same depth in order to compare. In general, the effective widths of FRP decks were smaller than comparable concrete decks by approximately 80%. The reduced effective width is due to lower shear stiffness of the deck, non-continuous shear stud connections and shear lag effect of through-deck which reduced the participation of the top flange in the composite action of the deck. Moreover, it was observed that the engaged effective widths in FRP decks show degradation with time, which is most likely due to the reduction in shear transfer efficiency required to develop composite behaviour.

Distribution factors are design tools to determine the maximum expected load each supporting girder might be able to resist given the strength contributions of adjacent superstructure elements. Distribution factor of a girder were computed according to equation (2.1) in the study of (Moses *et al.*, 2006).

$$\boldsymbol{DF_{girder,j}} = \frac{\boldsymbol{strain_j}}{\sum_{\boldsymbol{all\ girders}} \boldsymbol{strains}} \qquad (2.1)$$

where $strain_j$ is the strain in one girder which is divided by the total strain of all girders to compute the load distribution factor of one supporting girder

These factors appeared to be higher than equivalent concrete decks, which mean that the girder closer to the load will carry most of the load in case of FRP deck. The reason is that the transverse stiffness of the FRP decks is lower than concrete decks leading to reduced transverse distribution of wheel loads.

The effective deck width of FRP deck connected by shear studs with steel stringers under service loads is assessed by (Keelor *et al.*, 2004) as well. Basically the same procedure as explained in the previous study was followed. The bridge consisted of steel stringers connected with shear studs with DuraSpan deck. The shear studs had a spacing of 610 mm along the longitudinal distance of the bridge. Strain gages were placed along the girder in the middle between the shear stud connections. The resulted effective deck widths were computed as 75% of the theoretical effective width (which is the total of half widths of the deck between the girders) for the middle girders and 90 % of the total distance composed of half girder spacing plus the overhang distance (see Figure 2.42).

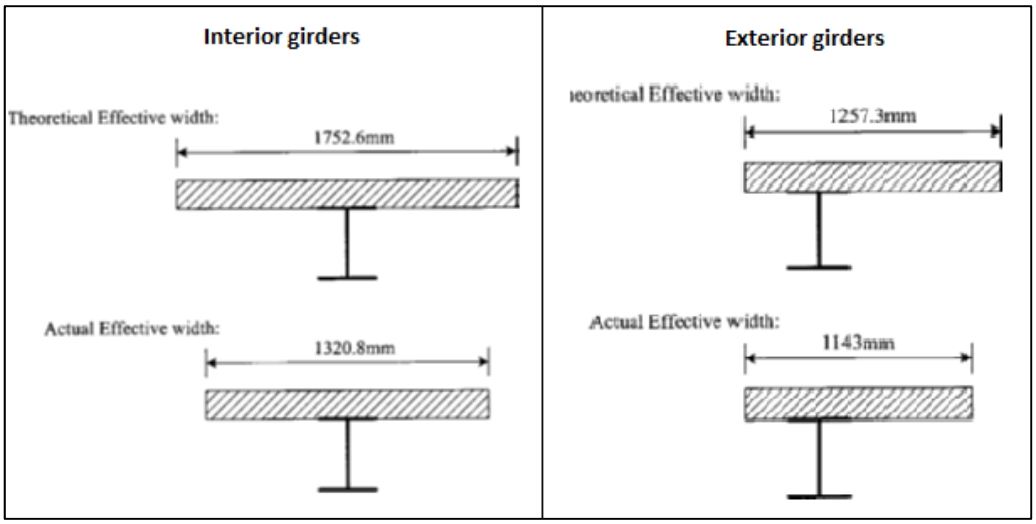


*Figure 2.42 Effective widths of interior and exterior girders at serviceability limit state(Keelor et al., 2004)*

The outcome of these investigations is that the connections between the girders and the steel girders affect the degree of composite action. FRP decks have lower stiffness than comparable concrete decks which leads in reduction of effective width of the FRP deck contributing as top flange to the steel girders and reduced transverse distribution of forces. In addition, not both top and bottom flanges contribute the same to the composite action, but there exists through-deck shear lag effect which reduces the participation of the top flange to the composite action.

### 2.5.4 Tests performed on connections

Several studies are done by researchers on system level connections which are mainly shear studs and adhesive bonding connections.

*Shear stud connection tests*

A study to develop an innovative effective deck to girder connection was done by (Righman, 2002). The criteria of the connection were prevention of the uplift of the deck, ease in installation, cost effective, ease in replacement and structural efficient. Based on these criteria a conceptual design of a connection consisting of welded threaded shear studs housed inside steel sleeves was developed. The sleeves will be installed with the FRP deck. Tests were performed on four modified versions of the main concept of the connection (see Figure 2.43). The fourth connection type is the same as type 1, but the connection is filled with high strength epoxy grout.

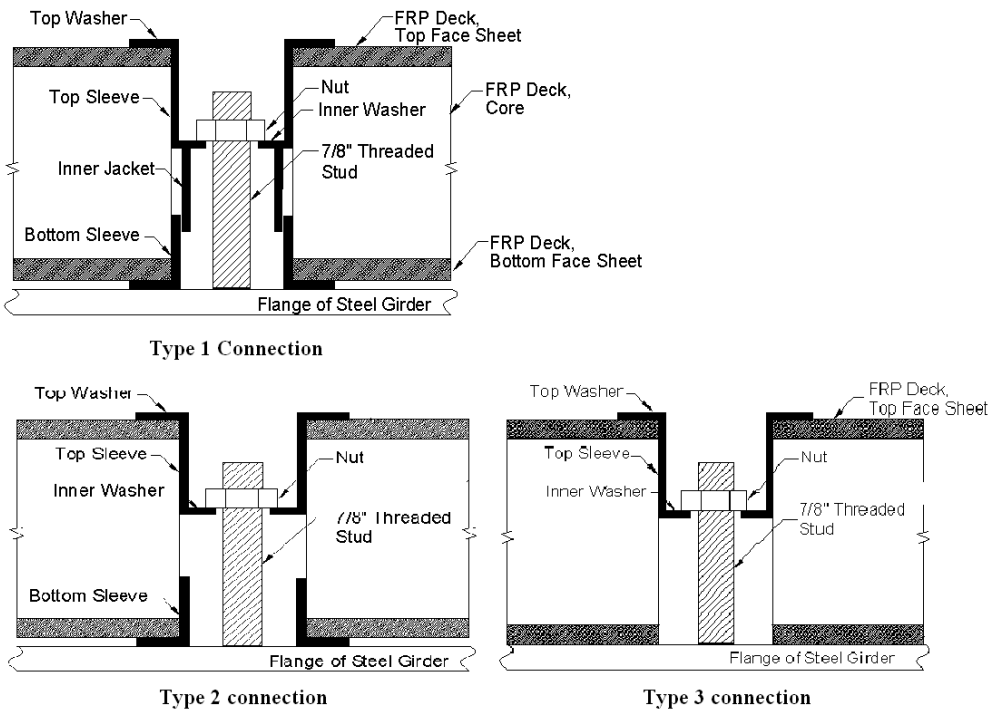


*Figure 2.43 Configuration of FRP deck to girder different type connections developed by (Righman, 2002)*

Static shear strength tests were performed to evaluate the strength of the various types of connections. In Figure 2.44, the load-deflection curves resulting from the test are depicted.

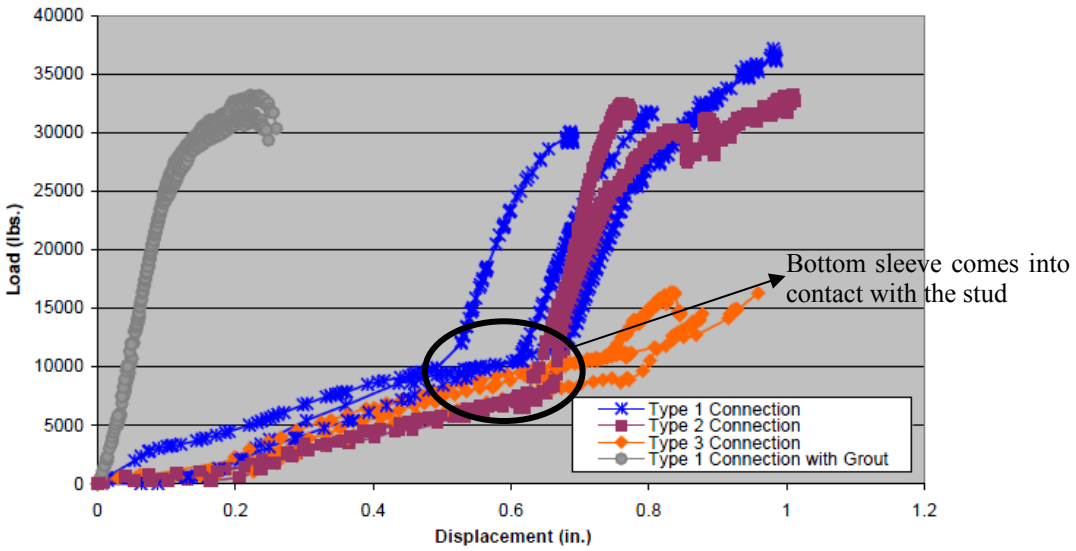


*Figure 2.44 Load - deflection curves for ultimate load connection specimens (Righman, 2002)*

As it can be observed in the figure above, type one and type two connections have an increase in stiffness after a certain displacement of the stud which corresponds to the stud coming into contact with the bottom sleeve. This is not observed in type three since it does not have a bottom sleeve. The connection filled with grout shows a higher stiffness from the beginning because the grout allows uniform loading of the stud. However, the ultimate loads of type one, two and grouted connection are nearly

the same. The failure of the first three types of connections was due to excessive damage of FRP panels, but the failure of the fourth type of connection was due to fracture of the shear stud. In these connection types, the shear force was primarily controlled by the strength of the FRP panels. Therefore, when designing a connection it should be taken care to avoid the bearing failure of the FRP panels.

(Moon *et al.*, 2002) have investigated three concepts of shear stud connections between steel girders and FRP decks. The first two connections consisted of three shear studs welded to the top flange of the supporting girder and housed inside steel sleeves and confined with grout that were installed within holes drilled through the FRP deck. The third type of connections consisted of threaded shear studs containing larger volume of grout (see Figure 2.45). The difference between the first and second connection was the location of the sleeve where in the second case it was placed between the inclined webs. It has to be noted that type 1 connection was tested with a deck having thicker face sheets.

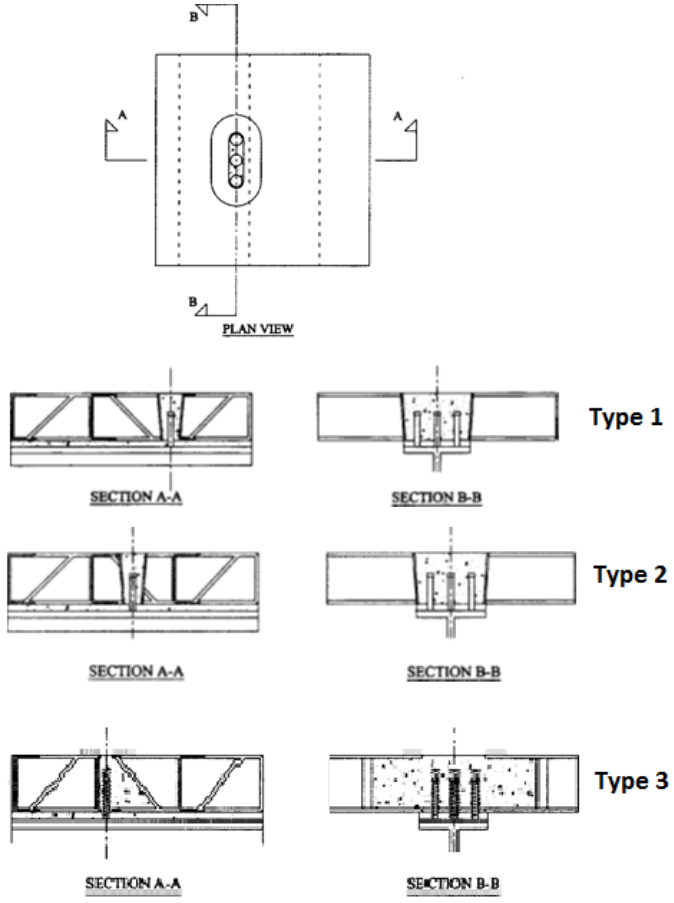


*Figure 2.45 Schematic of three types of connections investigated by (Moon et al., 2002)*

The load deflection curves of the static tests done on these connections are given in Figure 2.46.

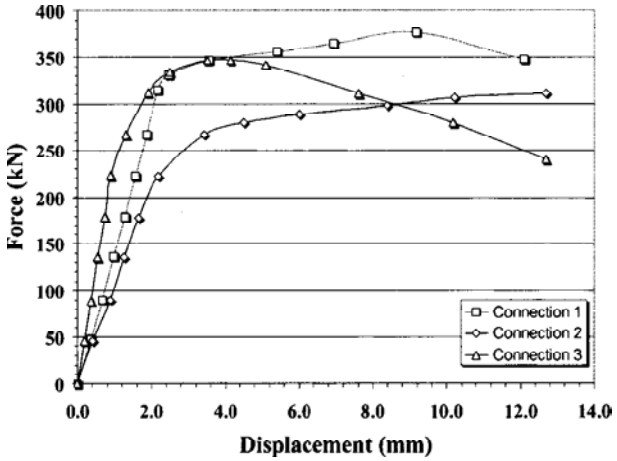


*Figure 2.46 Comparison of load deflection curves of the three types of connections (Moon et al., 2002)*

As observed in Figure 2.46, connection type 1 exhibited the largest strength when the deflection was 11 mm that is when the shear studs started bearing on the bottom flange of the deck. Connection type one exhibited the largest strength and this is because the deck flanges were 35% thicker than the other decks tested with the other connection types. The thickness of the deck flanges contributes to the strength of the connection. Connection types two and three were tested with the same deck and it can be observed that connection type 3 exhibits larger capacity due to higher volume of concrete which helps in decreasing the stress concentrations directly after shear studs. The failure mode of connection type one and two was identical. The confinement of the grout was lost and the shear studs came into contact with the bottom plate of the deck causing bearing failure of the FRP (local crushing). Shear lag effect became significant during loading of connection type 3 whereas the load increased; the top plate was translating more load than the bottom plate. Thereafter, type 3 connections failed due to significant connection rotations which caused delamination in the top face sheet near the bonded parts (see Figure 2.47). Delamination was due to peeling and shear stresses created between FRP plate and concrete occurring during rotation of the connection.

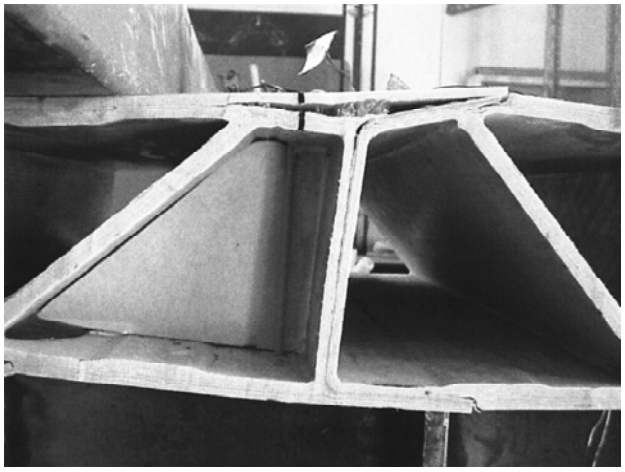

*Figure 2.47 Delamination of the deck near bonded lines of the deck elements (Moon et al., 2002)*

It was observed that 60-70% of the capacity of the shear studs was consumed up to failure (delamination) of the FRP decks. It was a bearing failure of the FRP panels.

*Adhesive bonding tests*

Experiments to investigate the performance of epoxy bonded balanced double-lap and single-lap joints between pultruded GFRP flat sections were performed by (Keller & Vallée, 2005a). The joints were subjected to quasi-static axial tensile loading. It was observed that failure was initiated as a result of combination of peeling tensile stresses and shear stresses. Failure modes were delamination in the outer fibre mat region of FRP coupon and not in the adhesive (see Figure 2.48).

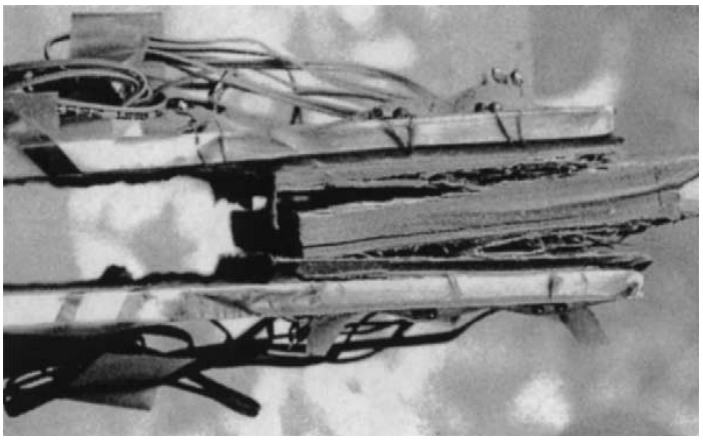

*Figure 2.48 Fibre tear failure of adhesively bonded lap joints (Keller & Vallée, 2005a)*

Through-thickness strength of the adhesive-adherend interface was higher than that of interface between the fibre mats. The adhesive thickness which was changed from 1-3mm had a small influence in the distribution of the stresses.

Furthermore a design method to predict the strength of these joints was developed (Keller & Vallée, 2005b). FRP coupons were tested using a shear-tensile device which allows the measurements of through-thickness tensile stresses and shear strength (see Figure 2.49).

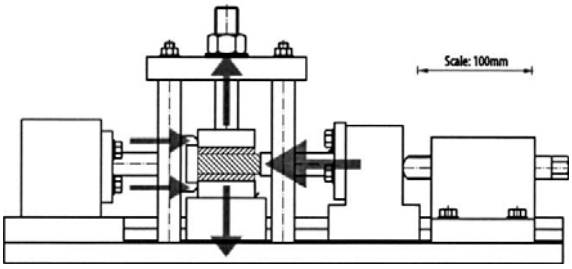


*Figure 2.49 Shear-tensile device used to test the bonded FRP coupons(Keller & Vallée, 2005b)*

The resulting combined through-thickness tensile and shear strength is given in Figure 2.50. The failure mode was the same as the previous tests the classical fibre-tear failure in the outer mats of adherends. The joint strength is principally determined by the low tensile peeling stress of the adherends. Partial material safety factor was calculated as well to be 1.34. It should be noted that the influence of temperature, moisture and fatigue on GFRP joint strength has not been taken into account in this investigation.

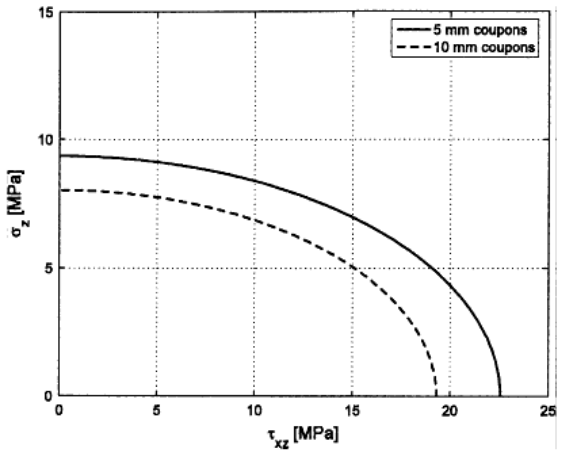


*Figure 2.50 Combined through-thickness tensile and shear strength of 5mm and 10 mm thick FRP coupons(Keller & Vallée, 2005b)*

In tests of adhesively bonded FRP decks (Asset and DuraSpan) to steel girders done by (Keller & Gürtler, 2005b), it was observed that the adhesive bonding was stiff enough to guarantee full composite action between the girder and the bottom face panel of the deck up to failure. Keller et al. observed also that even flexible adhesives in layers up to 50 mm thick gave full composite action between the bottom face panel of FRP decks and steel girders. In these test the adhesives were subjected to just longitudinal shear stresses and these stresses were far below the ultimate stresses at failure. Peeling stresses were absent in this test and the performance of adhesive joints subjected to peeling forces is investigated further by (Keller & Schollmayer, 2009).

Tensile peeling forces in the adhesives develop due to uplift forces created by the load-bearing behaviour in the transverse direction of the bridge (see Figure 2.51).

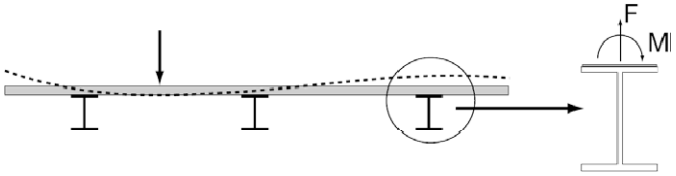


*Figure 2.51 Resulting uplift forces and moments due to load-behaviour of the deck in the transverse direction of the bridge (Keller & Schollmayer, 2009)*

Experimental tests were performed on steel girders adhesively bonded to DuraSpan deck subjecting tensile forces. The experimental test set-up is illustrated in Figure 2.52.

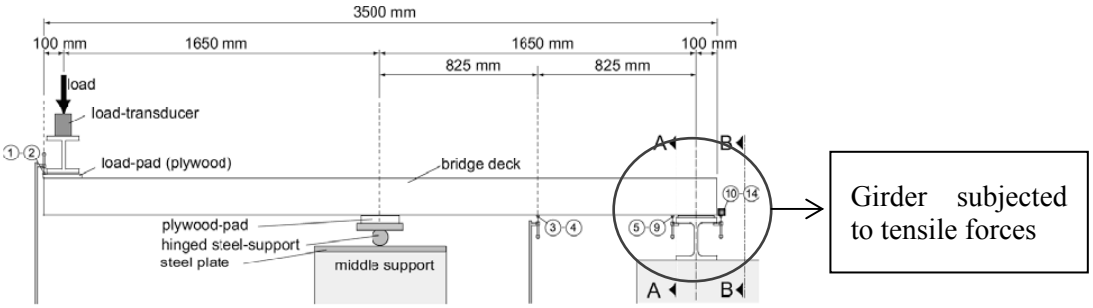


*Figure 2.52 Test set-up of the hybrid girder subjected to tensile forces (Keller & Schollmayer, 2009)*

The girders were loaded up to failure. The failure mode was observed to be fibre-tear failure in the outer mat layers of the deck flanges (see Figure 2.53). This was consistent with the failure modes of the lap joints presented above.

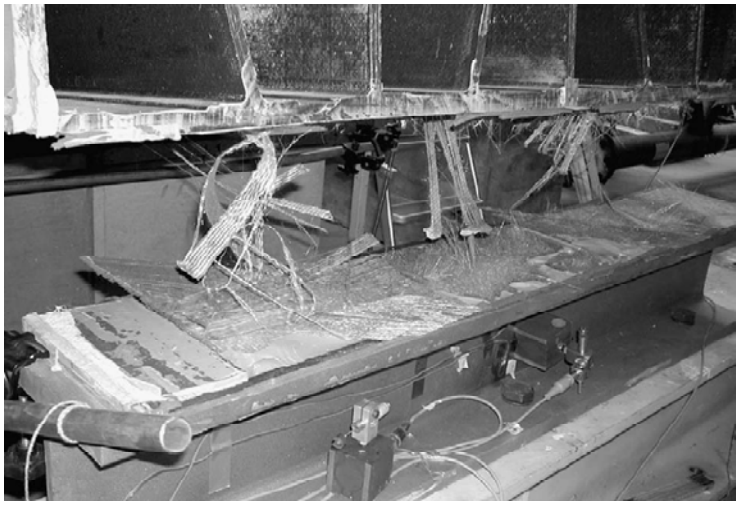

*Figure 2.53 Fibre-tear failure of the outer mat layers of the adhesively bonded FRP deck to steel girders subjected to tensile forces(Keller & Schollmayer, 2009)*

The average failure loads and stresses are presented in the table below.

*Table 2.8 Average experimental results of adhesively bonded deck to girder subjected to tensile forces*

| Property | Mean value |
|---|---|
| Ultimate load [kN] | 176 |
| Crack initiation load [kN] | 119 |
| Average joint uplift stress at failure [MPa] | 0.79 |
| Total safety factor | 5.2 |
| Failure mode | Fibre-tear |

In order to understand the flow of the stress on joints numerical analysis was done from (Keller & Schollmayer, 2009). A portion of deck adhesively bonded to the girders was modelled (see Figure 2.54). It was noted that under vertical and inclined webs there are peak stress concentrations. These stress concentrations are more pronounced under the vertical web (see Figure 2.55). This indicates that the loads are transferred directly from the webs through the adhesive joints to the girders. The average joint uplift stress at failure was determined as 0.79 MPa by the experimental results (see Table 2.8). If this value is multiplied by the stress concentration factors the failure stress is obtained. The stress concentration factors in this case were determined as 12.4 from the numerical analysis results and when this factor is multiplied by 0.79 MPa, joint tensile failure stress is computed as 9.1 MPa. This tensile failure stress corresponds to the tensile failure stress determined in lap joint tests under pure tensile loading (see Figure 2.50).

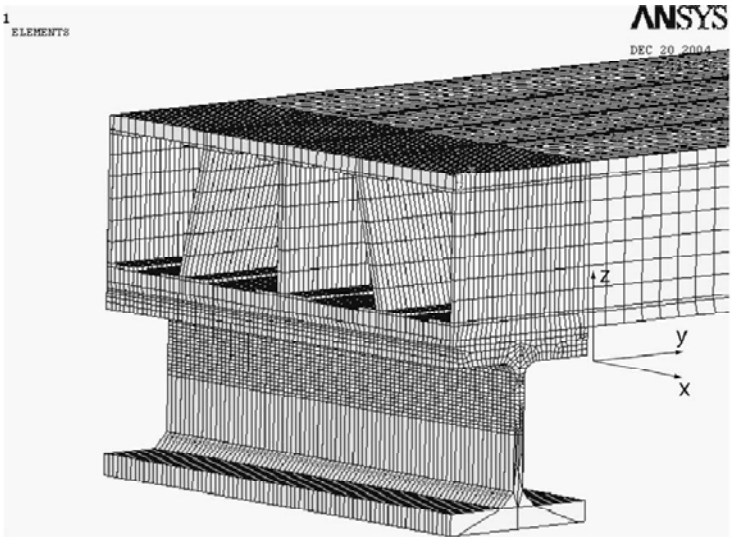


*Figure 2.54 Finite element modelling of deck adhesively connected to steel girder (Keller & Schollmayer, 2009)*

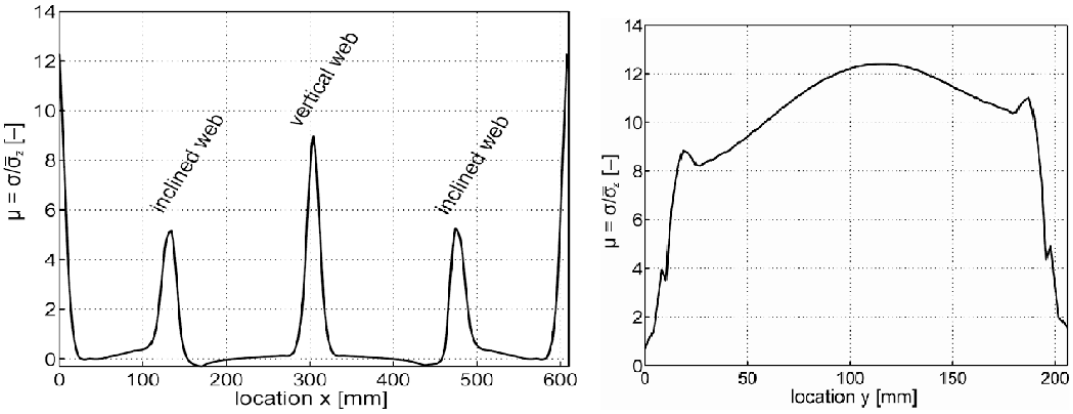


*Figure 2.55 The results of normalized through-thickness tensile stress distribution in the adhesive joints; left: along the longitudinal direction, right: along transverse direction under a vertical web (Keller & Schollmayer, 2009)*

The adhesive joint was tested for fatigue loading up to 10 million cycles during static test analysis as well. No stiffness degradation was observed but the ultimate load was significantly decreased. The deflection response of the hybrid girder subjected to fatigue loading is shown in Figure 2.56.

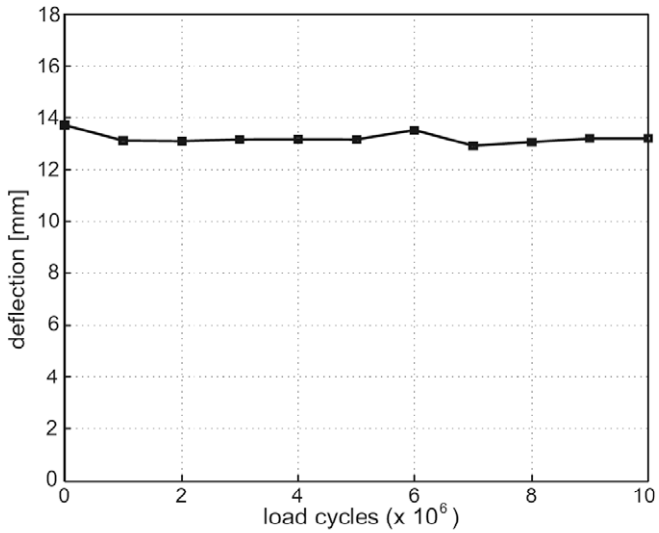


*Figure 2.56 Deflection response of the hybrid DuraSpan-steel girder subjected to 10 million fatigue cycles (Keller & Schollmayer, 2009)*

As it is observed in Figure 2.56, the deflection response is almost linear during the fatigue load cycles which shows that the stiffness is not degraded.

The load-displacement responses of two hybrid girder are depicted in Figure 2.57.

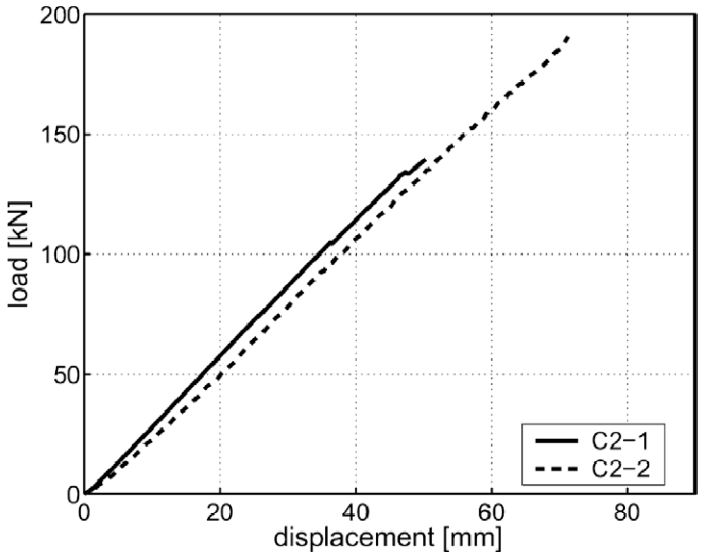


*Figure 2.57 Load-displacement response of two hybrid girders (Keller & Schollmayer, 2009)*

C2-1 hybrid girder was subjected to fatigue loading of 10 million cycles then to static loading and as it can be observed in the figure above, the ultimate load is lower than the other hybrid girder C2-2 which was subjected to just static loading.

The investigations show that in case of shear stud connections mainly bearing failure of FRP plates take place. This also leads to the strength of the connection being dependent on the thickness of FRP plates. When the deck is adhesively bonded to the girders fibre tear failure mode is observed due to low through-thickness strength of FRP plates. Moreover, stress concentrations are attained under the webs.

### 2.5.5 Other tests performed on FRP decks

An experimental test was done to survey the feasibility, constructability of FRP decks on steel stringers as supports by (Majumdar *et al.*, 2009). The deck was manufactured by Strongwell Corporation which is composed of adhesively bonded square tubes and top and bottom plates (see Figure 2.58).

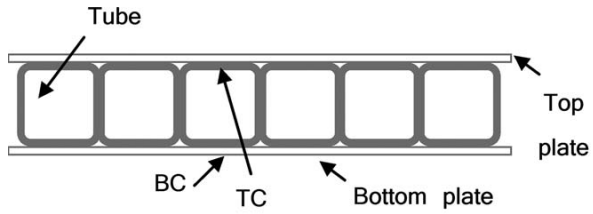


*Figure 2.58 Cross-section of Strongwell FRP deck (Majumdar et al., 2009)*

The test was done on a two-bay bridge having six wide flange stringers (see Figure 2.59).

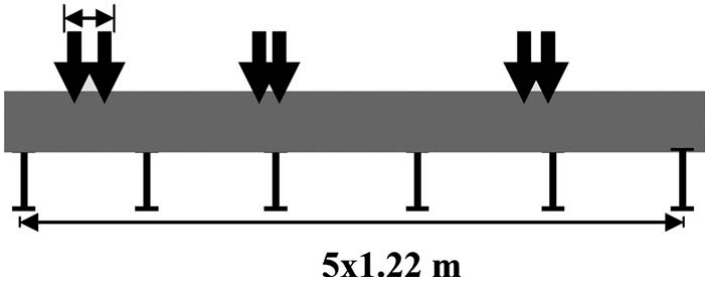


*Figure 2.59 Elevation of the bridge (Majumdar et al., 2009)*

The connection between the deck and the stringers was designed to have no composite action. Loading was done by simulating a tire patch load instead of using steel plates, since the steel plates might not represent the actual stress contour as was verified by a study of (Majumdar *et al.*, 2007). In case of steel plates stress concentrations are observed around the edges of the steel plates. On the other hand, the contact pressure of the tire patch load is non-uniform and concentrated in the middle of the contact area. Thus, it was concluded that the tests should be conducted with simulated tire patch instead of steel plates to get a better performance evaluation of the deck.

After loading the simulated bridge under service loads, there was no indication of damage in the FRP deck. The response was linear and the deflections were small. The load distribution factors were checked as well and it was observed that the deck had sufficient stiffness to distribute the load to all the stringers. Then the deck was loaded until initiation of failure and it was observed that local failure due to patch loading at the top plate and top flange of the tube occurred (see Figure 2.60). The failure load was 4.5 times greater than the service load.

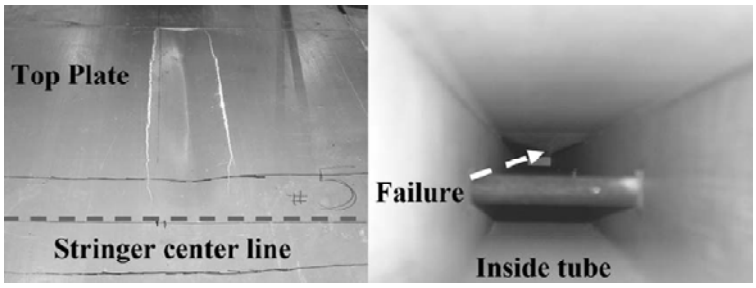


*Figure 2.60 Local failure of the deck due to patch loading of the tire (Majumdar et al., 2009)*

The deflections and strains were higher in the top plate. Furthermore, the strains in the pultrusion direction are higher than the ones in the transverse direction, due to principally uni-directional load carrying behaviour (see Figure 2.61).

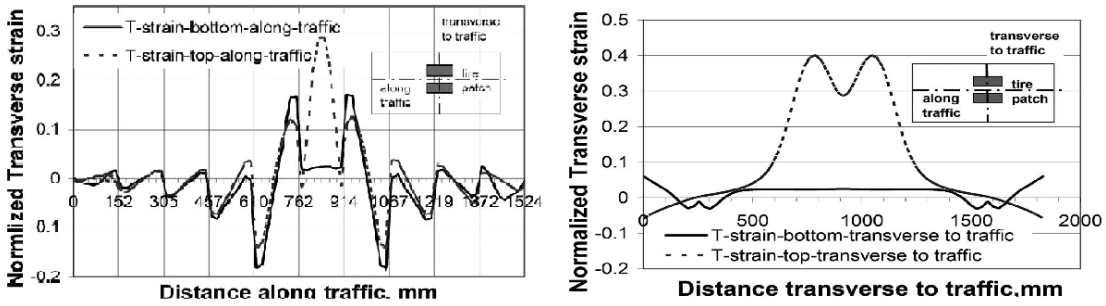


*Figure 2.61 Strains of top and bottom plates under service load in the direction perpendicular to the pultrusion left and parallel to the pultrusion right*

Another investigation of the failure modes and mechanisms under patch loading simulated by steel patch and truck tire patch was done by (Zhou *et al.*). The investigation was performed in laboratory on Strongwell deck panels (see Figure 2.62).

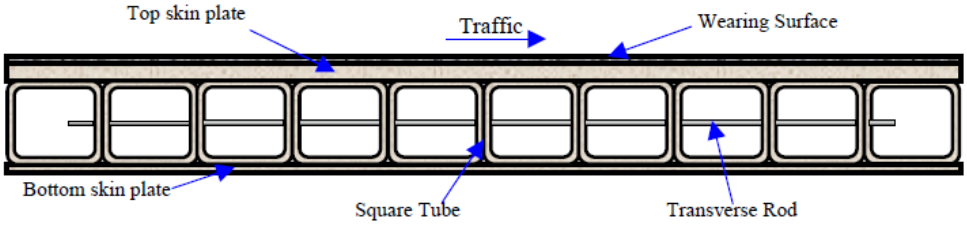


*Figure 2.62 Cross-section of Strongwell deck system (Zhou et al.)*

Transverse rods as seen in Figure 2.62 were mainly used for fabrication purpose.

It was observed that the failure modes were different for the different load patches. The failure mode when using steel patch is punching mode (see Figure 2.63). The failure mechanism was the initiation of a shearing crack from underneath the loading patch and the propagation of the crack up to failure.

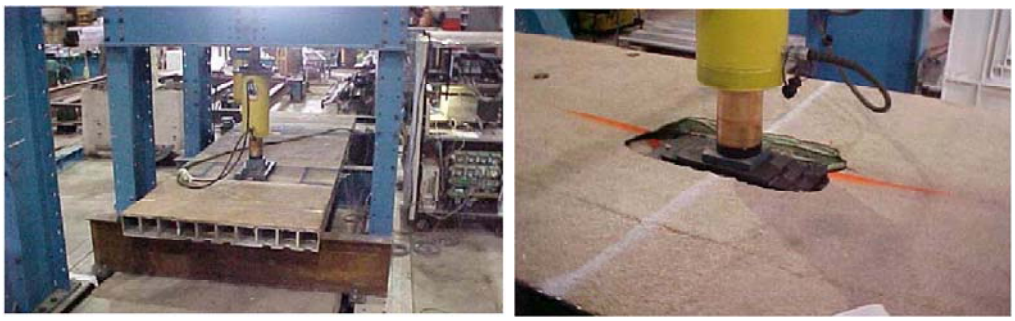

*Figure 2.63 The punching failure mode of FRP deck under steel patch loading (Zhou et al.)*

The failure mode when using tire patch is bending failure of the top plate as indicated in Figure 2.64.

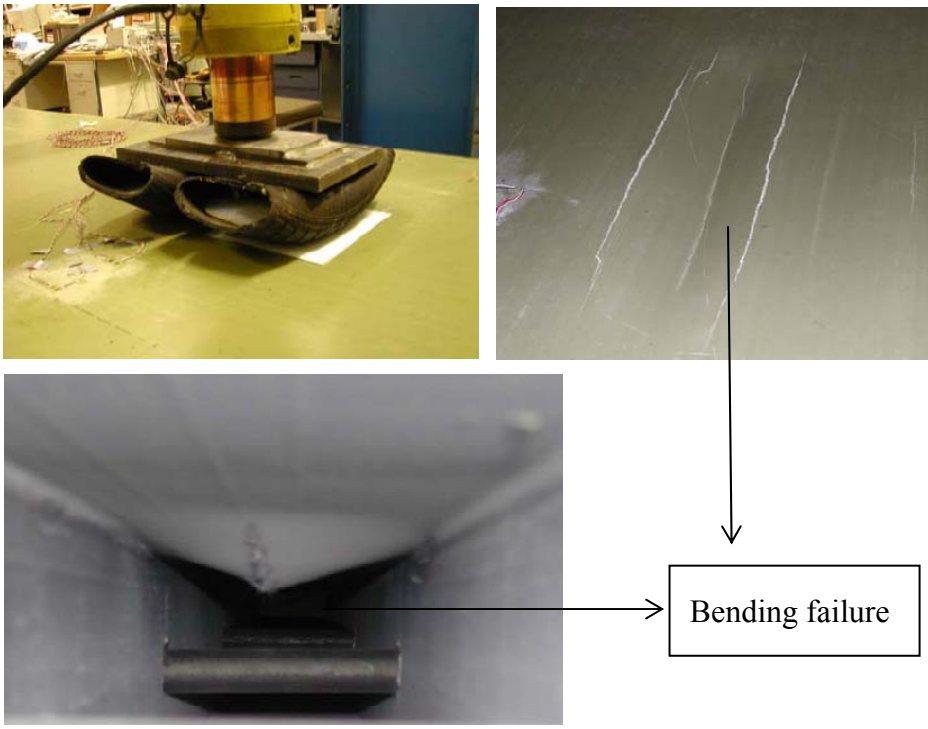


*Figure 2.64 Bending failure mode when the deck is loaded with simulated tire patch (Zhou et al.)*

Thus, the loading way can lead to different failure loads. Moreover, the ultimate strength using tire patch was higher (10% and 28%) than the ultimate strength using steel patch.

### 2.5.6 Fatigue behaviour

Generally, FRP decks have shown satisfying results under fatigue loading. In experimental fatigue tests performed by Keller et. al no significant degradation or damage in the deck has been observed (Keller & Gürtler, 2005b). The experiments were performed on adhesively bonded FRP deck (DuraSpan and Asset) to steel girders and loaded up to 10 million cycles which corresponds to the design life of 75 years. No degradation or damage of the adhesive bond was observed either (Keller & Gürtler, 2005a). However, it is stated that long term fatigue loading behaviour of the adhesive bond must be further researched.

Conversely, degradation of the stiffness on FRP decks has been observed in some other tests performed by (Brown & Berman, 2010). Two different deck types were tested (see Figure 2.65). Deck A was composed of adhesively bonded tubes sandwiched by adhesively bonded top and bottom plates and deck B had a bottom section consisting of I-profiles and a mechanically connected top plate. Different connections of these decks to steel girders were utilized (see Figure 2.66). The spacing between the connections in deck A was 1.8 m and in deck B 0.36m.

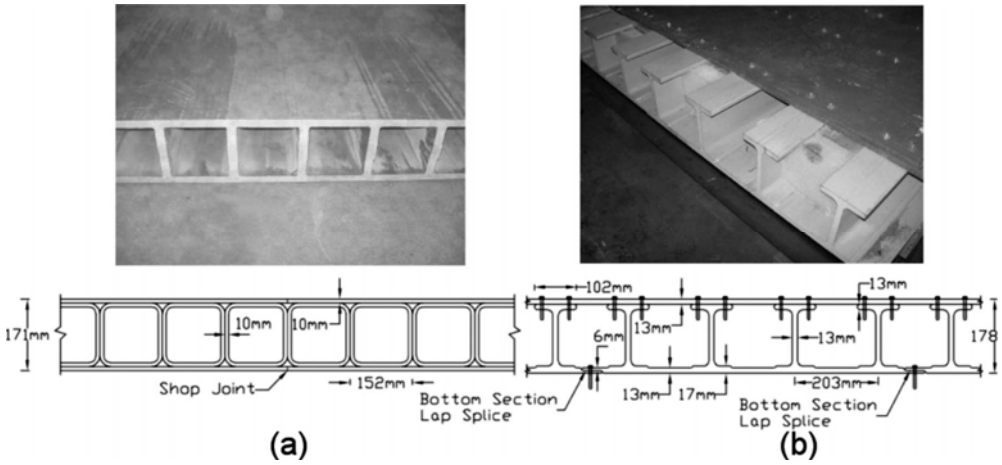


*Figure 2.65 Deck types a) Deck A b) Deck B tested for fatigue evaluation by (Brown & Berman, 2010)*

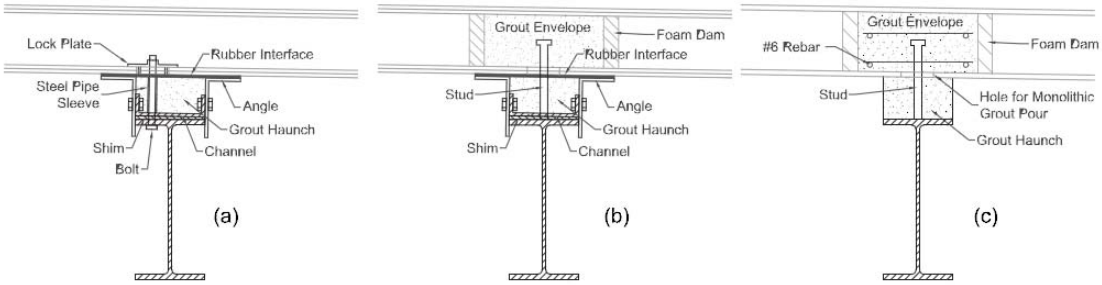


*Figure 2.66 Deck to girder connections: a) Bolt and lock plate used for deck A b) Shear stud used for deck A c) Shear studs used for deck B (Brown & Berman, 2010)*

These decks were loaded up to 2 million cycles. Degradation of the stiffness in both decks, more pronounced in deck A, during fatigue loading was observed. The higher degradation of deck A was due to failure of the shop joint (panel level connections) during loading, the scarceness and flexibility of system level connections and imperfections at the adhesive joints between the deck panels. Deck type B showed less degradation of stiffness which might be due to bearing deformations of the screwed connection of the upper panel. Some degradation of the composite action between the girders and the decks was detected by comparing the location of the neutral axis. However, in laboratory tests done by Keller et al. of adhesively bonded FRP deck to steel girders no degradation of composite action was detected. In other tests performed by (Moon *et al.*, 2002), negligible degradation of the shear stud connections of FRP deck to steel girders was observed when they were fatigued for 10.5 million cycles. Therefore, if the system level connections are done properly they behave well under fatigue loading.

In case of composite bridges when replacing the concrete deck by a FRP deck particular care must be taken if there are fatigue prone details. The lighter FRP deck will likely result in lower total stresses in the supporting girders, but due to the reduced composite action and effective width and increased distribution factors, the live load induced stress range is likely to be increased. This was studied by (Harries & J.Moses, 2007) and it was observed some increase in live load stress range. The increased transient stress range must be considered if there are prone fatigue details in the bridge. Thus, existing fatigue-prone details may become a concern and require additional attention in the design.

A fatigue testing under extremely high (50$^{o}$C) and low temperatures (-30$^{o}$C) was performed to evaluate the FRP deck performance by (Dutta *et al.*, 2003). Degradation of the stiffness of FRP deck following 10 million cycles under the two extreme temperatures was observed. The degradation of the stiffness of the FRP decks is believed to be more affected by the extreme temperature levels. The decks are affected more by the high temperatures. The degradation of stiffness in low temperature was not as significant as in high temperature.

### 2.5.7 Thermal behaviour of FRP composites

A large concern in the application of FRP materials is the possibility of accidental fire. FRP composites show lower heat resistance compared to conventional materials. All thermal and mechanical properties of FRP composites are dependent on the temperature. The deterioration of the properties in elevated temperature depends on the fibre and resin type of FRP composites. In case of fire incident on FRP bridge decks, the degradation of the strength and stiffness of the deck is experienced in early stages (Alnahhal *et al.*, 2006). In Figure 2.67, it can be noticed that the stiffness degradation of FRP is higher and earlier compared to steel.

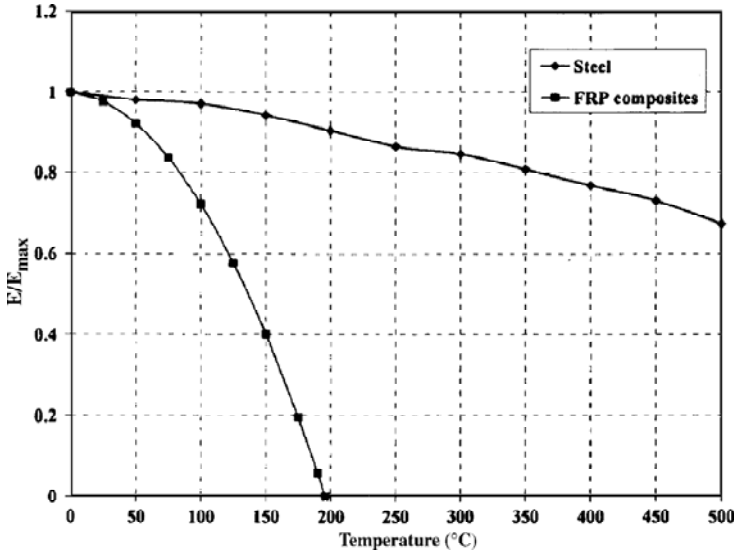


*Figure 2.67 The stiffness degradation of FRP and steel in elevated temperatures(Alnahhal et al., 2006)*

In case of rapid temperature changes in the surfaces of FRP decks, thermal gradients will occur between the top and the bottom of the deck causing internal thermal stresses. The hollow portions of the deck in case of hollow FRP deck profiles are not

able to dissipate the heat from the top surface to the bottom as effectively as concrete decks. Thus, these thermal induced stresses have to be considered in the design.

When FRP materials are exposed to low temperatures the resin shrinks relative to the fibres arising residual stresses in the material microstructure. This can cause micro cracking which contributes to the material stiffness degradation and increasing permeability and water ingress through the fibre/resin interface (NCHRP). However, the induced stresses are of concern in extreme cold environments.

### 2.5.8 Durability and other load effects of FRP decks

FRP decks have high tensile strength compared to conventional materials such as steel or concrete and they are unlikely to fail or be damaged due to purely bending stresses. However, FRP deck components such as face sheet are relatively weak under directly applied loads. Therefore, when high load per unit area (punch load) is applied directly to the FRP deck, punching type failure of the deck surfaces occurs.

FRP composites are prone to creep. Creep comes from the visco-elastic behaviour of the polymer resin and very little form the glass fibre reinforcements. Creep would exist mainly in high sustained shear and compression loads. Creep levels are higher in high temperatures or FRP submerged in liquid other than air. However, in creep tests performed in hybrid FRP deck-steel girders creep was not decisive for the design (Gurtler, 2004). The creep tests lasted for four hours and after unloading the hybrid girder turned to the initial state (see Figure 2.68). Creep deformations appear the first hours after loading, but more creep tests under long-term loading has to be executed.

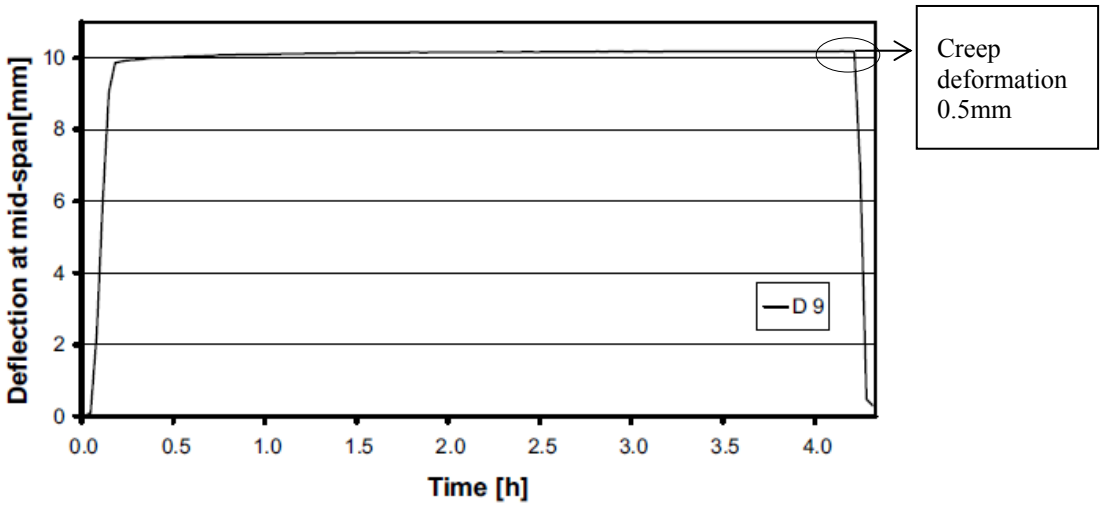


*Figure 2.68 Creep deformation of FRP-steel composite girder under 4 hours of loading (Gurtler, 2004)*

There exists some impact of moisture in the structural performance of the FRP pultruded decks. There is a reduction in the strength of the material rather than the stiffness (Smith, 2001b).

Fibre reinforced composites are sensitive to ultraviolet rays, but UV inhibitors are added to the constituent materials to improve the resistance to UV.

Freeze-thaw cycles have little effect on FRP decks because of the low void content of the material. However, severe freeze-thaw cycles can cause micro cracks which can grow and lead to the degradation of stiffness of the FRP deck (NCHRP).

## 2.6 Deflection/design criteria of FRP decks

Owing to the relatively low E-modulus of glass fibre composites, the design of FRP decks is more often governed by stiffness requirements rather than by strength of the deck. This does not allow the designer to exploit the full strength of fibre reinforced polymer decks. In general, the live load deflection criteria (serviceability limit state) govern the design. The deflection limit of L/800 has been adopted in the design of many bridges with FRP decks. However, some researchers have argued that a direct application of this limit is not recommended without understanding the dynamic response of the component. A deflection limit of L/400 has been suggested by some researchers. In any case, since FRP deck bridges show distinct dynamic characteristics from their concrete deck counterparts, any proper deflection limit should be derived based on suitable tolerances for deflection under static loads as well as dynamic motion due to vehicular traffic. Currently, there is no established standard or design guideline for FRP decks. This is the reason that the researchers try to adopt a deflection limit and to come up with the best one.

Strain limit state for structural FRP application, under flexure of service loads, is usually proposed to be kept 20% of the ultimate strain. However, when comparing the allowable span of the deck, deflection limit state governs the design, not strain limit state.

The response of the FRP decks has been observed to be linear elastic under service load conditions with no damage initiation. FRP decks usually exhibit adequate strength with high factors of safety for ultimate limit design. Test results have shown that the governing type of failure of the pultruded modular FRP decks is the delamination of the web from the face sheets when subjected to wheel loads. Delamination is typically classified as a separation of plies within the face sheet laminate (see Figure 2.69).

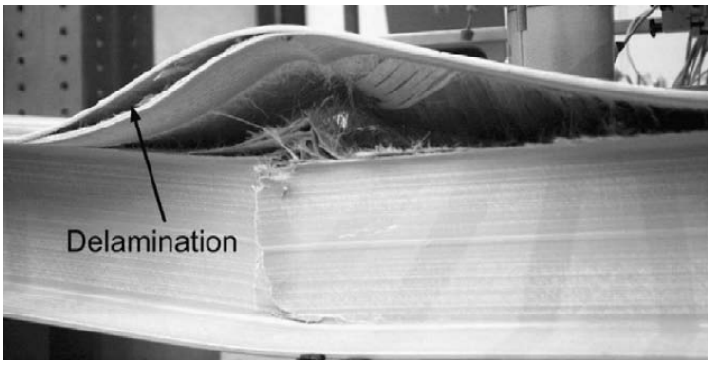


*Figure 2.69 Delamination in the face layer of FRP bridge deck (Bai et al., 2009)*

Safety factors to incorporate any loss of strength and stiffness of the deck during service life are not yet established. Some of the impacts that should be considered in the determination of these factors are moisture effects, sustained stresses, aging, creep effects. Research is going on to determine these factors by employing long term experimental tests.

## 2.7 Environmental impact and cost efficiency

The energy consumption to produce pultruded FRP profiles is lower than the energy consumption of manufacturing with conventional materials. A study is done by Fiberline Inc. and a comparison of the energy consumption for different materials is provided (see Figure 2.70).

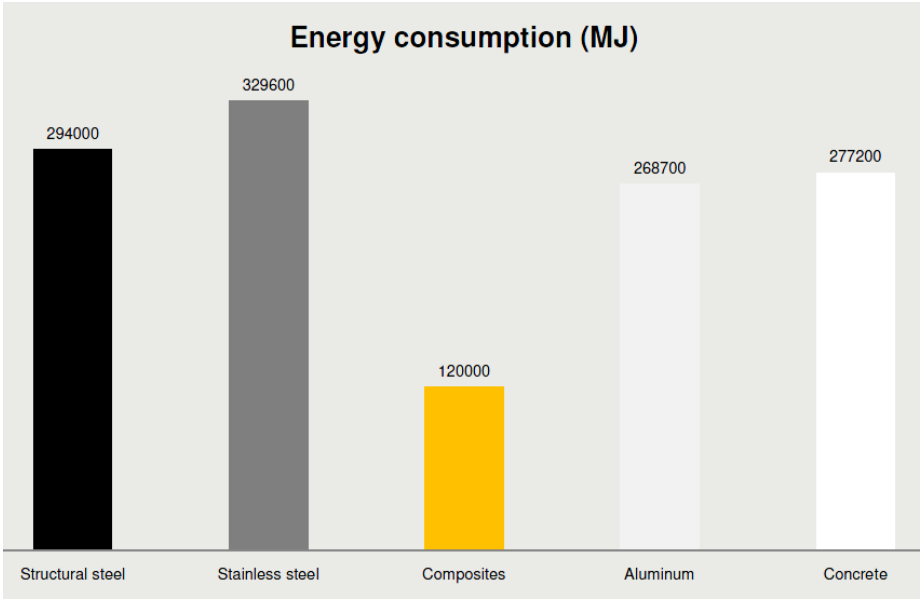


*Figure 2.70 Comparison of energy consumption in manufacturing different materials (courtesy of Fiberline Inc.)*

As it can be observed in the figure above the energy consumption of composites is much lower compared to the other materials.

Recycling of the composites is possible as well. The composites can be crushed and granulated. The granulated material can be used as filler and to a limited level as a reinforcing material. Composite material release high amounts of energy in controlled incineration which makes them energy carriers for heating or electricity. The remains after incineration are glass fibres which can be used further for manufacturing glass wool or as landfills. More research is going on to discover an enhanced solution in recycling composite materials.

The cost of FRP decks is higher compared to decks made of conventional materials. In Figure 2.71, upper and lower cost estimate of FRP decks for different spans compared to the costs of concrete and steel decks is depicted. It is observed that the cost of FRP decks is higher.

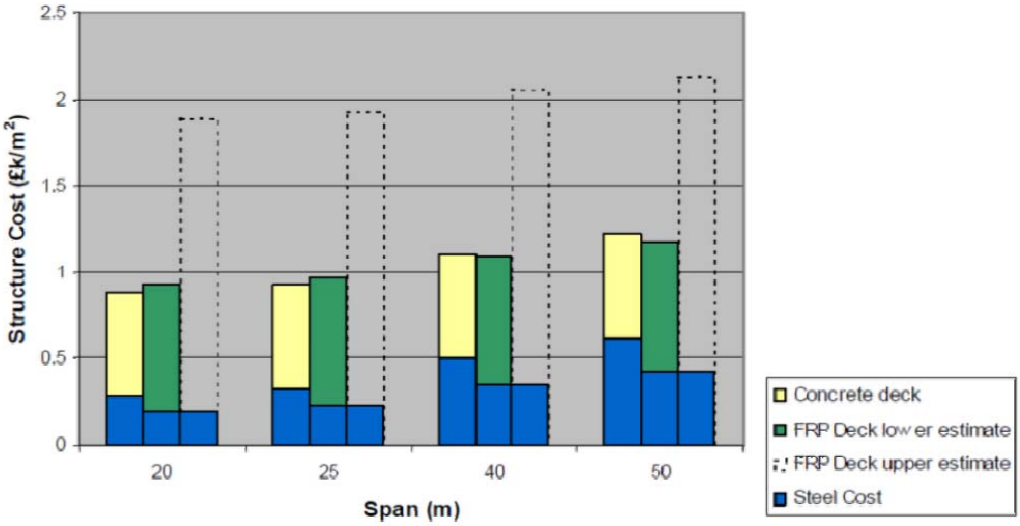


*Figure 2.71 Cost comparison of decks made of FRP, concrete and steel for different spans (courtesy of Fiberline)*

The high material cost of FRP decks limits the application of these decks. However when considering the savings during construction of these FRP decks, actually the cost gets lower. Extra material costs versus savings during construction for a 6 meter wide bridge with different spans is illustrated in Figure 2.72.

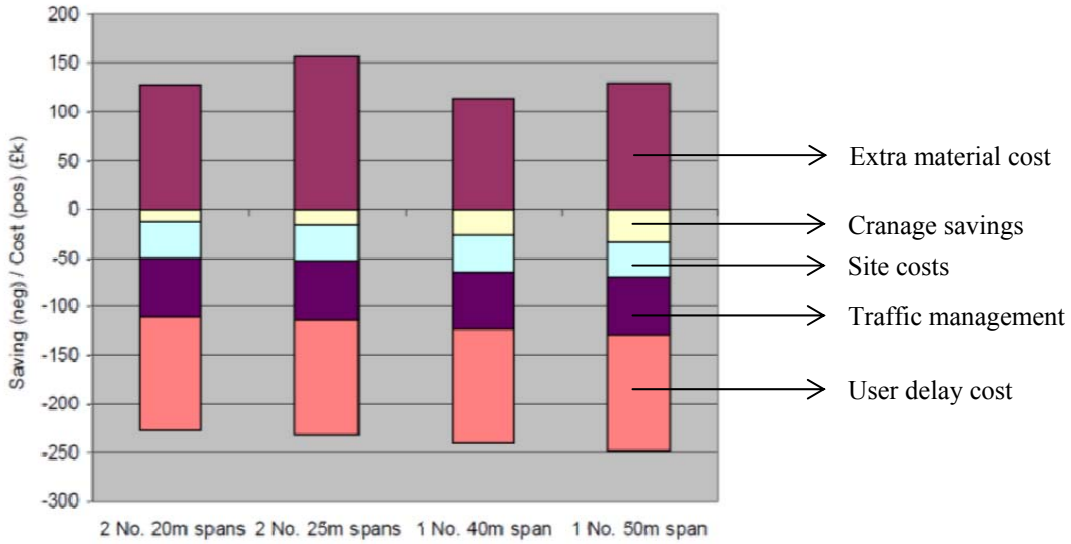


*Figure 2.72 Extra costs versus savings for a 6 m wide bridge (courtesy of Fiberline)*

Installation of FRP decks is done under a very short time compared to traditional decks which leads to a lot of savings considering different aspects such as construction equipment costs, site costs, traffic management and user delay costs. Therefore, in all of the cases presented in Figure 2.72, savings dominate. In addition, life cycle costs of FRP decks are competitive to traditional materials because the service life is greater with minor maintenance.

## 2.8 Alternative deck systems

One of the main issues in the design of FRP decks is to attain composite action with the girders. Apart from the connections, if the stiffness of the FRP decks is higher enhanced composite action between the deck and the girders can be attained. To make the best use of the materials in order to increase the stiffness of the deck, combinations of FRP and conventional materials have been researched. Hybrid construction of FRP composites with concrete is one of the most researched deck systems.

A hybrid deck system was proposed by (Alnahhal *et al.*, 2008), which consists of trapezoidal cell units with a thin layer of concrete on the compression zone of the section surrounded by a shell forming an integral bridge deck (see Figure 2.73). The concrete layer enhances the stiffness of the deck and reduced the local deformations under concentrated loads. This deck type was tested by connecting the deck panels to steel girders with shear connection. It was expected to have composite behaviour even though no full composite behaviour was developed. Overall, the deck satisfied the stiffness and strength limits.

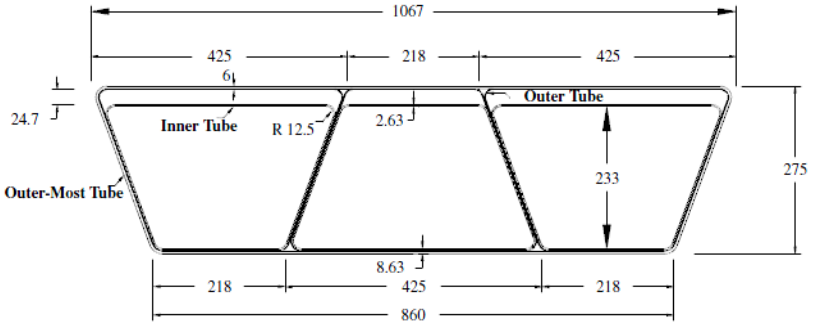


*Figure 2.73 Cross-section of hybrid FRP–concrete deck developed by (Alnahhal & Aref, 2008)*

Another developed deck type is GFRP-steel hybrid honeycomb sandwich concept (Lombardi & Liu, 2011). To increase the stiffness of the GFRP honeycomb sandwich deck incorporation of steel in the core was suggested. Thus the existing GFRP reinforced sinusoidal honeycomb core was replaced with an over-expanded hexagonal honeycomb constructed with steel roof deck (see Figure 2.74). This deck type was tested and it resulted that the stiffness of the deck in the longitudinal direction had a significant increase in both flexural and shear stiffness. In the transverse direction the flexural stiffness was about the same with the GFRP sandwich deck but the shear stiffness was increased.

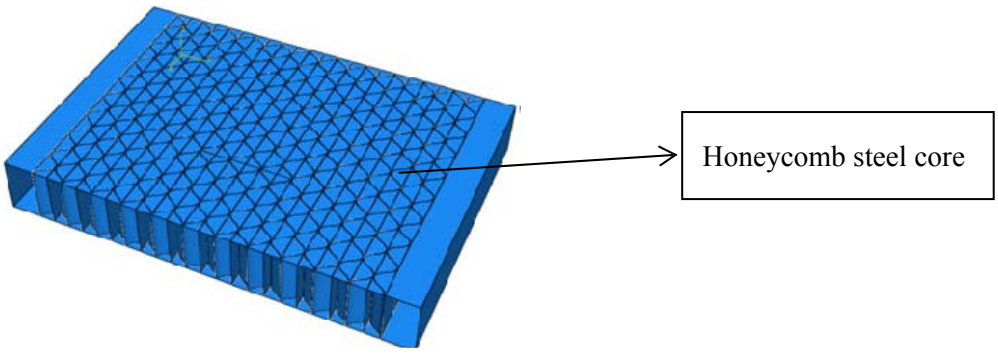


*Figure 2.74 Sandwich deck system with steel core (Lombardi & Liu, 2011)*

A deck composed by pultruded square hollow glass and carbon FRP tubes was investigated by (Kumar *et al.*, 2004). This deck is supposed to act as a beam as well. This tubes were adhesively bonded together to form a deck of four identical I-beams running along the length of the bridge (see Figure 2.75). This deck type was tested for fatigue and strength. It indicated very good performance considering the strength and deflection limits. The deck behaved well under fatigue testing and no degradation of stiffness resulted after 2 million cycles.

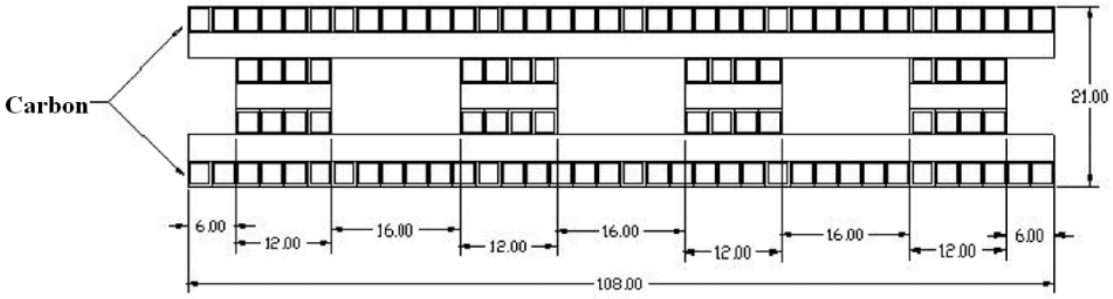


*Figure 2.75 Schematic side view of the bridge deck investigated by (Kumar et al., 2004)*

3-D FRP sandwich panels are introduced by (Hassan *et al.*). In order to overcome the delamination problems between the core and the layer and increase the shear stiffness and strength, through-thickness fibres are added to the core. These fibres connect the top and bottom GFRP layers using weaving or injection technology, thus delaying delamination-type failure (see Figure 2.76).

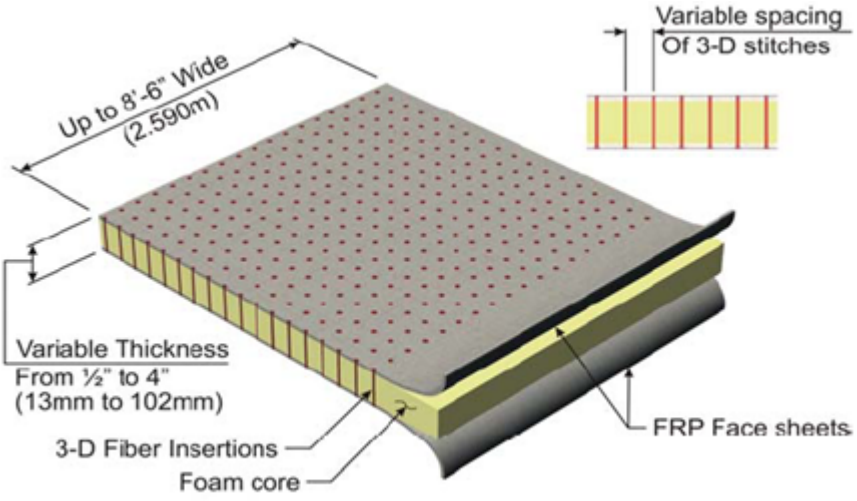


*Figure 2.76 Schematic of 3-D sandwich panels(Hassan et al.)*

Test results have shown that the strength and stiffness of the core is increased by increasing the number of fibres and in some cases the failure type is shear failure instead of delamination.

## 2.9 Installation and construction

FRP composite bridge decks are faster and easier to install than conventional bridge decks. The standard procedures that need to be implemented are:

- Pre-fabrication
- Assembly
- Connections
- Application of wearing surface

The factors that must be considered in the pre-fabrication step are manufacturing, erection, shipping and handling. The manufacturer together with the deck panels should provide an installation guide including connection details (deck-to-deck, deck-to-girder) since there is a lack of guidelines written about the installation of FRP decks. FRP deck panels are pre- fabricated to maximum deck dimensions that make possible the shipping.

The assembly time depends a lot on the experience of the contractor. A significant care must be put during the assembly of the deck panels in order to prevent cracks that might affect the performance of the deck afterwards.

As it is mentioned in the joining technique section, panel level connections are done adhesively or by mechanical shear keys. The connection type between the deck panels is described by the manufacturer which is based on the project requirements as well. Adhesive connection is the most common panel level connection which is done by applying epoxy adhesive in the tongue or groove faces of the deck panels. In general, the installation steps of adhesively bonded deck panels include: preparing of the surfaces of the joining faces, application of the adhesive in one of the faces, pressing the decks together to smear the adhesive and finally letting the adhesive to cure. In Figure 2.77, some panel level connections used by the manufacturers are illustrated. The first joint is a butt joint with shear splice plate strips and the other two connections are tongue and groove connections with different configurations. In the butt joint the adhesive is applied to the faces of the deck panel and then the splice plate strips are bonded to the top and bottom of the decks. Self-tapping screws are used to keep the splice strips in place while the adhesive is cured.

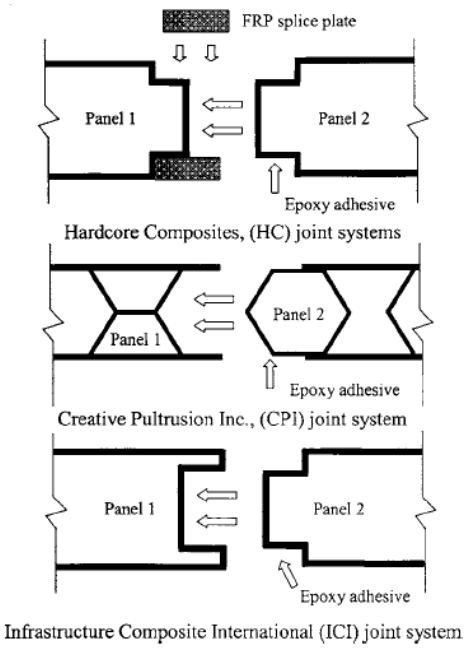


*Figure 2.77 Panel level connections (PLC) used by manufacturers (based on (Hong & Hastak, 2006))*

System level connections (deck to girder connections) can be mechanical or by adhesive bonding. In case of shear stud connections, the decks are pre-fabricated with pockets to receive steel shear studs (see Figure 2.78). One or more studs are required per connection pocket. Shear studs are welded to the steel girders and then usually non-shrink grout is poured to fill the joint (see Figure 2.79 and Figure 2.80).

In order to achieve the desired slope of the deck (in case of pultruded deck) and take up the irregularities between the girders and the deck, a haunch is built up by flowing grout between the top of the steel girder and the bottom of the deck (see Figure 2.79).

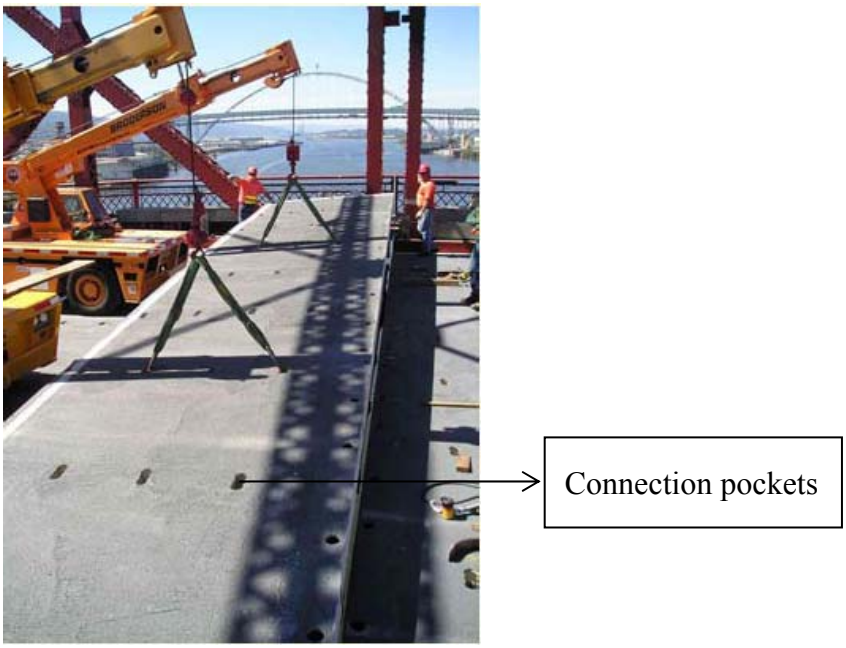


*Figure 2.78 Installation of an FRP deck panel in-site*

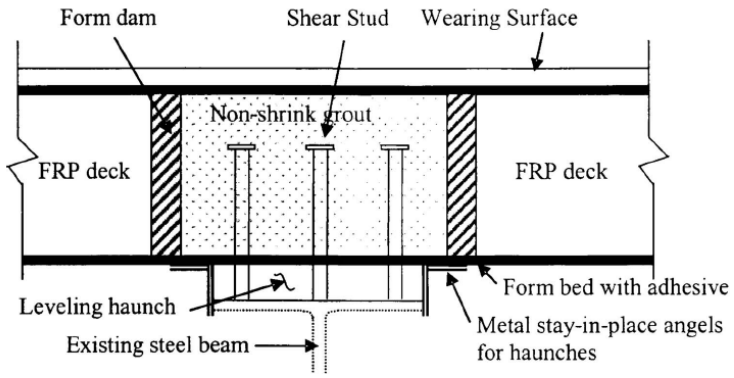


*Figure 2.79 Deck to girder connection by shear studs (Hong & Hastak, 2006)*

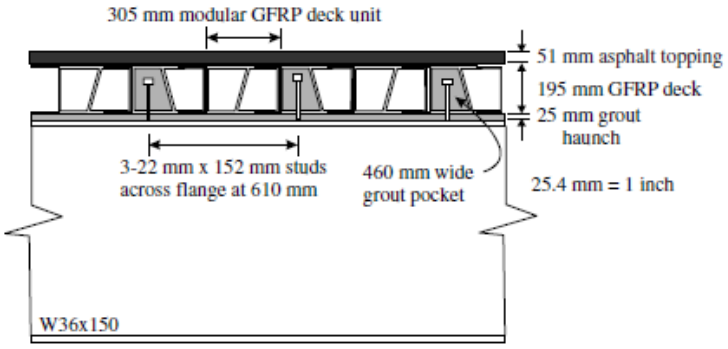


*Figure 2.80 A typical deck cross-section showing shear stud connection, haunch and grout pockets (Turner et al., 2004)*

The wearing surface is provided at the manufacturing site or at the construction site. It is predominantly bituminous material (asphalt) or polymer concrete, followed by epoxy overlay and latex modified concrete. The application of the wearing surface in the site should not be in the atmospheric temperature below 10$^{o}$C, or under wet conditions. The deck surface should be prepared by removing excess resin coat before applying the wearing surface.

The guardrails, pedestrian walkways and curbs of the bridge are installed directly on top of the FRP decks, or attached to an existing structure which is adjacent or connected to FRP decks. The curbs may be prefabricated concrete or concrete filled FRP delivered to site or may be constructed directly onto the deck, for example, cast in place concrete. In general the curbs are anchored into the deck with studs or reinforcement bars (see Figure 2.81). When the curb and railings are attached to independent superstructure components or fascia girders the lateral loads being applied to the FRP decks are eliminated. Another case is when the curbs are built typically on FRP decks but the railings are connected to fascia girders (see Figure 2.82).

*Figure 2.81 Reinforcing anchor details for cast in place curb(NCHRP)*

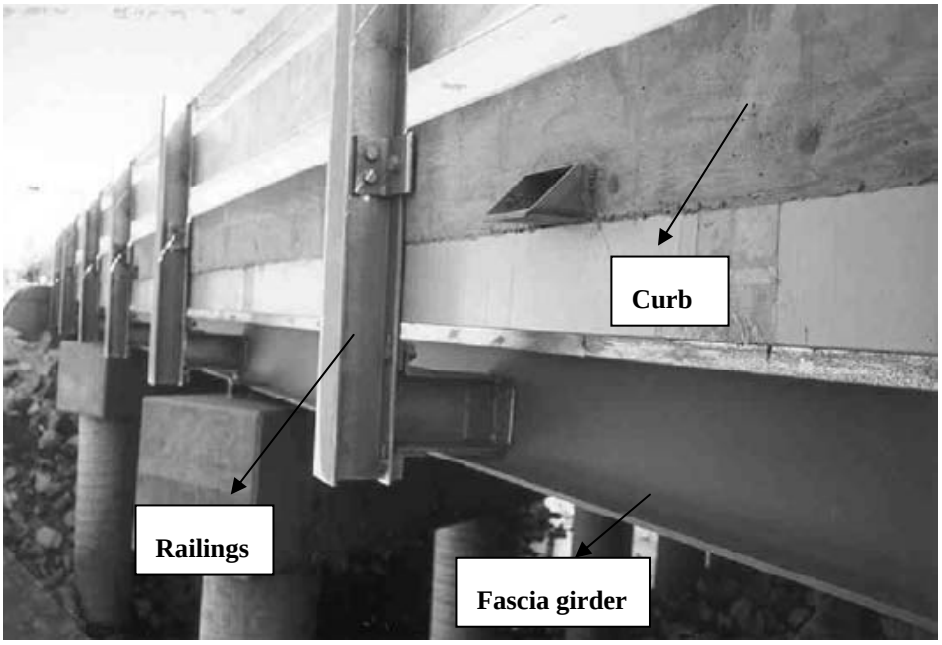


*Figure 2.82 Railings connected to the fascia girders and the curbs built on the FRP deck(NCHRP)*

## 2.10 Case studies

A lot of highway or pedestrian bridges have been build or rehabilitated with FRP decks up to now. The application of FRP decks is done mostly in USA, but the application has increased to a great extent in Europe in the last decade. These bridges are hybrid bridges (mainly FRP decks on steel supports) or all-composite bridges. The first bridge built in Europe using the all-composite method is the Bond Mill Bridge in 1994, in England. The deck and the girders were made of ACCS elements which consist of a plank; three-way connector and toggle bar for connection (see Figure

2.83). The bridge has a width of 4.24 m and a span of 8.5m. The bridge was investigated in detail after 1 and 9 years and the main problem was the poor resistance against the wheel loads. This was overcome by filling the hollow sections with foam.

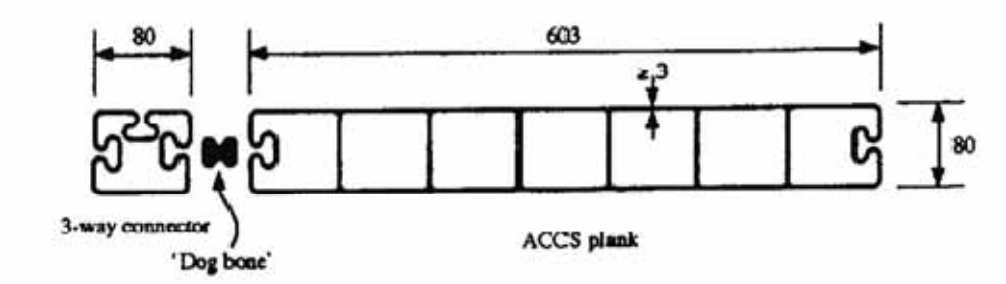


*Figure 2.83 Advanced composite construction system (ACCS)(Gurtler, 2004)*

The hybrid bridges are either new structures or replacement of existing concrete decks. Some of these bridge cases which have been monitored over a period of time are studied here and mainly their performance is being discussed. There is a lack of reports about the long-term performance of FRP decks in the field even though monitoring has been installed. That is the reason of describing a small number of bridges despite the fact that a lot of bridges have been built with FRP decks.

### 2.10.1 Bennett's Creek Bridge

This is a two-lane bridge, 7.8 m long and 10m wide with a skew angle of 30°. The reason of rehabilitating this bridge was that it was posted with weight restrictions because of the reduced load capacity of the deteriorated concrete deck (Alampalli *et al.*, 2002). The deck was replaced by hard core deck system and the existing abutments were reconstructed as well. The hard core slab system was fabricated in two pieces and connected by a combination of shear key and resin glue (see Figure 2.84 and Figure 2.85). The wearing surface was polymer concrete and was applied in the shop.

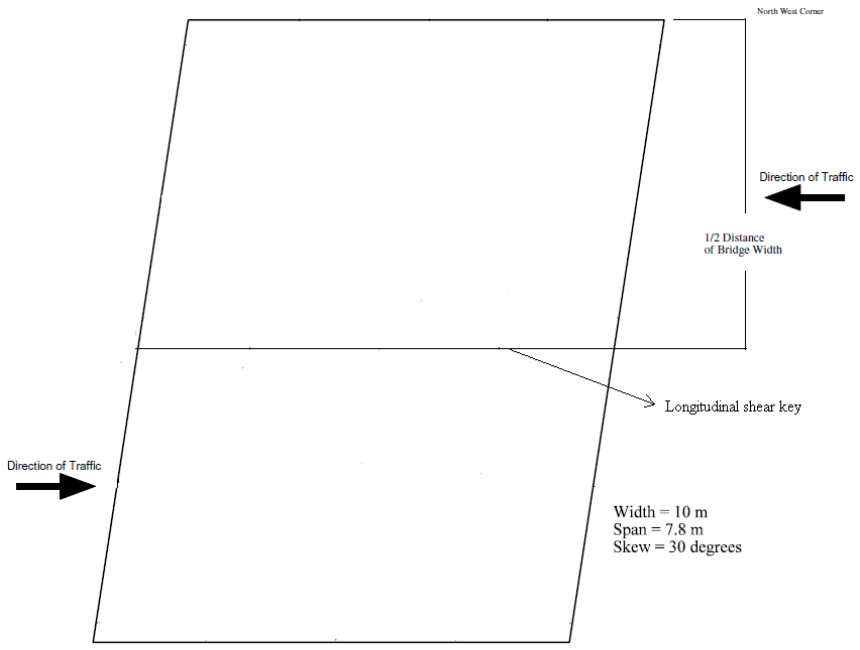


*Figure 2.84 Sketch of Bennett's Creek Bridge (reproduced by (Alampalli, 2006) )*

*Figure 2.85 Longitudinal shear key of the FRP deck (Alampalli, 2006)*

In-service performance over a period of four years was investigated (Alampalli, 2006). It was indicated that the maximum strains were below the predicted in design stage and the shear key/longitudinal joint was effectively transferring the loads. The visual inspections noted delamination in the slab and thus causing cracks in the wearing surface. Each year the delamination problems were repaired, but delamination of other portions were observed.

### 2.10.2 Snohomish county bridge

This bridge has a span and width of 9.14 m. The aim of building this bridge was the investigation of performance of GFRP deck types over steel girders for use as a replacement option for the concrete deck. The cross section of the bridge is shown in Figure 2.86.

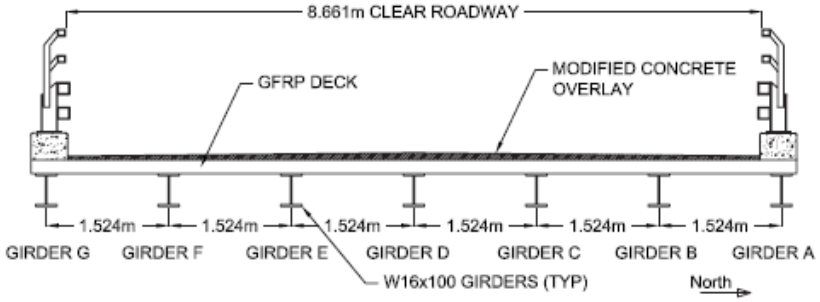


*Figure 2.86 The cross-section of Snohomish county bridge(Berman & Brown, 2010)*

GFRP deck panels were prefabricated and they were connected by adhesive bonding. Epoxy concrete was used as an overlay. The deck to girder connection is done by using bolts and no composite action was designed between the deck and the girders (see Figure 2.87). Neoprene rubber was placed to ensure uniform bearing surface between the deck and the girders.

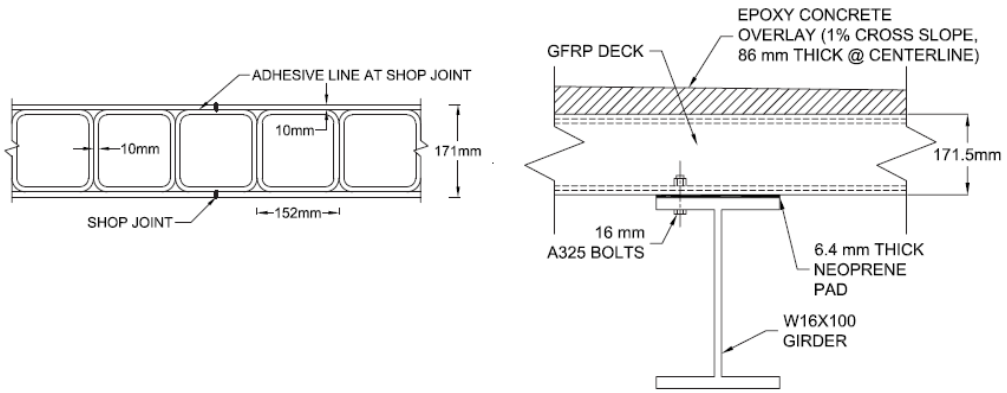


*Figure 2.87 Deck type and deck to girder connection of Snohomish county bridge (Berman & Brown, 2010)*

Field monitoring was done for nine months to check the performance of the deck. Cracking of the wearing surface was observed after 7 months and this was caused by the delamination of the deck (see Figure 2.88). The delamination was triggered by non-proper adhesive bond between some deck panels. Deflections of the deck were increased considerably in the delaminated parts. Thus to meet the objectives of long-term performance of the deck proper connection between the panels must be done to prevent delamination.

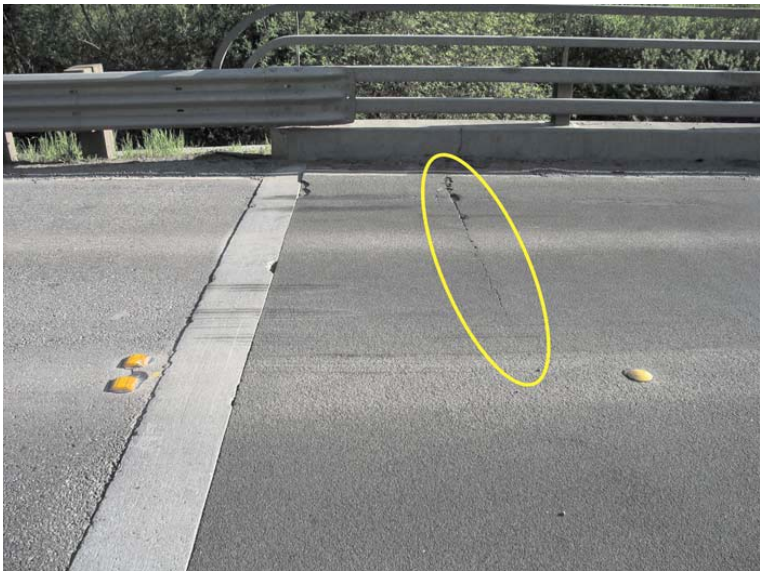

*Figure 2.88 Cracking of the overlay observed in Snohomish county bridge(Berman & Brown, 2010)*

### 2.10.3 Salem avenue bridge

This bridge consisted of steel girders and deteriorated concrete deck which needed to be replaced. Four deck systems were used as decking of this rehabilitation project in order to compare the performance of different deck systems (Reising *et al.*, 2004). The used deck systems were: superdeck system,VARTM sandwich deck, hand lay-up sandwich deck and concrete deck reinforced with FRP bars. Panel level connection of FRP deck was done by adhesive bonding (see Figure 2.89). FRP decks were connected by shear studs to the steel girders but no composite action was intended to be provided in the design. The panels were delivered to the site with pre-drilled shear

stud pockets at an interval of 1.2 m. Polymer wearing surface was used as an overlay. The installation of the FRP reinforced concrete deck was similar to the regular concrete decks and no wearing surface was needed.

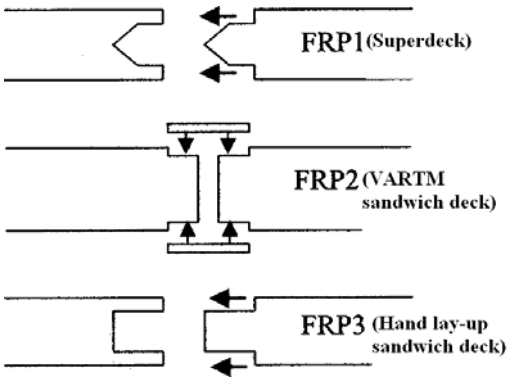


*Figure 2.89 Panel level connection for FRP decks(Reising et al., 2004)*

Pultruded FRP panels were identified as having the most accurate dimensions which was beneficial for the installation. The advantages of FRP deck system over standard reinforced concrete deck were proved in the terms of reduced construction time.

Thermal characteristics of FRP panels especially VARTM sandwich deck panels resulted in unexpected lifts and significant thermal gradients. Thermal induced stresses and movements must be allowed in detailing the deck to girder connection in future design. Thermal temperature differences between the faces of the panels are illustrated in Figure 2.90.

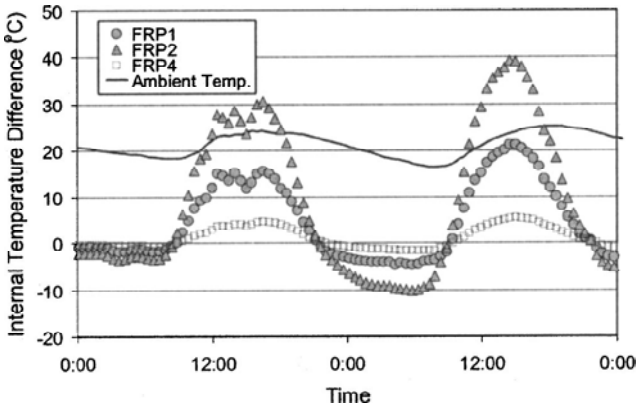


*Figure 2.90 Variation of internal panel temperature difference over two random days(Reising et al., 2004)*

As it can be observed in the figure above the temperature gradient in FRP2 deck system can reach to 40$^{o}$C, which is quite a high value.

Functional problems started developing on the decks shortly after the bridge was reopened to the traffic. After two months delamination areas were found in FRP2 deck system and FRP3 deck system. Sandwich deck types seem to be more prone to delamination due to small and relatively fragile connection between the core and the faces and due to the thermal characteristic of the panels. There was observed joint incompatibility between different deck systems and there were problems in field and shop joints. Some joint deficiencies stemmed from manufacturing flaw such as no bonding between face sheets and core webs in some areas. Cracking and spalling was observed in the wearing surface. Water accumulation in the cavity of the deck was seen.

*Outcome of field performance of FRP decks*

The overall performance of FRP decks in the field has been rather good. However, since these decks are a relatively new concept some problems which require minor maintenance have been observed in some cases.

One typical problem observed in applications of FRP decks is delamination and debonding of wearing surface. This has to be corrected by better surface preparation of the FRP decks. Lack of experience of the crew in installation of FRP decks is also a factor of not installing properly these decks and leading to these problems after opening the bridge to traffic. Another problem that has been observed is delamination of the deck components. Delamination problems have occurred due to not proper adhesive bonding between the deck components during manufacturing process Delamination of the deck components is of great concern as it can result in a significant reduction in the stiffness of the deck sections. Therefore, a great care must be taken during component level connections to assure that no areas between the components' surfaces are left without adhesive. This localized delamination can be repaired in the field by epoxy injections. In other bridge applications, some problems have been detected on the haunch supports, where a gap between the bottom face of the deck and the haunch would be created and thus causing impact to the deck due to the passage of vehicles.

In most of bridge designs, FRP decks are not designed to work compositely with the stringers or girders. The design is done without considering composite action even though partial composite action is achieved between the deck and the girders. This design is a conservative design. This factor limits the inspection and assessment of the composite action between the deck and the girders in real bridge designs.

# 3 Upgrading existing concrete-steel bridge

## 3.1.1 Introduction

After collecting the experience of previous research and practical applications done on FRP decks it was decided to study further the feasibility of FRP decks on upgrading existing steel-concrete bridges. Replacement of a deteriorated concrete deck with an FRP deck in an old bridge is investigated. The bridge is picked from a master thesis done by Mattias Nilsson which consists of the replacement of the old bridge with a new prefabricated one (Nilsson, 2002). The bridge is built in north of Sweden over a small watercourse called Rokån. It is located 10 km northwest of Roknäs in the motorway 373 which runs between Piteå and Arvidsjaur (see Figure 3.1). The bridge was built in 1948 and it consisted of two steel girders and reinforced concrete deck. The girders were not designed to act compositely with the concrete deck. Due to increased traffic loads over the years the load carrying capacity of the girders was not sufficient. Another problem was deterioration of the concrete deck and the bridge needed to be widened. The bridge was decided to be replaced with a new composite bridge with steel girders and prefabricated concrete slabs in year 2000. The carriageway width was upgraded by one meter as well. At that time, this was claimed to be the best solution fulfilling the requirements of which the most important one was fast construction in order to minimize the inconveniencies for road-users which leads to savings in both terms of time and cost. The main focus on Mattias' study was to make a cost evaluation considering investment and road-user's costs for different building techniques. These techniques include replacing the old bridge with a cast in place concrete slab or prefabricated slabs lying on steel girders. It was concluded that the prefabricated building technique was a more economical solution due to fast erection of the bridge. In that time FRP decks were not considered as a solution, therefore in this thesis it is decided to study another building technique of the bridge by utilizing FRP decks.

This building technique will be replacing the concrete deck with an FRP deck and keeping the steel girders which actually were still in good condition. To assess the deck replacement scenario, two cases are studied:

1. FRP deck acting non-compositely with the supporting girders
2. FRP deck acting compositely with the supporting girders

Furthermore, connections between the deck and the steel girders are studied for both cases.

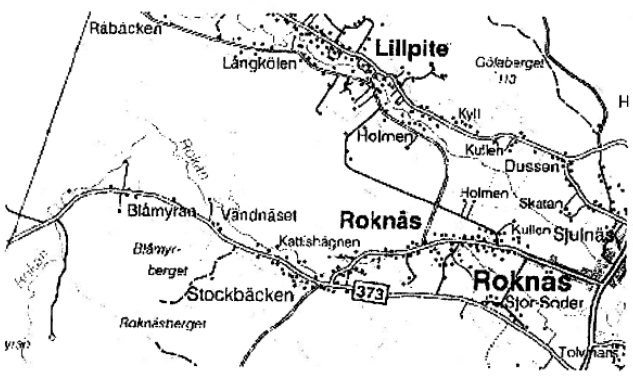


*Figure 3.1 Map of the location of the bridge(Nilsson, 2002)*

### 3.1.2 Background of the bridge

Rokån bridge was a simply supported bridge spanning 12 meters (see Figure 3.3). The load bearing structure was composed of two steel girders having a c/c distance of 3.8 m (see Figure 3.2). The deck was composed of reinforced concrete with an average depth of 265mm. Concrete bridge deck did not have a composite action with the steel girders. The bridge was a two lane bridge and had a free width of 6 meter. The width of the new bridge has to be upgraded to 7 meters. The steel material used for the girders was ST44. The properties of ST44 are given in Table 3.1.

*Table 3.1 Steel material data of the girders*

| Material | Yielding stress | Ultimate strength |
|---|---|---|
| | $f_y$ [MPa] | $f_u$ [MPa] |
| ST44 | 255 | 431.5 |

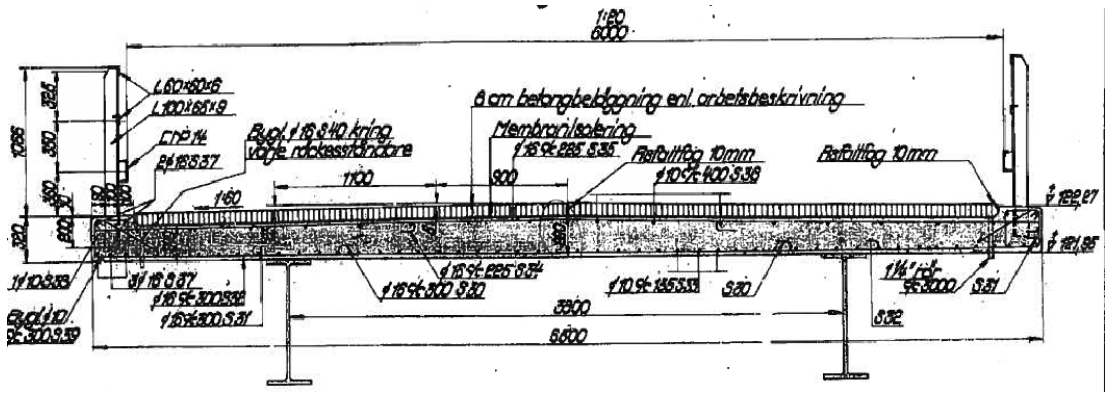


*Figure 3.2 Cross-section of the old Rokån bridge*

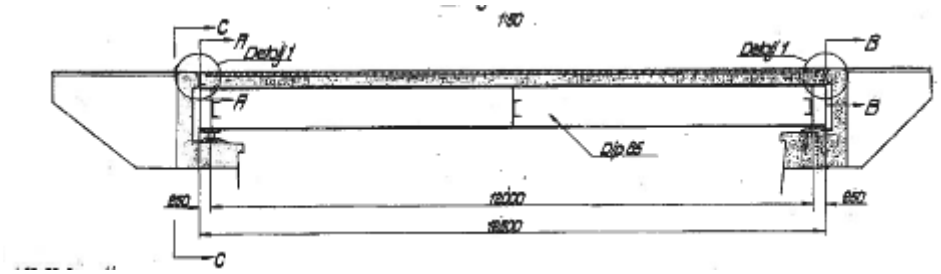


*Figure 3.3 Elevation of the old Rokån bridge*

### 3.1.3 Organization of the study

The organization of the study of upgrading this bridge is illustrated in Figure 3.4.

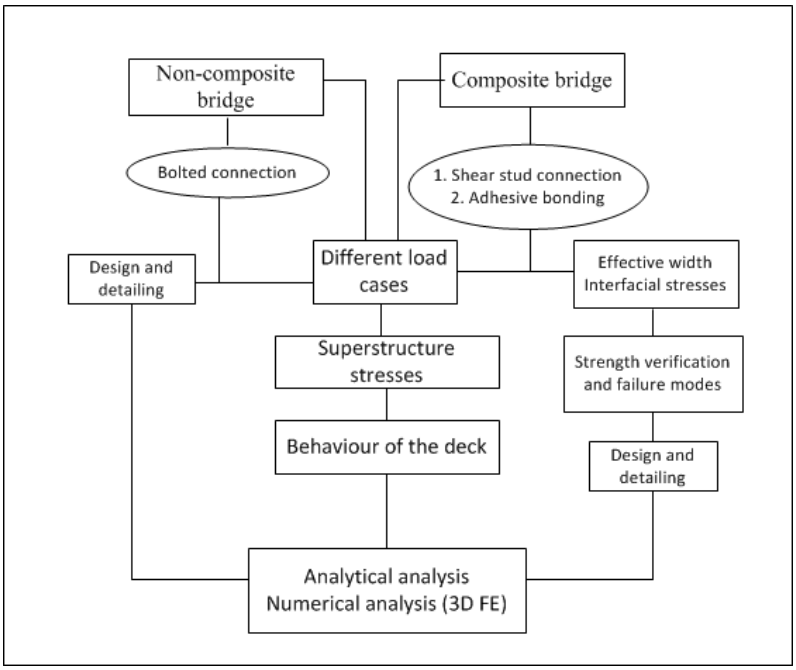


*Figure 3.4 Scheme of the organization of the study*

As mentioned previously, two scenarios of replacing the concrete deck are considered: FRP deck working non-compositely and compositely with the steel girders. In case of non-composite bridge, bolted connections are studied. These connections are intended to prevent the deck from uplifting and transverse displacements, but not providing composite action between the deck and the steel girders. In order to provide composite action between the girders and the deck two different connections that is shear stud connections and adhesive bonding are studied. Under different load conditions, the stresses and behaviour of the deck are examined. The incorporation of the FRP deck to the composite action that is the effective width is computed as well. Interfacial stresses under different loadings between the connections of the FRP deck to the steel girders are analysed in order to design the connections in case of composite action. The study is conducted by method of both analytical and numerical (3D finite element) analysis.

## 3.1.4 Applied Loads

Different loadings are considered in the analysis of the bridge. These loads are chosen according to EC1 and are presented in the following.

### 3.1.4.1 Vertical loads

The vertical loads considered in the analysis of different scenarios are the dead load of the structural components and the live traffic loads. The dead load includes the loads of deck, girders, diaphragms and parapets and the dead weight of asphalt layer. The road traffic loads are used according to load model 1 in European Code EC1((CEN), 2003). Load model 1 covers most of the actions of the traffic of cars and trucks and it is used for general and local verifications. It consists of double axel concentrated loads and uniformly distributed loads (see Table 3.2*)*. The distance between two axles is 1.2 m and distance between the wheels of one axle is 2 m. The concentrated load patch dimensions are 0.4x0.4m per wheel. These loads have to be multiplied by the national adjustment factors $\alpha_Q$ and $\alpha_q$. These factors are picked from the national

annex. In this study, these factors were set as shown in Table 3.2. For ultimate limit state (ULS), the characteristic loads have to be increased by a load factor of $\gamma_F$=1.35. The considered load combination is shown in equation (3.1):

Ultimate limit state (ULS) $1.35 * DL + 1.35 * LL$ (3.1)

where DL is dead load and LL is live load.

*Table 3.2 Load model 1(characteristic values): traffic loads according to EC1*

| Location | Axle loads $Q_{ik}$ | Uniform load $q_{ik}$ | Adjustment factor | Adjustment factor |
|---|---|---|---|---|
| | [kN] | [kN/m$^2$] | $\alpha_Q$ | $\alpha_q$ |
| Lane 1 | 300 | 9 | 0.9 | 0.7 |
| Lane 2 | 200 | 2.5 | 0.9 | 1.0 |
| Remaining area | 0 | 2.5 | - | 1.0 |

In Figure 3.5, the application of load model 1 in the upgraded bridge is depicted. The width of one lane is 3 meters and half meter on each side of the lanes is the remaining area. Characteristic load values are presented in the figure.

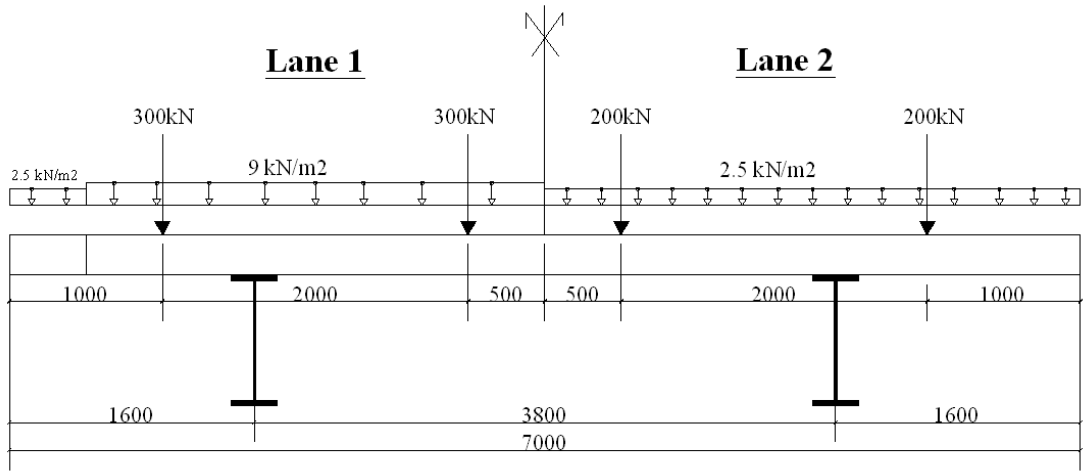


*Figure 3.5 Schematic of Load model 1 application used in the analysis for traffic loads*

### 3.1.4.2 Horizontal loads

The horizontal forces acting on the surface of the deck are braking or acceleration forces and lateral forces. The braking force is calculated as a fraction of total maximum vertical forces corresponding to load model 1.

$$Q_{hk} = 0.6\alpha_{Q1}(2Q_{1k}) + 0.1\alpha_{q1}q_{1k}w_1L \quad (3.2)$$

Equation (3.2) shows the calculation of the braking force for lane 1. The braking force is applied along the width of the lane as a line load (see Figure 3.6). The acceleration

force is the same magnitude as the braking force but in opposite direction. The lateral forces caused by skew braking or skidding are taken into account with a value equal to 25% of the braking force. The lateral forces should be considered acting in the finished carriageway level at the same time with the braking loads (see Figure 3.6). The magnitudes of the horizontal forces are presented in Table 3.3. The design ultimate loads have to be multiplied with the partial factor of 1.35.

*Table 3.3 Horizontal and lateral forces (characteristic values)*

| Location | Braking load $Q_{hk}$ | Acceleration load $Q_{ik}$ | Lateral force $Q_{trk}$ |
|---|---|---|---|
| | [kN] | [kN] | [kN] |
| Lane 1 | 346.7 | 346.7 | 86.7 |

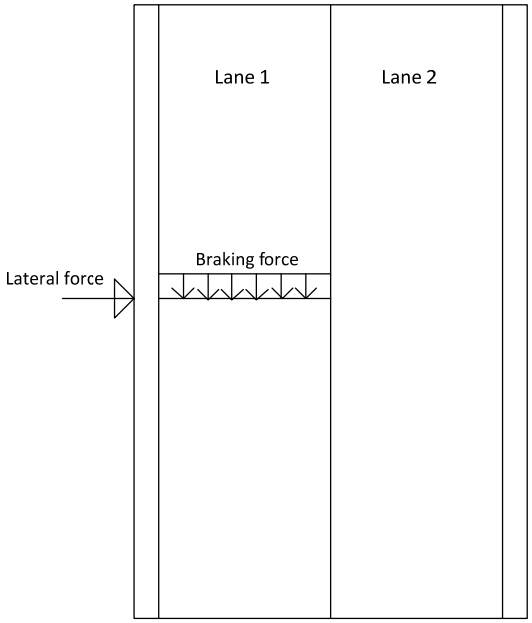


*Figure 3.6 Schematic of application of horizontal and lateral loads on the bridge*

### 3.1.4.3 Fatigue loads

Fatigue loading was considered in the study to analyse the fatigue resistance of the shear studs used in the connection with the steel girders in case of composite action between FRP deck and steel girders. Fatigue load model 3 in European Code EC1 was used. This model consists of four axles, each of which has a load of 120 kN. The load configuration used in this study is shown in Figure 3.7.

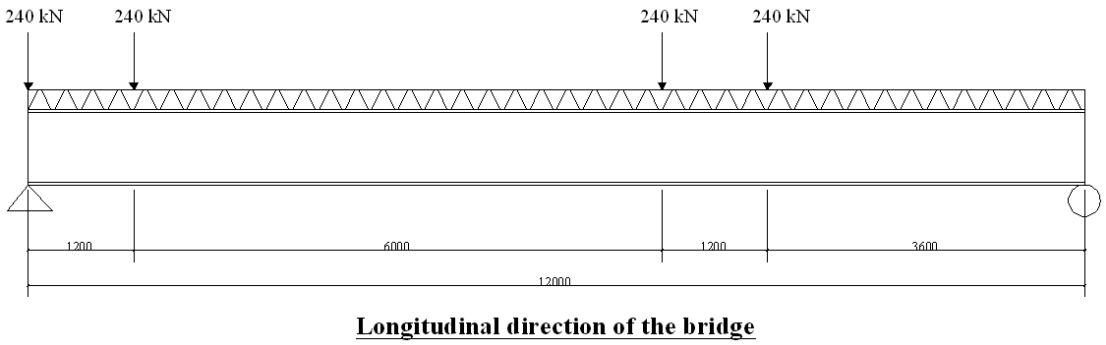


*Figure 3.7 Configuration of fatigue load model 3*

In this bridge it was relevant to take into account one vehicle per lane. The loads presented in this case are double the axle load because the bridge consists of two lanes. Fatigue loads are placed starting from the edge of the bridge in order to obtain maximum shear forces acting on the shear studs.

## 3.1.5 Reduction of superstructure stresses

In this section, the stresses on the steel girders when replacing the concrete deck with FRP deck are presented. These stresses are obtained when vertical loads are applied and the different scenarios of composite and non-composite girders are compared.

### 3.1.5.1 Non-composite FRP bridge

The self-weight of an FRP deck is approximately 20% of an equivalent concrete deck. In this study the self-weight of the FRP deck is 0.925 kN/m$^2$. This makes these decks beneficial in reducing the stresses induced by the self-weight of the deck. The first case of replacing the reinforced concrete deck with FRP deck having non-composite action with the steel girders is studied and assessed in this section.

The maximum tension stresses in steel girders for the load combination in ultimate limit state are presented in Table 3.4 for RC bridge and FRP bridge. The stresses are calculated by simple mechanics using elastic section properties (see Appendix for further calculations).

*Table 3.4 Superstructure stresses for dead and live load*

| Bridge | Self-weight | Stress from self-weight | Stress from traffic loads | Total stress (ULS) |
|---|---|---|---|---|
| | [kN/m] | $\sigma_g$ [MPa] | $\sigma_t$ [MPa] | $\sigma$ [MPa] |
| Non-composite RC bridge | 30.97 | 58.13 | 246.54 | 304.67 |
| Non-composite FRP bridge | 8.51 | 15.97 | 252.25 | 268.33 |
| Reduction (%) | 72.5 | 72.5 | - | 11.9 |

As it can be observed in the table above, the stress caused by the self-weight is decreased by 72.5% for the new bridge with FRP deck. The stress from the traffic loads in the new bridge is higher since the carriageway of the bridge was increased by one meter. The total stresses are lower in the new bridge and a decrease in stresses of the girders by 11.9 % is achieved. This proves that the decrease in self-weight of FRP decks allows for increase in traffic loads and the final stresses can still be smaller than the RC bridge. However, the stress values are higher than design yield stress of the girder steel material for the girders (see Table 3.1). A solution to decrease more the stresses in the girders is the design of hybrid girders by attaining composite action between the girders and the deck.

### 3.1.5.2 Composite FRP bridge

In order to achieve composite action between steel girders and FRP deck two types of connections have been considered in this study. Traditional shear stud connections and adhesive bonding between the FRP deck and steel girders have been investigated and the reduction of girder stresses in these cases is evaluated. These connections are presented in the following sections:

*Adhesive bonding*

One option to attain composite action between steel girders and FRP deck is adhesive bonding between the deck and the girders. In order to compute the effective width of the FRP deck contributing to the hybrid girder a finite element model is required. Finite element modelling is done in the software ABAQUS (ver. 6.8.2) and it is explained more in detail in the Section 3.1.6. To calculate the effective width of the FRP deck just the flanges of the deck are taken into account in the calculations. The level of assistance of FRP flanges to the composite girder is calculated based on the upward shift of the neutral axis by back-calculating the effective FRP flange width using standard transformed section properties. The shift of the neutral axis is obtained by the results of the analysis in finite element model of composite bridge. The calculation is done for the middle of the span where maximum moment is acting.

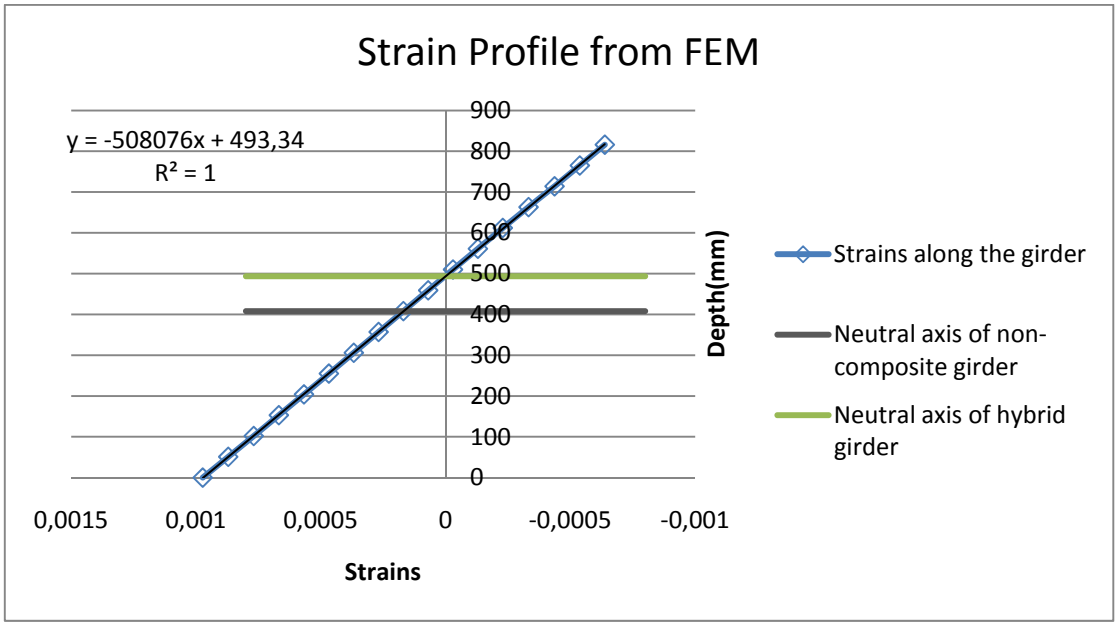


*Figure 3.8 The strain profile along the composite steel girders*

In the figure above, the upward shift of the neutral axis of the girder due to the composite action can be observed.

According to the calculations, the effective width of the FRP deck flanges was determined approximately 2.2 m (see Figure 3.9). If the whole width of the deck would work compositely with the girders, that would be half of the span between the girders plus the overhang (see equation (3.3)).Thus, approximately 63% of the deck is working compositely with the girders.

$$b_{th} = \frac{3.8\ \text{m}}{2} + 1.6\ \text{m} = 3.5\ \text{m} \quad (3.3)$$

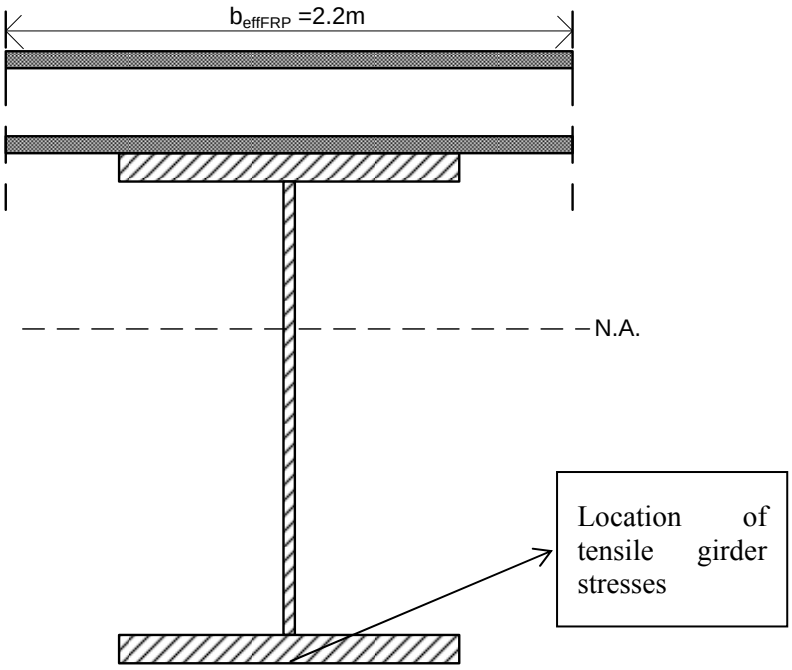


*Figure 3.9 The effective width of the FRP deck flanges contributing to composite action*

The superstructure maximum tension stresses in the girder (see Figure 3.9) for different scenarios is given in the table below.

*Table 3.5 Superstructure stresses in case of composite bridge with bonding*

| Bridge | σ [MPa] | Stress reduction [%] |
|---|---|---|
| Non-composite RC bridge | 304.67 | - |
| Non-composite FRP bridge | 268.33 | 11.9 |
| Composite FRP bridge with bonding | 239 | 21.5 |

As it is observed in Table 3.5, there is a decrease of approximately 11% between the non-composite FRP bridge and composite FRP bridge with bonding. The total reduction compared to the original bridge is 21.5%.

**Shear stud connection**

The next option to provide composite action is by having shear stud connection between the girders and the deck. In applications up to now, shear stud connections have been discrete and non-shrink grout or concrete has not been continuous (see Figure 3.10). This discrete nature of shear stud connections rather than continuous affects the efficiency of the decks to contribute as a top flange of the hybrid girder.

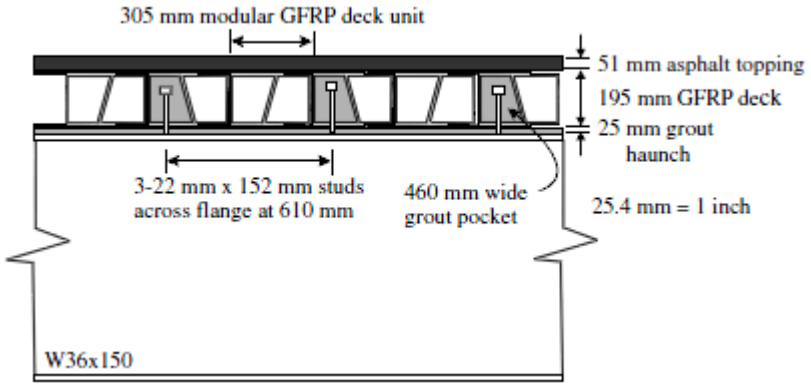


*Figure 3.10 Configuration of discrete shear stud connection(Turner et al., 2004)*

In this study, the concept of having shear stud connection with continuous concrete along the span of the bridge is studied. The cross-section of the shear stud connection concept is shown in Figure 3.11.

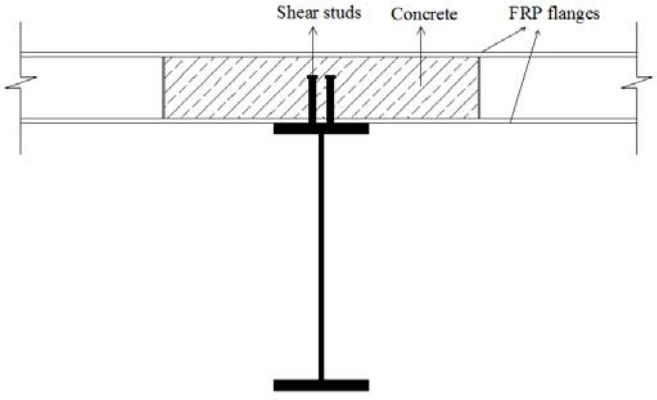


*Figure 3.11 Illustration of shear stud connection concept*

The width of the concrete needed in the connection is decided based on the percentage desired for the reduction of superstructure stresses. To start with, an overall decrease of 30% of the total stress in the girders was desired. This is a criterion that is set by the author, since a reduction of 30% is considered to be a reasonable high percentage. A backward calculation was done to calculate the effective width of the concrete needed to provide this decrease by working compositely through the shear studs with the girders. Concrete class that was considered in the calculations is C30. The effective width of the concrete was computed to be approximately 600 mm to achieve the desired reduction. Afterwards, a more detailed calculation was done to design the shear studs and the hybrid FRP-steel girder. The effective width of the concrete is

decided to be 1000 mm because the efficiency of this width is reduced when considering the effect of shrinkage and creep. The shear studs are designed to have a diameter of 22 mm and a height of 150 mm. The spacing of the connectors in the cross-section is determined to be 55 mm and in the longitudinal direction the shear studs are spaced by 350 mm. The calculations are presented in Appendix. In Figure 3.12, the design of the shear studs welded to the girders is shown.

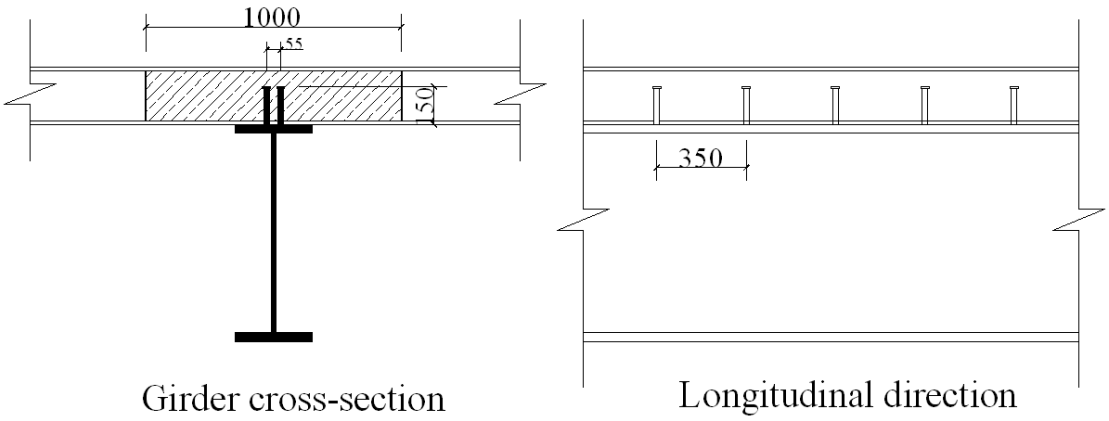


*Figure 3.12 Configuration of shear stud connection between FRP deck and steel girders*

In case of shear stud connection with concrete the contribution of effective FRP deck flanges should be considered as well. The maximum tensile stresses in the girders are computed for this case as well and the stresses for the different scenarios are compared in the following.

### 3.1.5.3 Comparison between different scenarios

In Table 3.6 maximum tensile stresses in the girders and the percentage of reduction for the different cases is presented. The reduction of the stresses for the different scenarios is calculated with regard to the non-composite RC bridge.

*Table 3.6 Maximum stresses in girders for different scenarios*

| Bridge | Maximum tension Stress | Reduction |
|---|---|---|
| | σ [MPa] | [%] |
| Non-composite RC bridge | 304.67 | - |
| Non-composite FRP bridge | 268.33 | 11.9 |
| Composite FRP bridge with bonding | 239 | 21.5 |
| Composite FRP bridge with shear studs + concrete | 215 | 29.4 |

As it is observed in Table 3.6, the maximum reduction of approximately 30% is achieved in the case of composite FRP bridge with shear stud. In this case concrete contributes as a compressive flange of the hybrid girder and increases the efficiency of the composite action by resulting in maximum stress reductions. Furthermore, the stress values of the girders in case of composite bridge are smaller than the design yield stress of the girder steel material which makes possible in keeping the original steel girders. The stress reductions for different cases are presented by means of a chart as well in Figure 3.13.

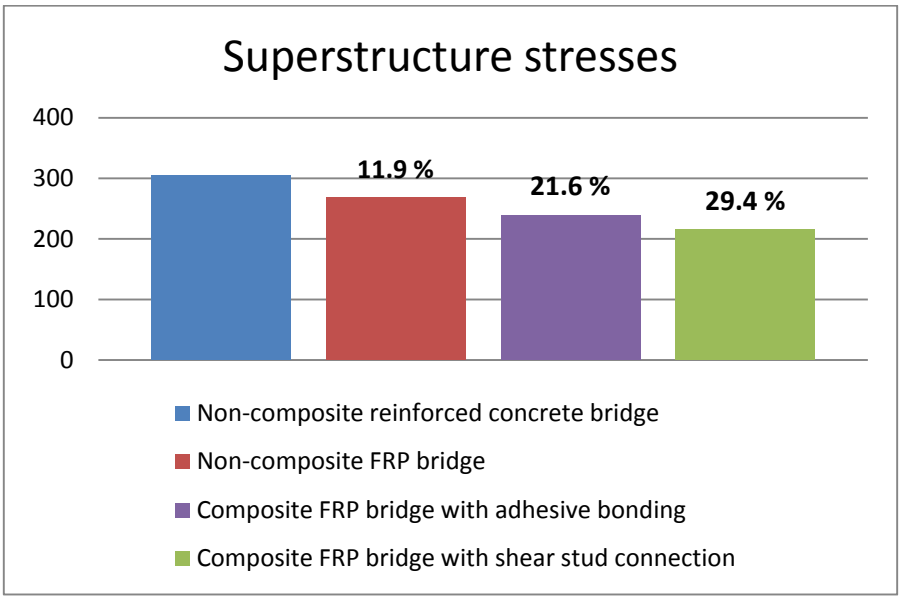


*Figure 3.13 Illustration of girder stresses when replacing concrete deck with FRP deck for different scenarios*

### 3.1.6 Finite element modelling

A finite element model was created in software ABAQUS (ver. 6.8.2) in order to simulate the structural behaviour of the composite FRP-steel bridge. The focus here was to evaluate the global behaviour of the bridge.

FRP deck is modelled using the actual geometry model, where each subcomponent of the deck is modelled. FRP deck and steel girders are modelled by 3-D deformable shell elements since the structure is mainly dominated by flexure behaviour. The geometry and dimensions of one component of the Asset deck are illustrated in Figure 3.14. The reason of studying the Asset deck is the collaboration of Chalmers with Fiberline Inc. which provided with all the material and geometry data.

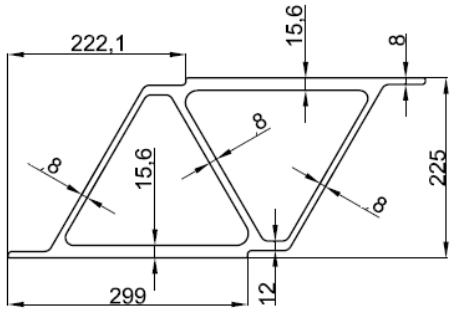


*Figure 3.14 Asset deck component*

It is noteworthy to mention that the webs and flanges of the deck are modelled as straight surfaces with a thickness in ABAQUS, while there exist some curvature between the webs and the flanges which would help in reduction of stress concentrations (see Figure 3.15). In ABAQUS the forces are transferred through the lines which would result in concentrated higher force results.

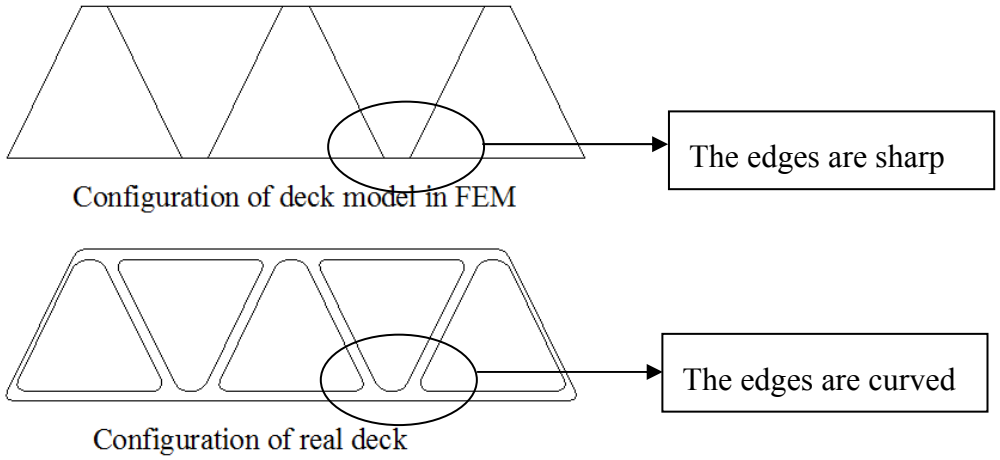


*Figure 3.15 Comparison between the configurations of the deck geometry in finite element analysis and the real one*

Element type S4 was used in modelling of the FRP deck and the girders. The adhesively bonded component level connections between deck components were not modelled. FRP deck is composed of orthotropic material. The deck was modelled using the characteristics and material properties (2D orthotropic material) of ASSET deck produced by Fiberline Inc. The material properties according to the orientation of deck's flanges and webs are presented in Figure 3.16 and Table 3.7.

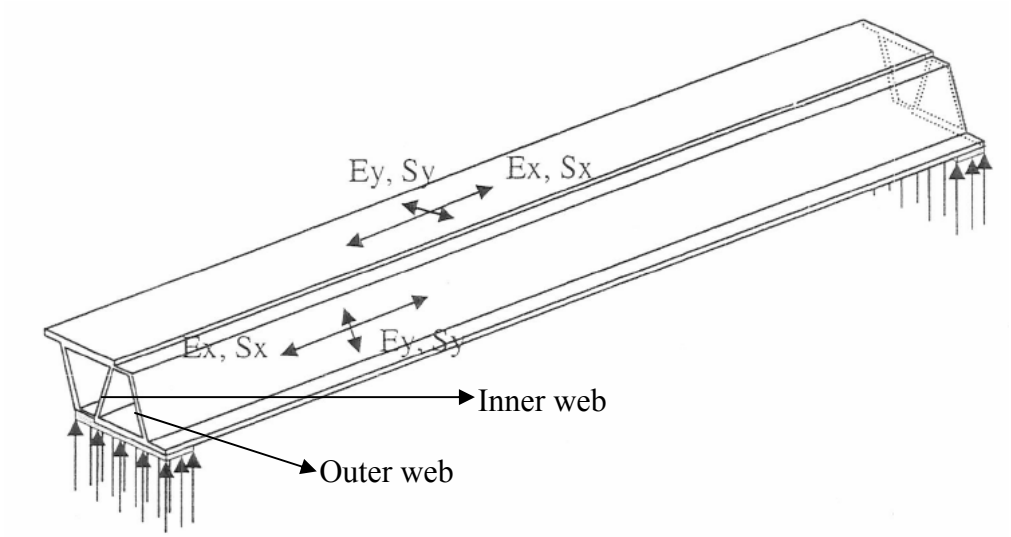


*Figure 3.16 ASSET deck profile typical component properties (Fiberline Inc.)*

*Table 3.7 ASSET deck material properties*

| Property | Flange plates | Outer web plates | Inner web plates |
|---|---|---|---|
| $E_x$ [MPa]* | 23000 | 17300 | 16500 |
| $E_y$ [MPa] | 18000 | 22700 | 25600 |
| $G_{xy}$ [MPa] | 2600 | 3150 | 2000 |
| $G_{xz}$ [MPa] | 600 | 600 | 600 |
| $G_{yz}$ [MPa] | 600 | 600 | 600 |
| $\nu_{xy}$ | 0.3 | 0.3 | 0.3 |

*X: pultrusion direction, Y: transverse direction, Z: vertical direction

The steel I-girders are modelled by using 3-D deformable shell elements for ease of compatibility in connection with the shell elements used to model the FRP deck. Steel material is modelled as linear elastic with isotropic behaviour having an elastic modulus of E=210 GPa and a Poisson ratio of ν=0.3.

*Interaction:*

Deck to girder connection adopted in this bridge model is intended to develop composite action. Thus, the deck to girder connection was modelled by using 'tie constraints' in the interaction module which provides a fully bonded connection between the steel girder flanges and the corresponding area of the deck flanges. The top flange of the girder was modelled as master surface and the corresponding area of the bottom flange of the deck was modelled as slave surface. One of the problems in case of 'tie constraint' is that in the connection face there is no force output available. In order to obtain the output of the interfacial forces between the deck and the girder, the connection was recreated as a contact surface to surface connection. The contact

properties were assigned as hard contact between the surfaces. The tangential behaviour was assigned as frictionless while the normal behaviour was assigned as 'hard' contact with constraint enforcement method as penalty. The surfaces were adjusted to be tied, where the translational degrees of freedom between the nodes of the master and slave surfaces are constrained. The adhesive between the girders and the deck was not modelled.

*Boundary conditions:*

The girders were modelled as simply supported and the boundary conditions were assigned at the end of the bottom flanges. On one support the vertical and longitudinal translations were constrained, and on the other support translation in the vertical direction was constrained.

*Loading:*

Different load configurations were applied to the model according to the analysis. The load configurations are consistent with the ones presented in Section 3.1.4. Sections of 400x400 mm were created in the deck in locations where the wheel loads are applied.

*Meshing:*

The mesh varied in size due to the requirements from the software ABAQUS where the slave surfaces should have a finer mesh than master surfaces in order to obtain better results and shorten the time of the analysis. Also, the partition faces where the wheel load was applied were meshed finer. Free and structured mesh controls were utilized. In Figure 3.17 the configuration of the bridge modelled in ABAQUS is illustrated.

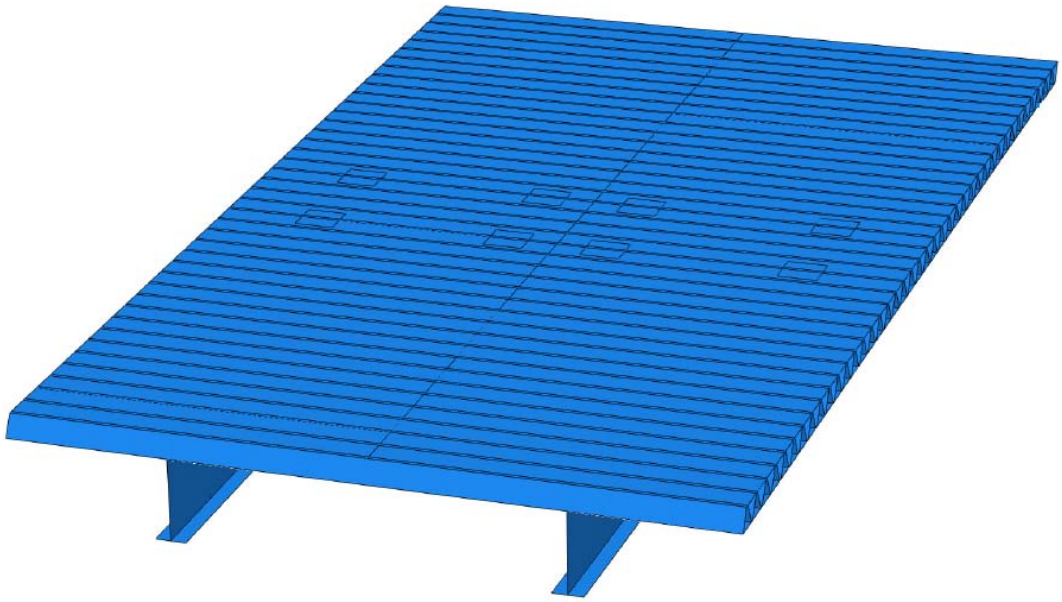

*Figure 3.17 Modelling of the bridge in the software ABAQUS*

### 3.1.7 Stresses in FRP deck

When vertical loading is applied in the bridge in ultimate limit state, tensile stresses resulting in FRP deck are checked as well. These stresses are compared with the tensile strength of the flanges and webs of the deck which were provided by Fiberline (see Table 3.8).

*Table 3.8 Tensile strength of flanges and webs of Asset deck*

| Property | Flange plates | Outer webs | Inner webs |
|---|---|---|---|
| Tensile strength-x[MPa]* | 300 | 180 | 213 |
| Tensile Strength-y [MPa]* | 220 | 255 | 255 |

*X and Y directions are the same as presented in Figure 3.16

Maximum resulting transverse and longitudinal tensile stresses obtained from finite element analysis are presented in Table 3.9. It is observed that these stresses are lower than the tensile strengths of the plates and minimum safety factor of 1.77 is computed. Thus, FRP deck has sufficient capacity to carry the traffic loads.

*Table 3.9 Resulting tensile stresses in flanges and webs of FRP deck*

| Property | Flange plates | Web plates |
|---|---|---|
| Transverse maximum stress [MPa] | 30 | 33.4 |
| Tensile Strength [MPa] | 300 | 180 |
| Safety factor | 10 | 5.4 |
| Longitudinal maximum stress [MPa] | 124 | 62.5 |
| Tensile strength [MPa] | 220 | 255 |
| Safety factor | 1.77 | 62.5 |

In Figure 3.18, the resulting transverse stress in FRP deck when applying vertical loading is illustrated.

Patch load capacity of the ASSET deck is 440 kN under an area of 300x300 mm. This capacity was provided by Fiberline Inc. In this study, maximum patch load of 405 kN under an area of 400x400 mm is applied which is lower than the patch load capacity. Thus, the capacity of FRP deck is sufficient for patch loading.

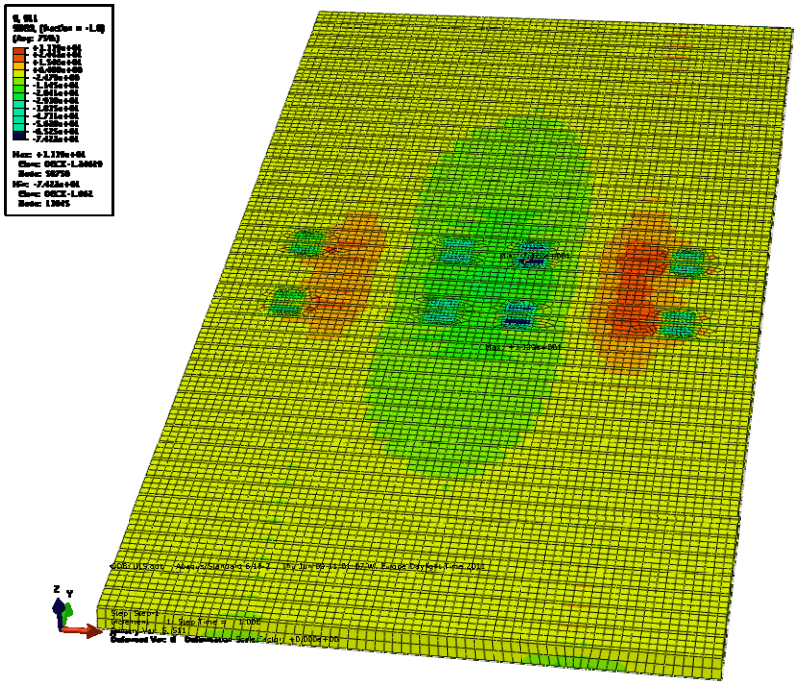

*Figure 3.18 Transverse stresses in FRP deck when vertical loading is applied*

### 3.1.8 Behaviour of ASSET deck

Behaviour of ASSET deck on how the loads are transferred between the flanges and the webs is studied. It is observed that the forces are mainly transferred through the webs by truss action (compressive and tensile forces in the diagonals) due to the triangular configuration of the deck (see Figure 3.19).

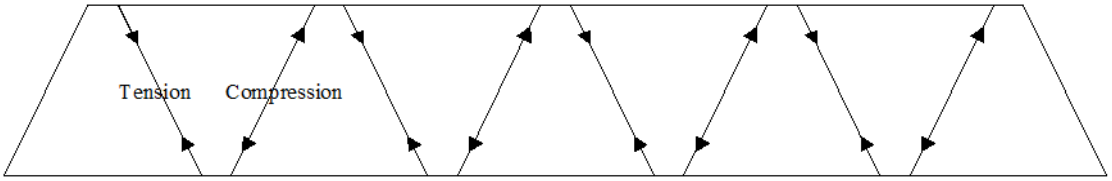


*Figure 3.19 Force distribution in ASSET deck*

One of the webs carries tension and the other compression forces. The components of these forces will create force couples in the flanges which will result in local moments and high shear forces between the intersections of diagonals (see Figure 3.20). The moments in the intersections are higher because the moment is a function of the length of the force couple. Thus, peak moments and shear forces result in the intersection between the web and the flange (see Figure 3.21).

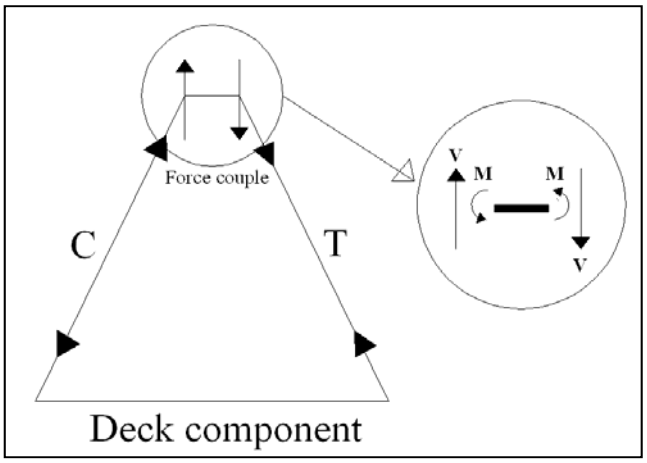


*Figure 3.20 The moments resulted from the force couple in the flanges of the deck*

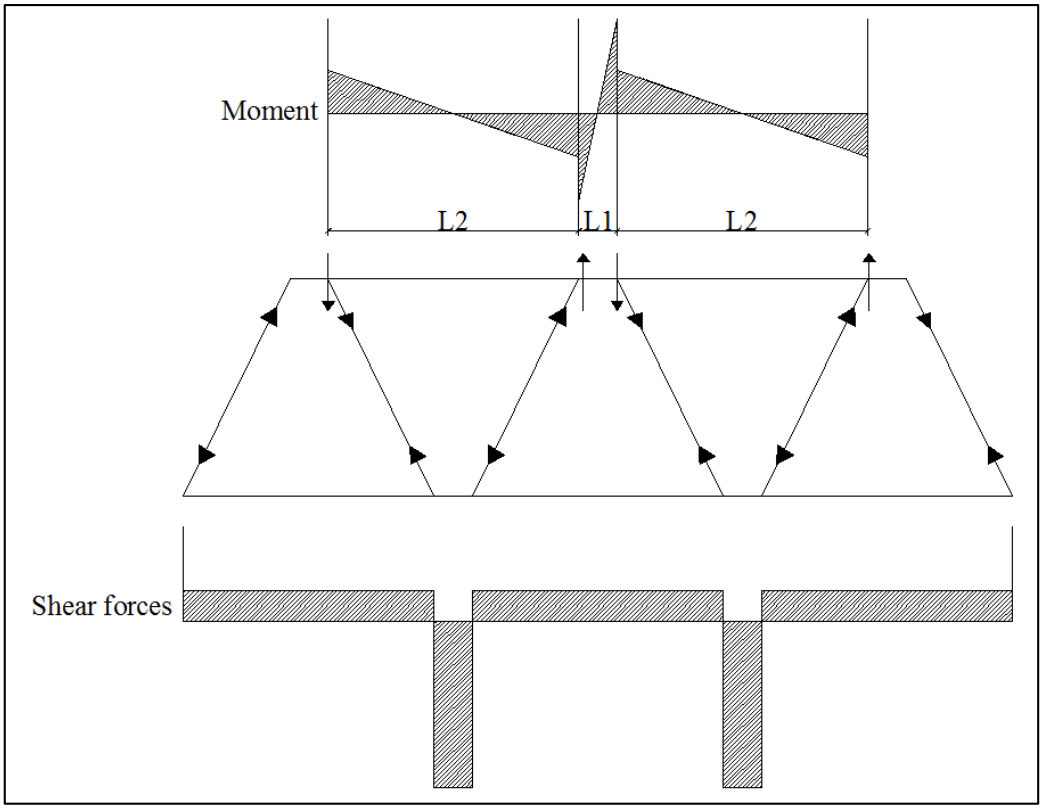


*Figure 3.21 Moment and shear force distribution in the flanges of the deck*

### 3.1.9 Deflections in Serviceability Limit State

Deflections of the girders and FRP deck are examined when the bridge is loaded in serviceability limit state. Vertical loading is applied the same as load model 1 in the finite element model of the bridge (see Figure 3.22). The square sections in blue and red colour are the sections where the wheel loads are applied and in the remaining areas uniformly distributed load is applied.

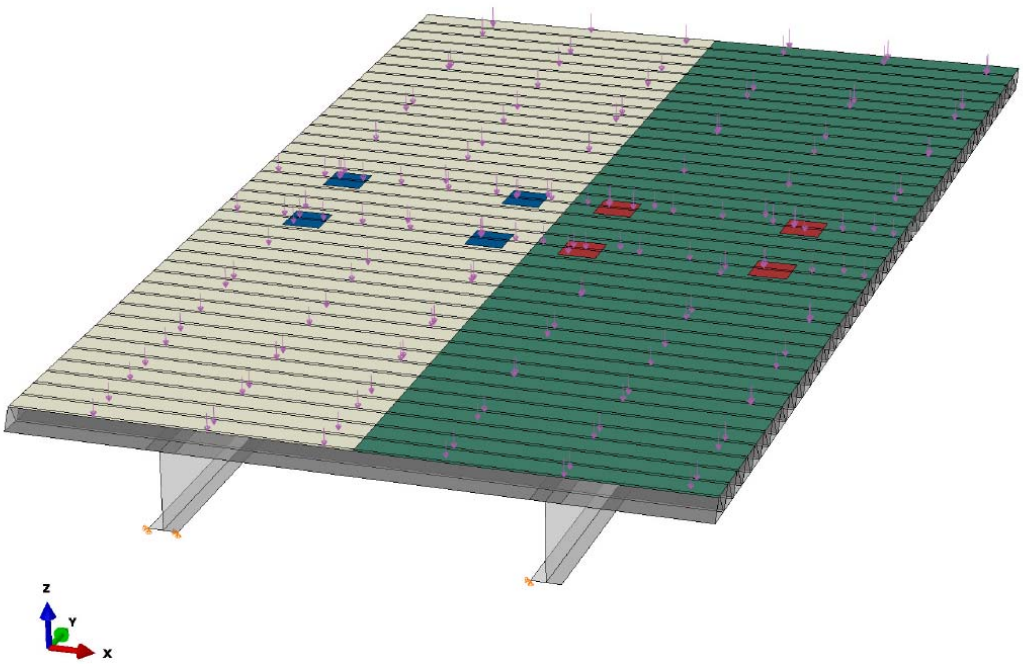


*Figure 3.22 Loading configuration of the bridge in finite element analysis*

The global deformation of the bridge is depicted in Figure 3.23. Obviously, the maximum deflection of the deck is in the middle where the load is applied. It can be noticed that the deflection is higher in the positions where the wheel loads are applied. The maximum deflection of the steel girder is in the middle as well where loading is applied and it has a value of 22 mm which corresponds to L/540. The maximum deflection of the deck has a value of 9.17 mm. This deformation corresponds to L/414. This deflection is reasonable if the deflection criterion is set to L/400.

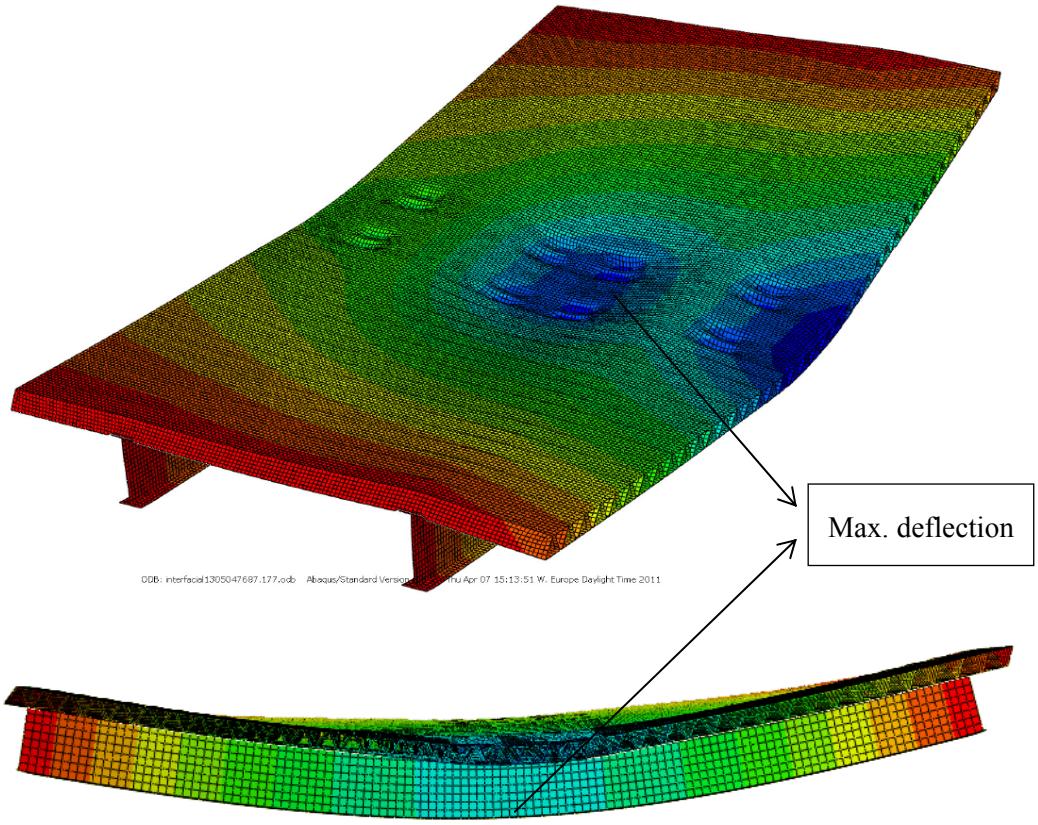


*Figure 3.23 Deformation of the deck (top) and the girders (bottom) in the bridge when vertical load model 1 is applied*

When concrete is incorporated in FRP deck in case of shear stud connections the deflection of the FRP deck will be even lower. This is because of the stiffness of the concrete which will prevent the deformation of the bridge up to the point where concrete is casted. Furthermore, the length of the deck is lowered by one meter (instead of 3.8 to 2.8 meters) due to the placement of concrete which will result in reduction of deflections.

### 3.1.10 Influence lines

In design of connections in case of composite action, peeling and shear stresses acting on the surface between FRP deck and steel girders are essential. The most critical forces for the design are the tensile forces resulting by the uplift of the deck. Uplift of the deck results when vertical loading is applied. The magnitude of this uplift force depends on the location where the load is applied (see Figure 3.24). In the case of applying the load in the middle of the bridge, the stresses in the interface are subjected in two different ways. According to the position of the section along the length of the girder, the joint is subjected just to compression or compression in one side and tension on the other side (see Figure 3.24 a). In case of applying the force in the edge of the deck one of the joints will be subjected to pure tension (see Figure 3.24 b).

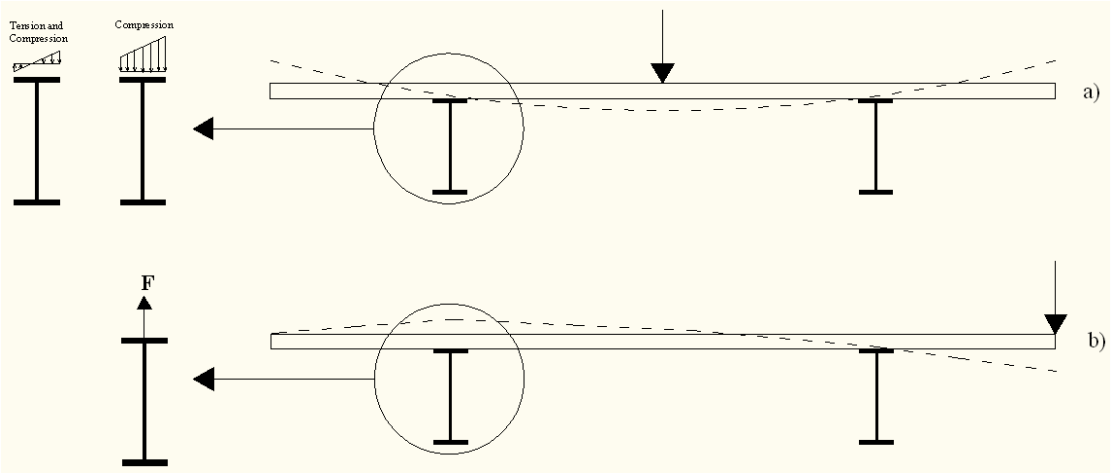


*Figure 3.24 Load bearing behaviour in transverse direction: a)when the load is applied in the middle; b) when the load is applied in the edge*

To determine where to put the traffic load in the longitudinal direction of the bridge with the intention of obtaining maximum tensile forces on the joint, influence lines were obtained in different positions for a unit moving load. A simplification of using simply a moving unit load in the middle of the bridge is done in this study. Essentially, an influence area analysis with different moving concentrated and uniformly distributed load positions has to be done to acquire a correct design. The load positions of the moving unit load are shown in the figure below.

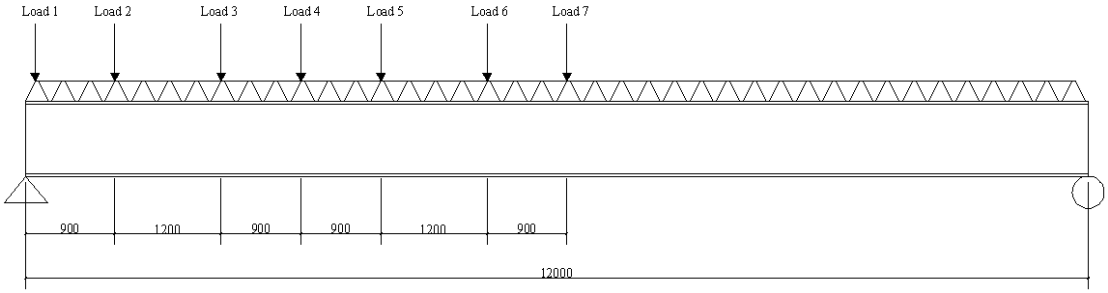


*Figure 3.25 The load positions of the moving unit load*

After each load application, the resulting forces on the interface were attained from finite element analysis. The forces are plotted along the longitudinal direction of the bridge and are illustrated in Figure 3.26. As it is observed the peeling forces vary from compression to tension under the webs.

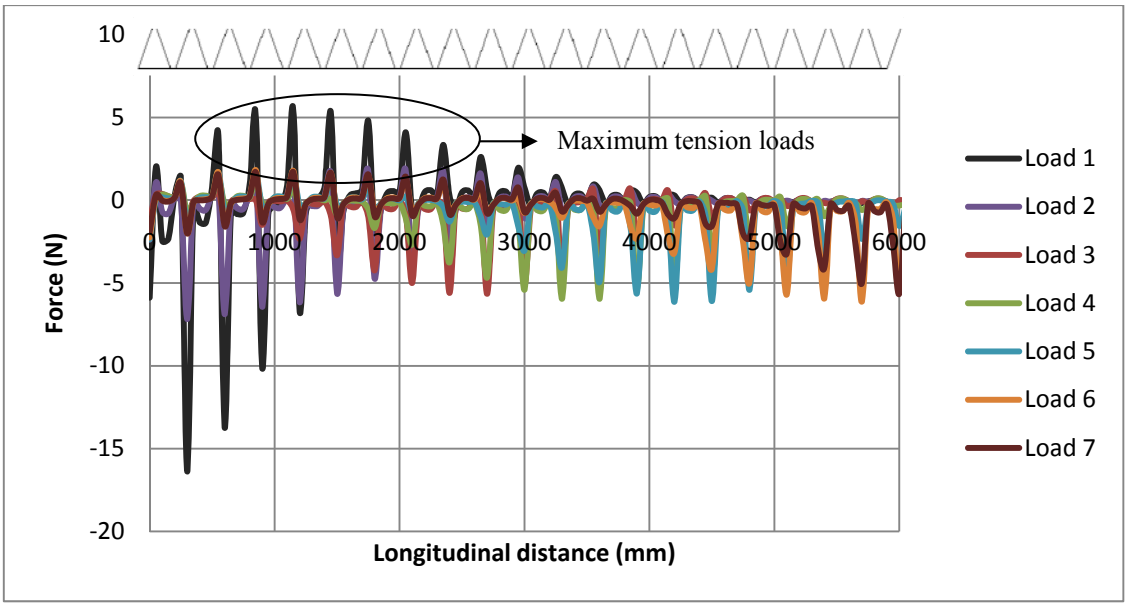


*Figure 3.26 Variation of the peeling load in the edge of the girder flange along the longitudinal direction of the bridge*

The reason of having compression and tensile forces under the webs is due to the local effect in the intersections between the webs and the flanges. As it was explained in Section 3.1.8 in the intersections between the webs and the flanges force couples are acting. Tensile or compression forces acting on the girders from the transversal load bearing behaviour (see Figure 3.24) are added together with force couples resulting from the rolling shear acting on the deck due to composite action(see Figure 3.27 and Figure 3.28). Depending on the magnitude of these forces the resultant might be tension or compression which explains the change of forces along the longitudinal direction of the bridge in Figure 3.26.

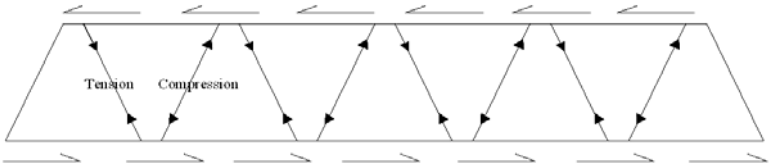


*Figure 3.27 Rolling shear forces on the deck due to composite action*

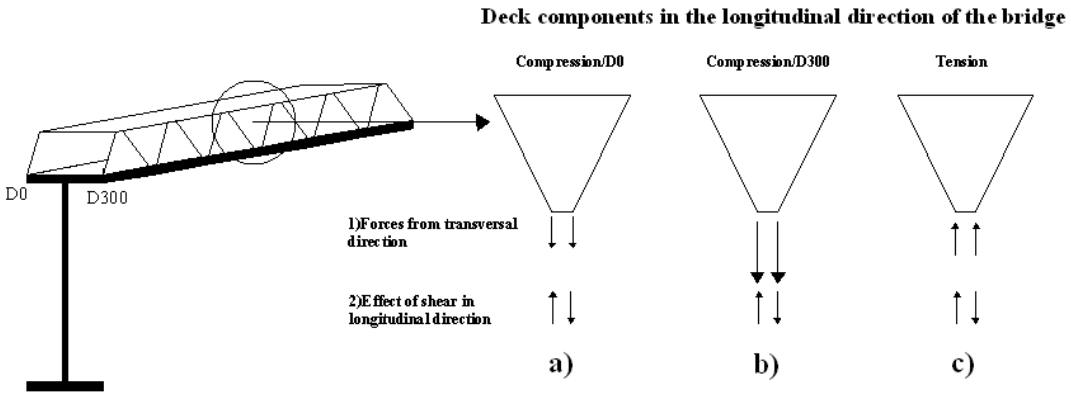


*Figure 3.28 Illustration of load bearing behaviour in longitudinal direction for one deck component: a) the compression forces in one edge of the flange D0 b) the larger compression forces in the other edge of the flange D300 c) tensile forces*

Maximum tensile forces resulted for the load position 1 which is marked by a circled area in Figure 3.26. In the positions where the maximum tension forces appeared the influence lines for a moving point load are drawn (see Figure 3.29 and Figure 3.30).

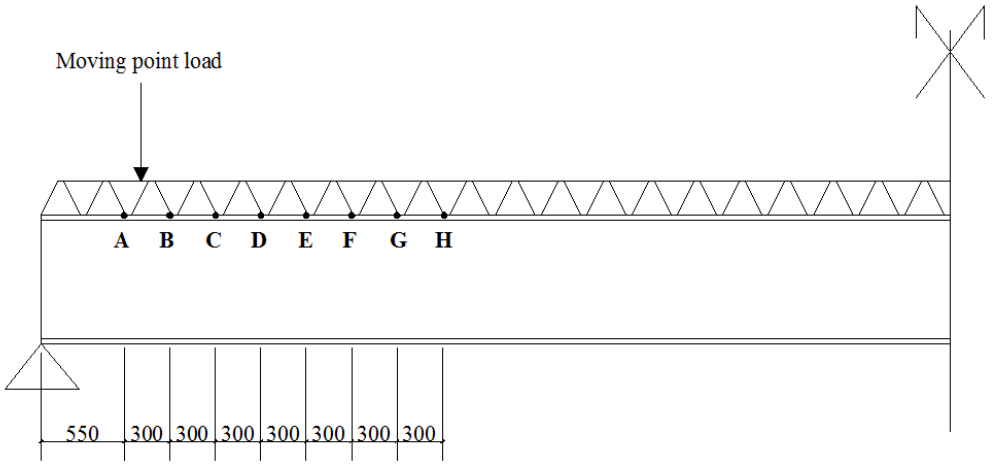


*Figure 3.29 Illustration of positions where the influence lines are obtained*

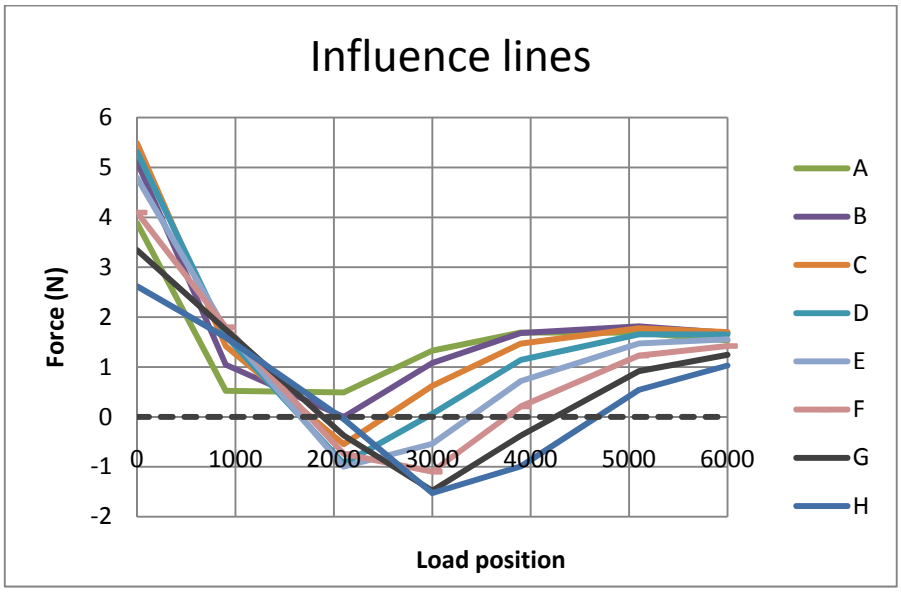


*Figure 3.30 Influence lines for various positions in the deck*

According to these influence lines, the position of the wheel loads in order to obtain maximum tensile forces can be decided. The wheel loads have a distance of 1.2 meters in the longitudinal direction of the bridge and the maximum tension forces will be the sum of the two forces under the wheel loads. It is observed that the maximum tension is obtained when these wheel forces are placed in the end of the bridge (see Figure 3.31). Some of the influence lines were directly excluded since it was obvious enough that maximum tensile forces could not be achieved in those positions.

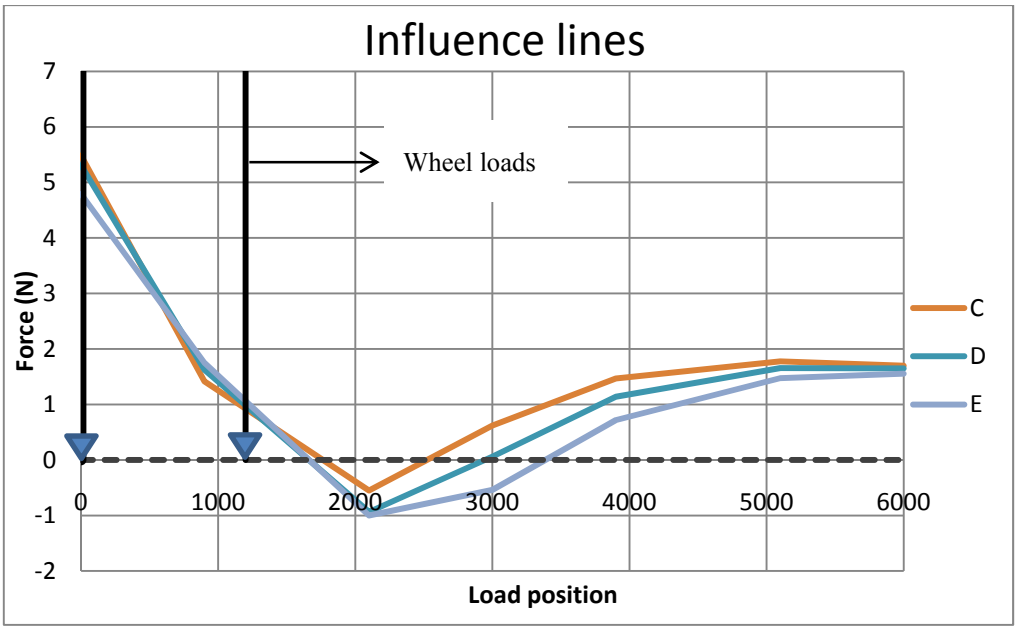


*Figure 3.31 Placement of the wheel loads in order to obtain maximum tensile forces*

Therefore, it was decided to precede the analysis by placing the loads starting from the end of the bridge in order to achieve maximum tensile forces in the interface of girder-deck connection.

## 3.1.11 Interfacial stresses

In the software Abaqus, the bridge model was analysed with different loading conditions with the intention to obtain the most severe cases in terms of high interfacial stresses between the FRP deck and the steel girders. The stresses acting on the contact area are peeling and shear stresses. These stresses are crucial to design an appropriate and safe connection.

### 3.1.11.1 Tensile peeling stresses

To attain the maximum peeling stresses the position of the wheel loads was determined in section 3.1.10 according to the influence lines. The wheel loads are applied at the end of the lane and just two wheel areas instead of four having a distance of 1.2 meters in the longitudinal direction of the bridge and the same load of axles are applied (see Figure 3.32). The load applied on one area is calculated as shown in equation (3.4) and it has a value of approximately 2.3 N/mm$^2$. It has to be mentioned that this is the worst case of obtaining the maximum peeling stresses. In reality, there are four wheel loads and it will help in distribution of the forces over a larger area and the resulting peeling stresses would be smaller. The reason of using two wheel areas was to have compatibility with the determination of the influence line where a sole point load was exerted.

$$\gamma_F * \alpha_{Q1} * Q_{1k}/A \qquad (3.4)$$

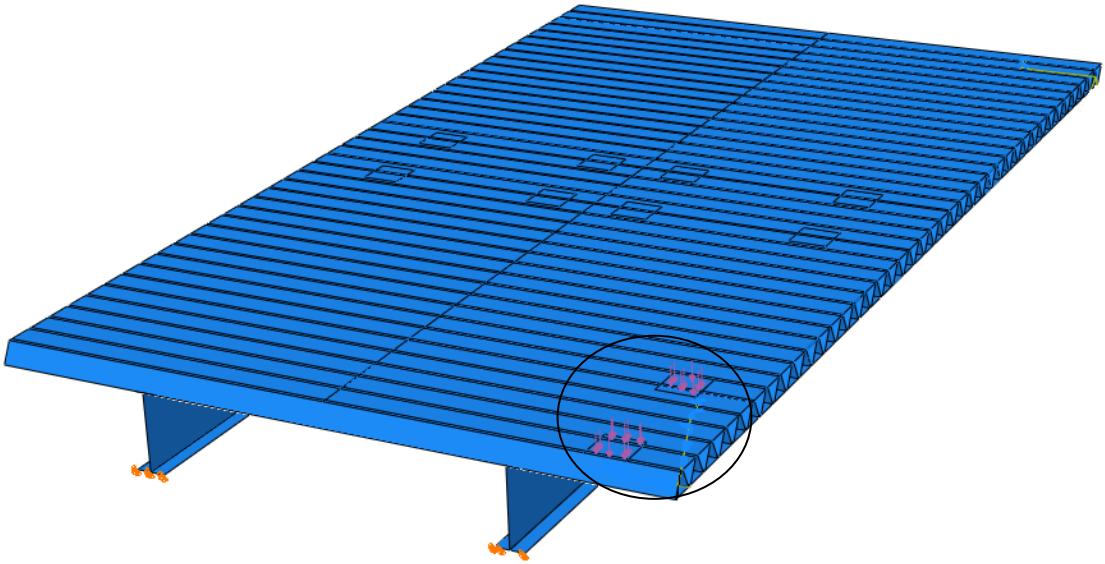

*Figure 3.32 The application of loads to obtain maximum peeling stresses*

In Figure 3.33, the deformation of the bridge and the location of the maximum peeling stress in the contact area between the girder and the deck are displayed.

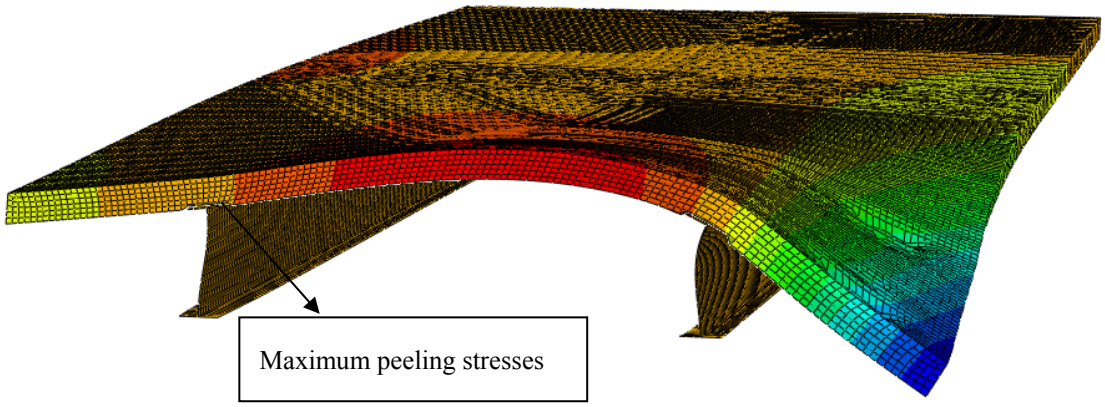


*Figure 3.33 The deformation of the bridge and the location of maximum peeling stresses*

The peeling stresses along the edge of the flange of the girder up to the length of 3 meters are shown in Figure 3.34. The maximum tensile stress obtained has a value of 11 MPa. This stress has to be taken into account while designing the connections between the girder and the deck.

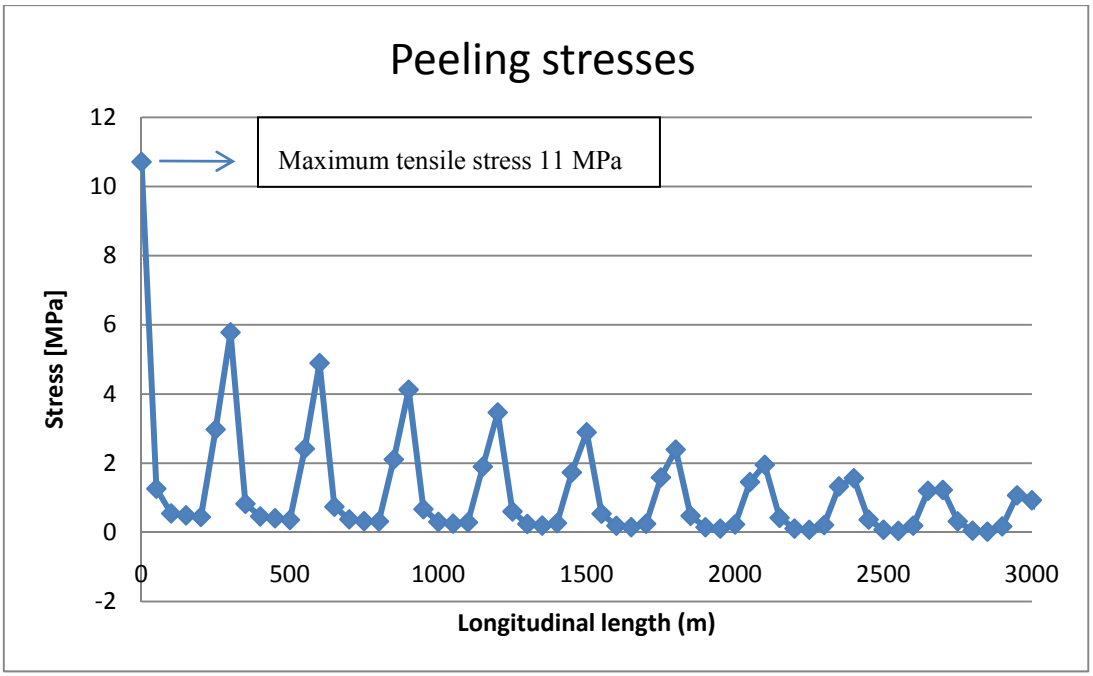


*Figure 3.34 Maximum peeling stresses along the edge of the girder flange in the longitudinal direction of the bridge*

### 3.1.11.2 Shear stresses

Maximum shear stresses between the girder and the deck are attained when the braking and lateral forces are applied in the model. Two different models were run in the software ABAQUS (ver. 6.8.2) by applying the braking load and the lateral load separately. These forces have to be applied in the same time according to Euro code, but for ease of understanding these loads are applied distinctly. Both loads are applied in the end and in the middle of the bridge in order to find the case where the shear stresses reach the maximum value. Braking load can be applied as a line load along one lane and the lateral force as a concentrated force in the same position as the braking load. In the software ABAQUS (ver. 6.8.2) the type of line load was not functioning thus the braking load was applied as a distributed traction load on an area of 40x3000mm on the surface of the deck. The lateral load was applied on the same way but in different direction (see Figure 3.35).

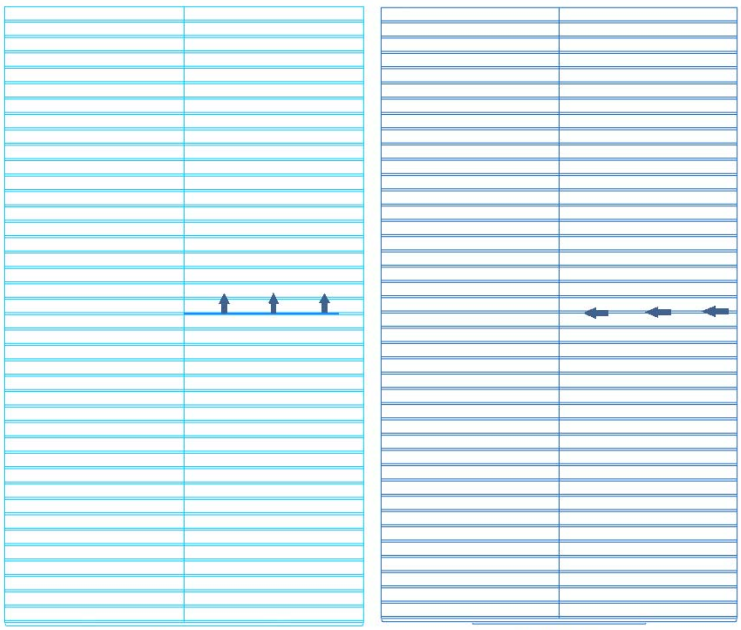


*Figure 3.35 The application of the braking and lateral load in the middle of the bridge in the software Abaqus*

In the case of applying the lateral load, the finite element model was modified by adding U-diaphragms as it was in the original old bridge (see Figure 3.36). Three diaphragms were assembled together with the girders. The necessity of the stiffeners in this particular analysis was to prevent the girders from large lateral torsional buckling and to get more reasonable and correct results.

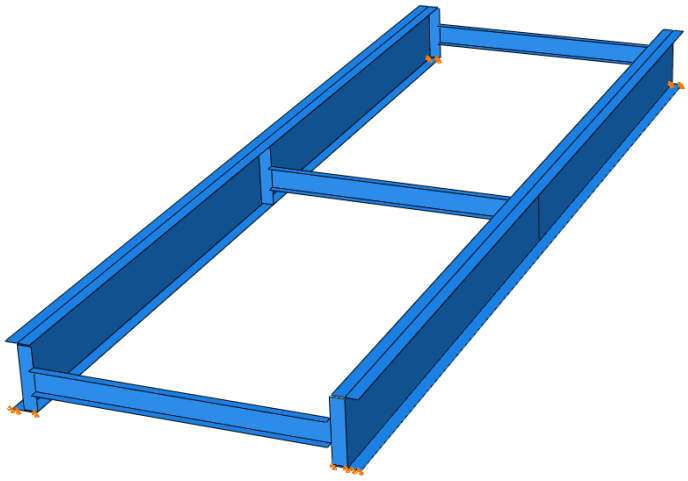

*Figure 3.36 The configuration of the girders and stiffeners frame*

As it was mentioned before, the braking load was applied in the end of the bridge and in the middle. It was seen that the maximum shear forces in the contact area between the girder and the deck were obtained when the load was applied in the end (see Figure 3.37). The global axis is as indicated in Figure 3.37; y-axis is in the longitudinal direction of the bridge, x-axis is in the transverse direction of the bridge and z-axis is perpendicular to the bridge.

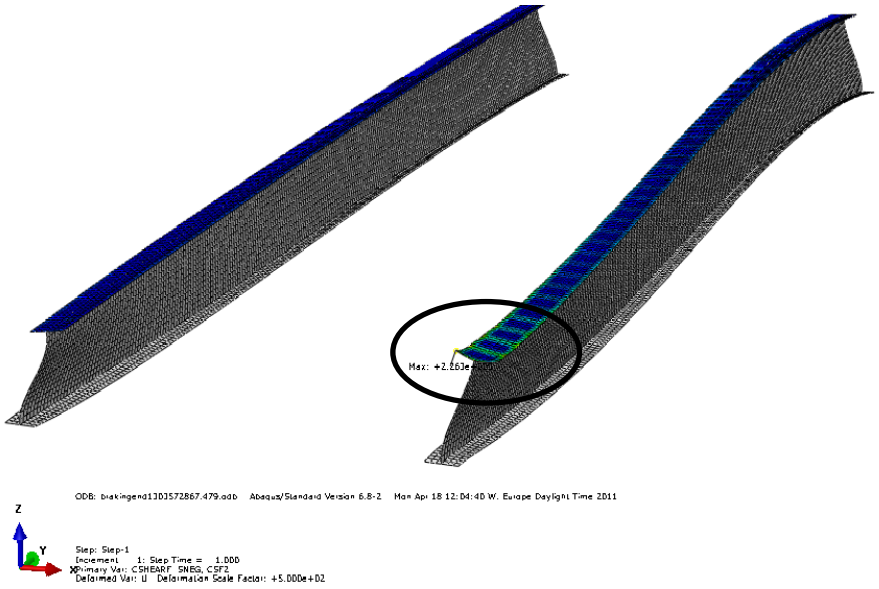


*Figure 3.37 Location of maximum longitudinal shear forces when braking load in the end is applied*

Along the edge of the girder flange where the maximum shear force acts, a path was taken and the shear forces were plotted. The maximum shear forces are at the location where the load is applied (see Figure 3.38 and Figure 3.39).

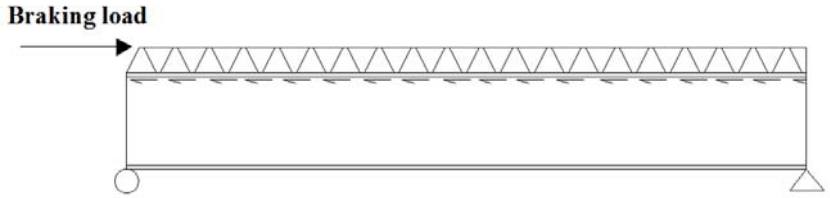


*Figure 3.38 Location where the braking load is applied in the model*

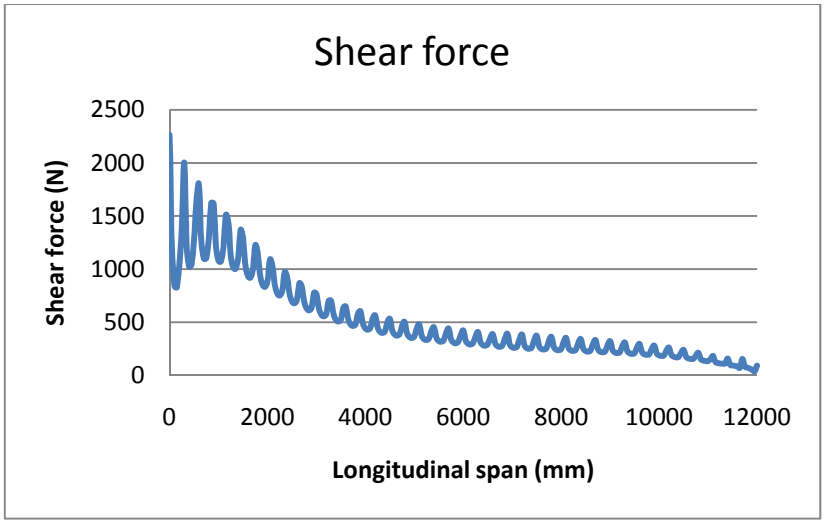


*Figure 3.39 Longitudinal shear force in the contact area between the girder and the deck*

The shear stresses were computed by dividing shear force output to the contact nodal areas extracted from ABAQUS. In Figure 3.40, longitudinal shear stresses are displayed.

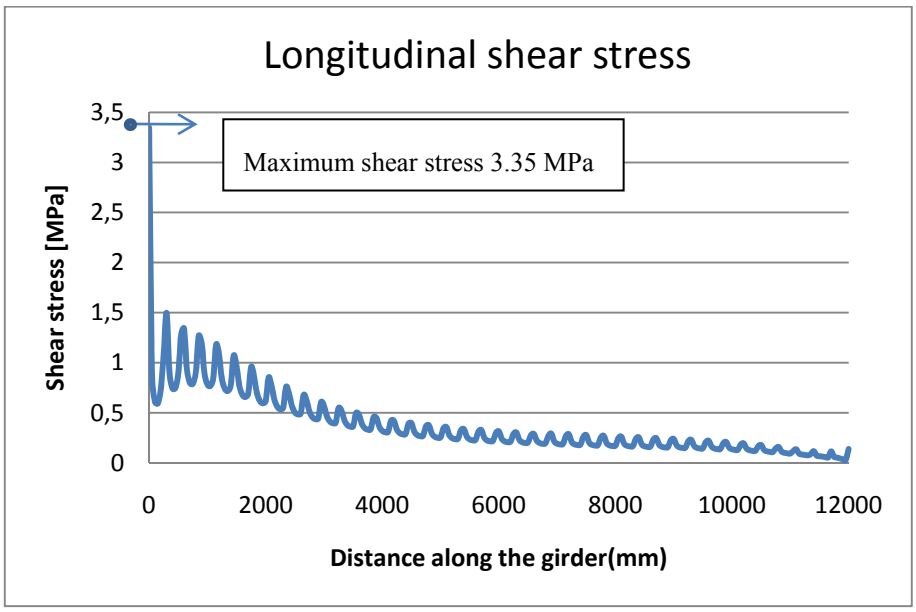


*Figure 3.40 Interfacial longitudinal shear stresses when braking load is applied in the end of the bridge*

The maximum contact longitudinal shear stress is 3.35 MPa. The transverse shear stresses were examined as well. The variation of the shear stress along the longitudinal direction of the bridge is illustrated in Figure 3.41.

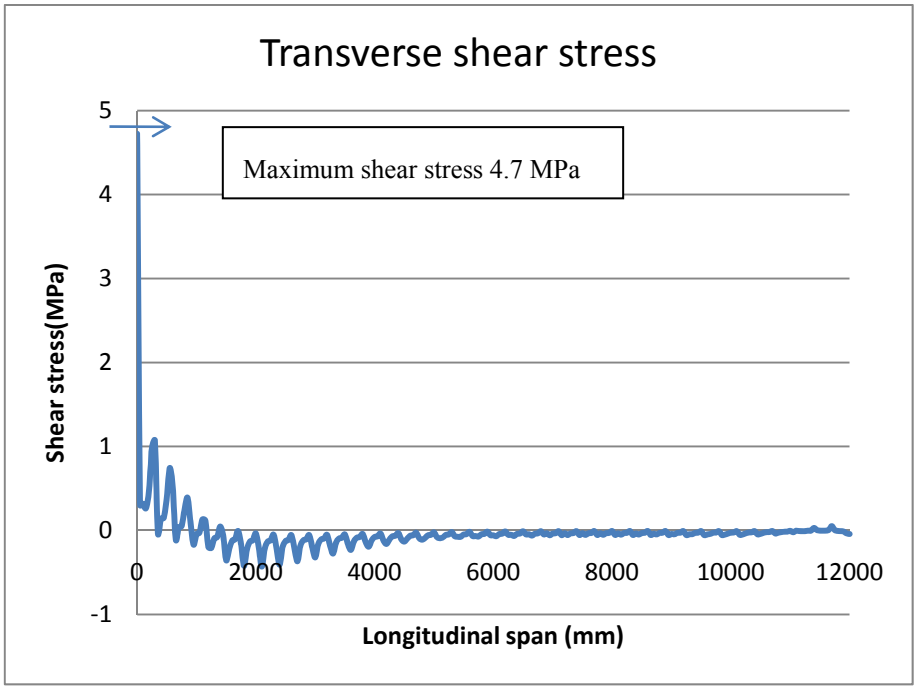


*Figure 3.41 Variation of transverse shear stresses along the longitudinal direction of the bridge*

The same procedure was followed when the lateral load was applied in two positions that are in the end and the middle of the bridge. When the lateral load is applied in the middle the deformation of the girders and stiffeners is displayed in Figure 3.42.

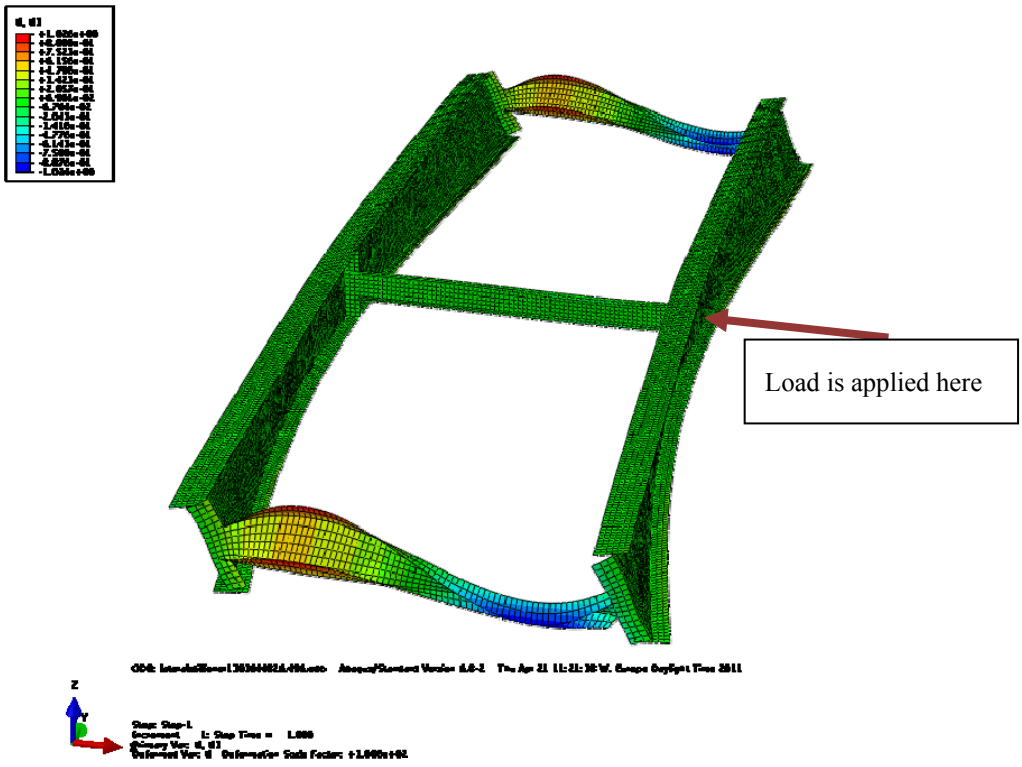


*Figure 3.42 The deformation of the girders and stiffeners when lateral load is applied in the middle*

The contact longitudinal and transverse shear forces in the longitudinal direction of the bridge are shown in the following figures.

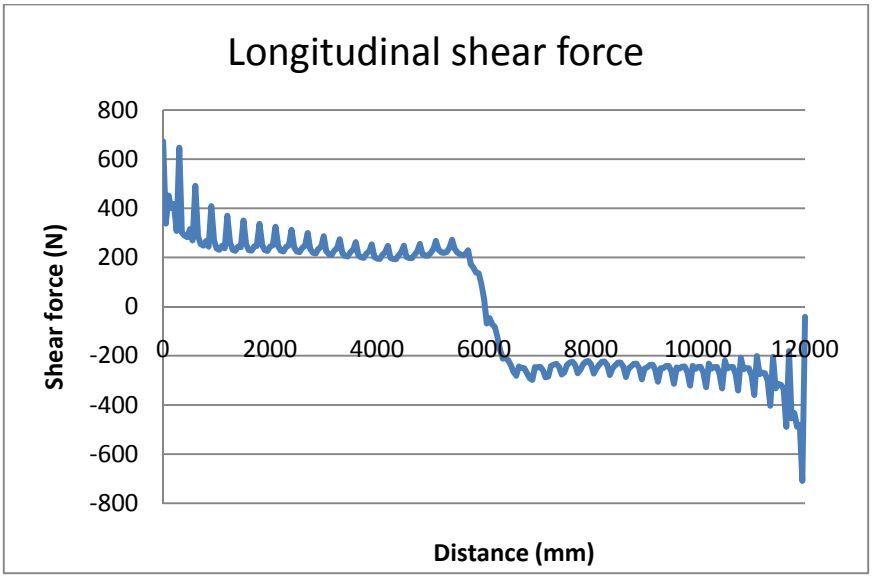


*Figure 3.43 Contact longitudinal forces along the girder*

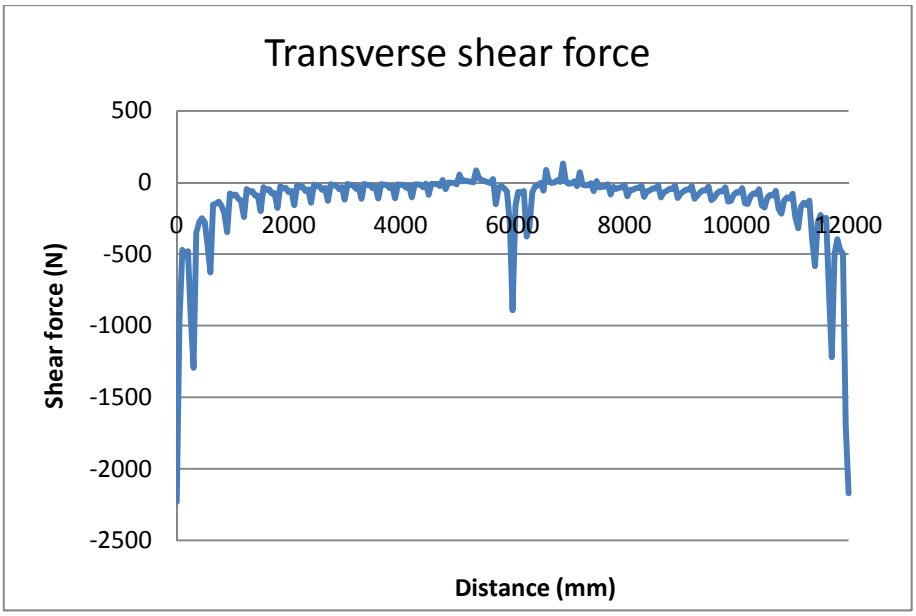


*Figure 3.44 Contact transverse shear forces along the girder*

Longitudinal shear forces are as they are expected when a load is applied on a simply supported girder as illustrated simply in Figure 3.45.

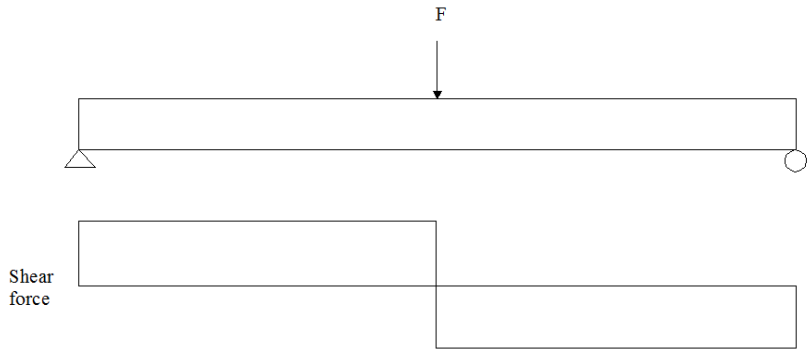


*Figure 3.45 Illustration of the shear force distribution in a simply supported girder*

The non-uniform distribution of the shear force with high concentrations is due to the cellular geometry of the deck where the deck webs are utilized to transmit the forces.

In Figure 3.44, three peak points of shear forces are observed. The first two are in the edges and the third one is where the load is applied. The forces are distributed according the stiffness of the system. The stiffer parts attract and carry more forces. In this case the stiffness of the system is larger at the ends of the bridge where the boundary conditions are applied. The middle of the bridge is less stiff than the edges (see Figure 3.46). Nevertheless the U-diaphragms contribute to the stiffness of the system. This can be verified as well by examining the deformation of the frame in Figure 3.42 where the U-diaphragms at the edges experience a higher deformation.

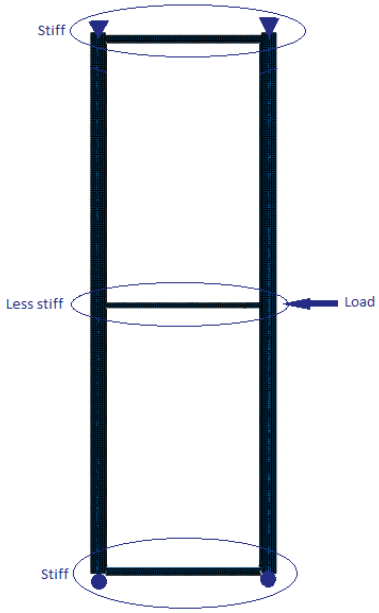


*Figure 3.46 Sketch of the stiffness of the system*

When the load is applied on the end of the bridge the force will be carried mostly by one of the stiff portions. Consequently, the contact shear stresses will be higher than the ones obtained in the previous case. The results when lateral load is applied in the end of the bridge are depicted in Figure 3.47 and Figure 3.48 for longitudinal and transverse contact shear stresses respectively.

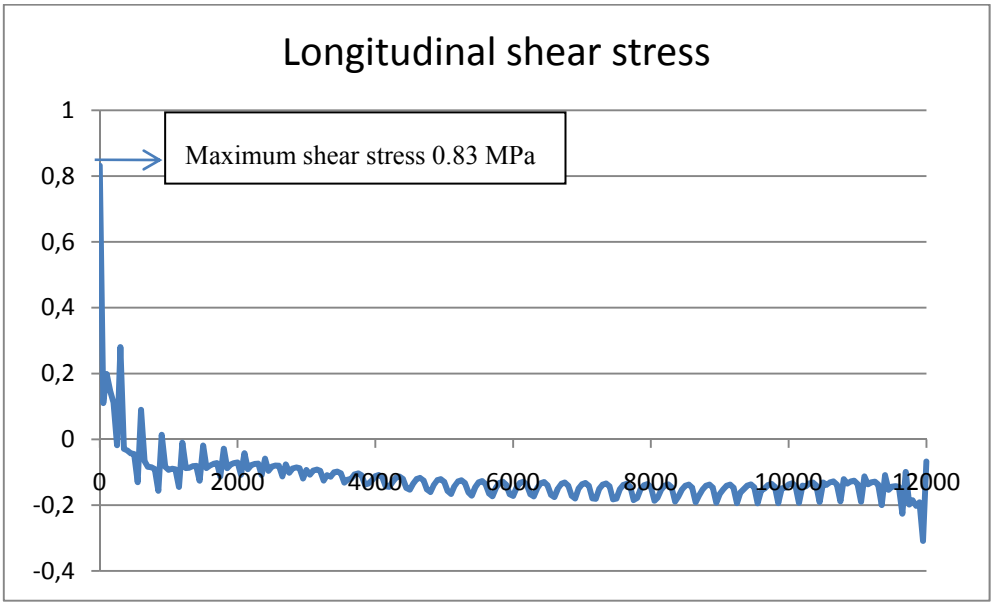


*Figure 3.47 Longitudinal contact shear stress*

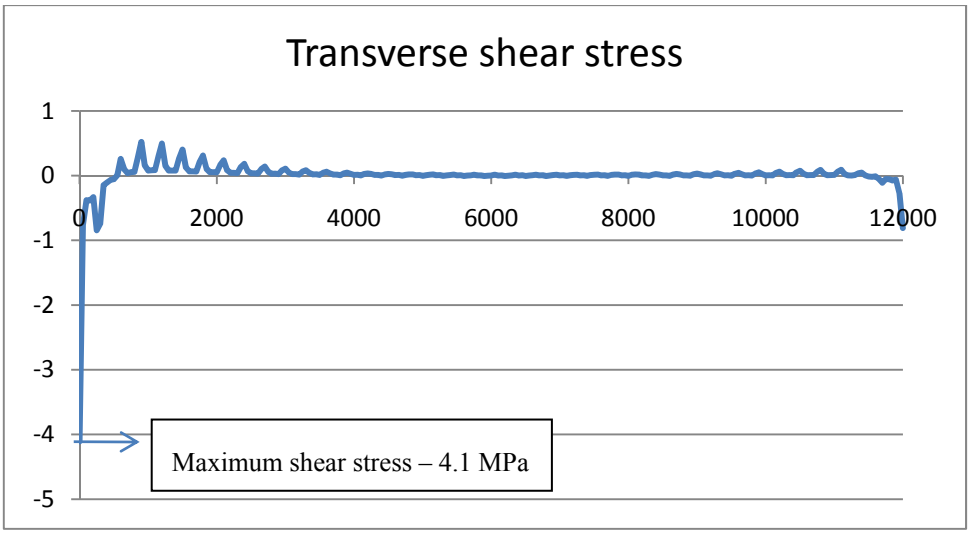


*Figure 3.48 Transverse contact shear stresses*

All of the results of maximum tensile peeling and shear stresses are summarized in the table below.

*Table 3.10 Maximum peeling and shear stresses in the interface between the girder and the deck*

| Property | Vertical load | Braking load | Lateral load |
|---|---|---|---|
| Tensile peeling stress [MPa] | 11 | - | - |
| Transverse shear stress [MPa] | - | 4.7 | 4.1 |
| Longitudinal shear stress [MPa] | - | 3.35 | 0.83 |

### 3.1.12 Strength verification of adhesive bonding

The maximum peeling and shear stresses acting on the interface between the steel girders and the FRP deck were determined by finite element analysis as presented in the preceding section. In case of adhesive bonding, the strength verification is done by referring to the literature review. In bonded connections it was observed that the failure mode is the delamination of the FRP in outer mat layer close to the bonding line but not in the adhesive. The adhesive used in this research was SikaDur 330 epoxy. Through-thickness tensile-shear interaction strength of adhesive bonding was developed by Keller et. al. The shear-tensile strength curves for 5 mm and 10 mm thick coupons are depicted in Figure 3.49. The strength values of 10 mm coupons are less and it is believed that fibre architecture of the coupons influences the strength. In this study, the thickness of the FRP deck flanges bonded to steel girder is 15 mm and the curve for 10 mm thick coupon is taken into account. The pure through-thickness tensile strength is 8 MPa and pure through-thickness shear strength is 19.3 MPa for 10 mm thick coupons.

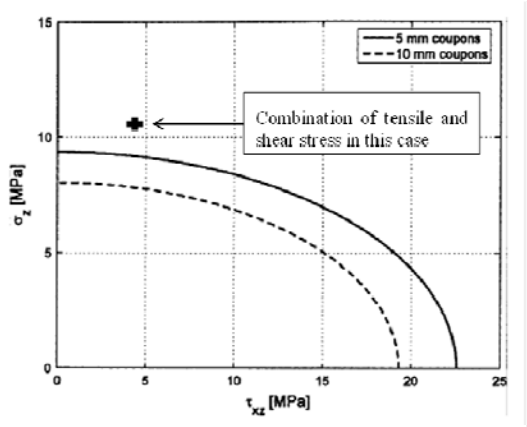


*Figure 3.49 Combined shear-tensile strength for adhesively bonded FRP coupons*

Maximum peeling stress in the interface between FRP deck and steel girders in this study was determined as 11 MPa. This value exceeds the pure through-thickness tensile strength of the bonded connection determined by Keller et. al. It has to be reminded that the worst case and conservative assumptions were considered while finding the maximum tensile stress acting on the interface between FRP deck and steel girders. The action of the vehicle was placed only by two wheel loads instead of four. Furthermore, the simplifications made while modelling the bridge in finite element analysis result in higher stresses. Shear stresses induced in the joint presented in Table 3.10 are well below the shear strength of the adhesive bonding. Thus, the critical stresses in the joint are peeling stresses.

### 3.1.13 Design and detailing of the connections

In this thesis, detailing has been covered by means of general solution but no detailed design has been done.

*Bolted connections*

The connections of non-composite bridges should be designed to prevent the transverse movement and the uplift of the deck. These connections in FRP-steel bridge applications have been done by using bolts between the steel girder flange and bottom flange of FRP deck. This design should be avoided when possible due to stress concentrations around the bolt holes of the FRP deck flanges which might cause rupture of the FRP deck.

In this study, a bolted connection combined with adhesive bonding is developed in order to avoid drilling holes in the FRP deck flanges. The bolts are inserted in a steel plate and this steel plate is adhesively bonded to the FRP deck. This procedure can be done off-site while manufacturing the deck panels. In site, another steel plate is placed between the deck and the steel flange and the bolts are tightened (see Figure 3.50). Between the girder flange and the deck a rubber pad can be located in order to make possible a uniform distribution of the forces.

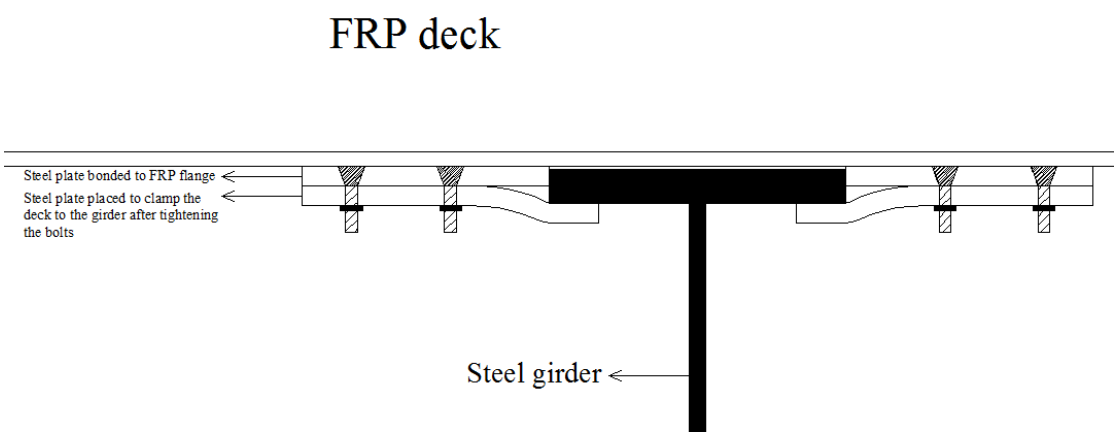


*Figure 3.50 Bolted connection between the FRP deck and steel girders*

The design of these connections is done by considering the lateral forces which cause shear stresses in the connection and the vertical loads which might cause lifting of the deck causing tensile forces on the connections. When lateral load is applied it is assumed that this load will be resisted by two connections (see Figure 3.51). These forces will be transferred to the bolts through the adhesive bonding. Thus the strength of the adhesive has to be taken into account in the design of the connection.

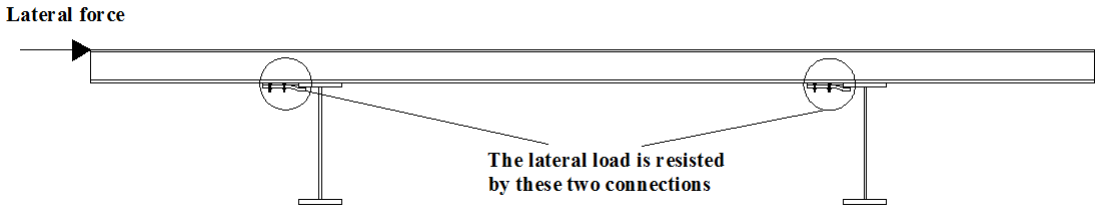


*Figure 3.51 Configuration of how the lateral load is resisted by the connections*

The adhesive which is used in the design is SikaDur 330 epoxy. The mechanical properties of this adhesive are given in Table 3.11.

*Table 3.11 Tensile and compression properties of SikaDur 330 epoxy adhesive*

| Property | Strength [MPa] | Flexural E-modulus [MPa] | Tensile E-modulus [MPa] |
|---|---|---|---|
| Tension* | 30 | 3800 | 4500 |

*These properties were taken by the manufacturer

In order to design the required spacing of the bolts uplift forces on the interface between the deck and the girders are attained from the finite element modelling. In Figure 3.52, peeling stresses along the girder for 3 meters is depicted. The total tensile forces for three meters are considered to decide the spacing of the bolted connections. The tensile forces will be resisted by the tension resistance of the bolts. It was observed that one bolted connection could carry the sum of tensile forces that act along 1 meter (marked area in Figure 3.52).

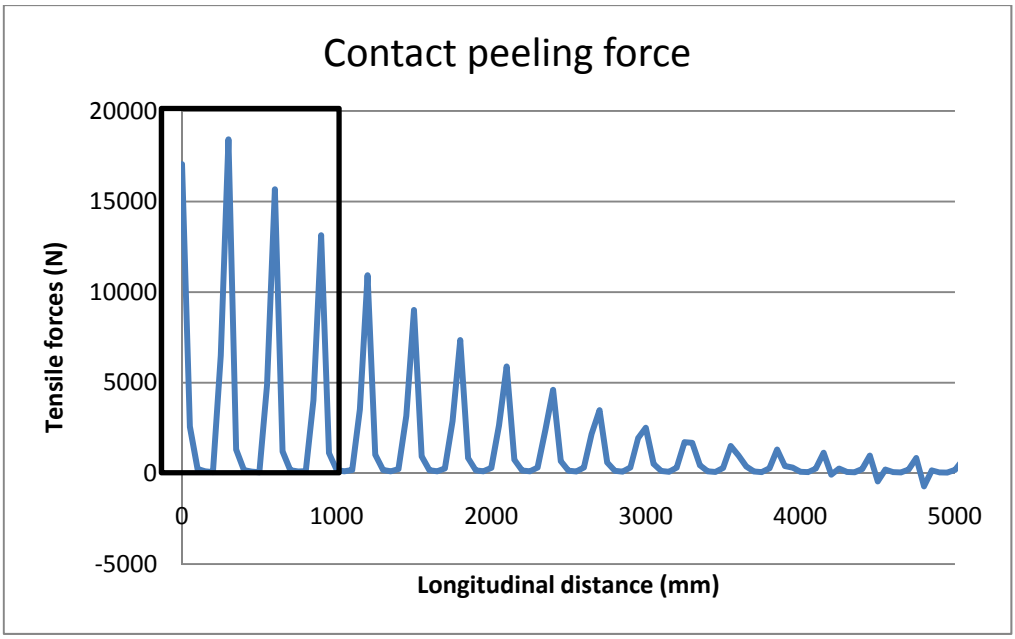


*Figure 3.52 Contact tensile forces on the contact interface between the girder and the deck*

The calculations can be followed in detail in the Appendix. Countersunk bolt class 8.8 having a diameter of 14mm were chosen. The steel plate which is bonded to FRP deck was found to be sufficient with an area of 200x80mm. The force is transferred from the adhesive to the bolts. The peeling stresses in the adhesive are computed to be 5.5 MPa which is smaller than 8MPa, the stress capacity of the bonded connection between FRP and steel determined by Keller et. al. The connections are placed in both sides of the girder flange but in the calculations in order to be on the safe side, there is done a simplification by considering that the peeling stresses are resisted by one bolted connection. Essentially, peeling stresses will be distributed to both connections. The spacing of the bolted connections is decided to be one meter. A total number of 13 connections will be installed for the bridge of 12 meter long in each side of the girder flange. The connection details are illustrated in Figure 3.53.

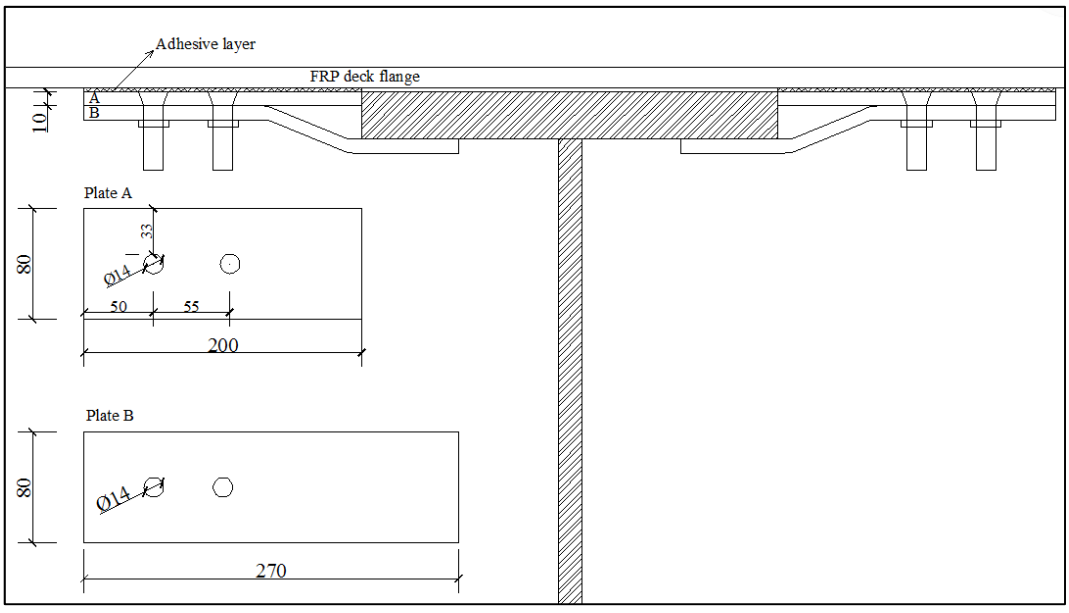


*Figure 3.53 Configuration and dimensions of the bolted connection*

This type of connection is easy to install. The steel plates with the bolts bonded to the FRP deck will be prefabricated and the tightening of the bolts will take place on-site which is a simple procedure and not labour intensive.

*Adhesive connections:*

The application of adhesive bonding is straightforward. The adhesive is applied on the steel flanges and the deck is placed on the top. Curing of the adhesive takes 48 hours.

*Shear stud connections:*

The shear stud connection developed in this study is different from the ones that have been applied by other researchers. The shear stud connections applied up to now are discrete and the composite action between the girders and the deck is consequently lower. In this study, a shear stud connection with continuous concrete over the girder is developed. The shear studs were determined to have a diameter of 22 mm and a height of 150mm. The spacing of the connectors in the cross-section was determined to be 55 mm and in the bridge longitudinal direction the shear studs are spaced by 350 mm (see Figure 3.54). These shear studs were checked for fatigue loading as well. The extended design life of the bridge was decided to be 25 years. The analytical calculations showed that these shear studs resisted fatigue loading.

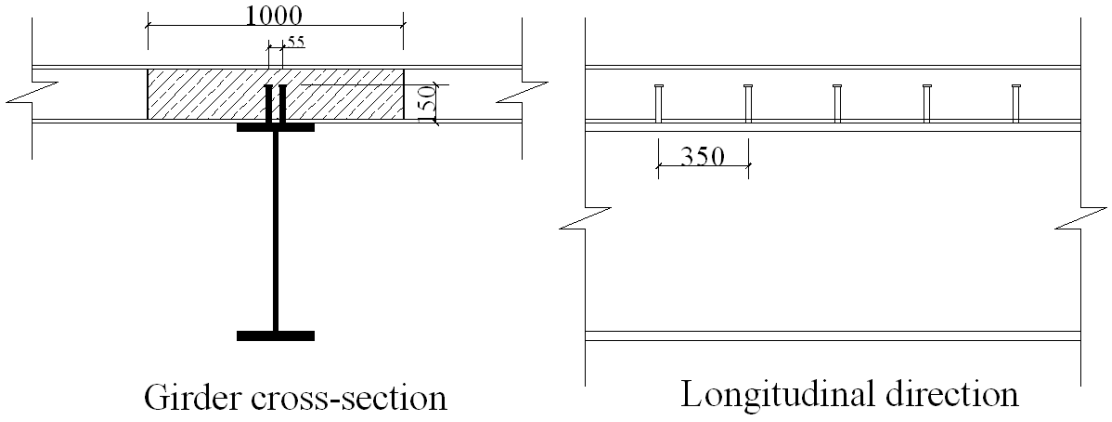


*Figure 3.54 Configuration of the shear stud connections*

In order to investigate the transformation of the loads from the FRP plates to the concrete and to get a basic perception of the stress values induced in the FRP-concrete face, a finite element analysis was performed in ABAQUS (ver. 6.10.2). The bridge was modelled with 3D-solid elements. The interface between the concrete and FRP plates was not modelled, instead they were merged together. Vertical loading in ultimate limit state was applied. Stresses in the concrete and FRP plates were checked. Transverse stresses of the deck are depicted in Figure 3.55. The marked area in the figure is the location where the concrete block ends and it can be observed some stress concentrations in the FRP plate. These stresses are of magnitude 25 MPa, which are quite lower than the strength of FRP plates.

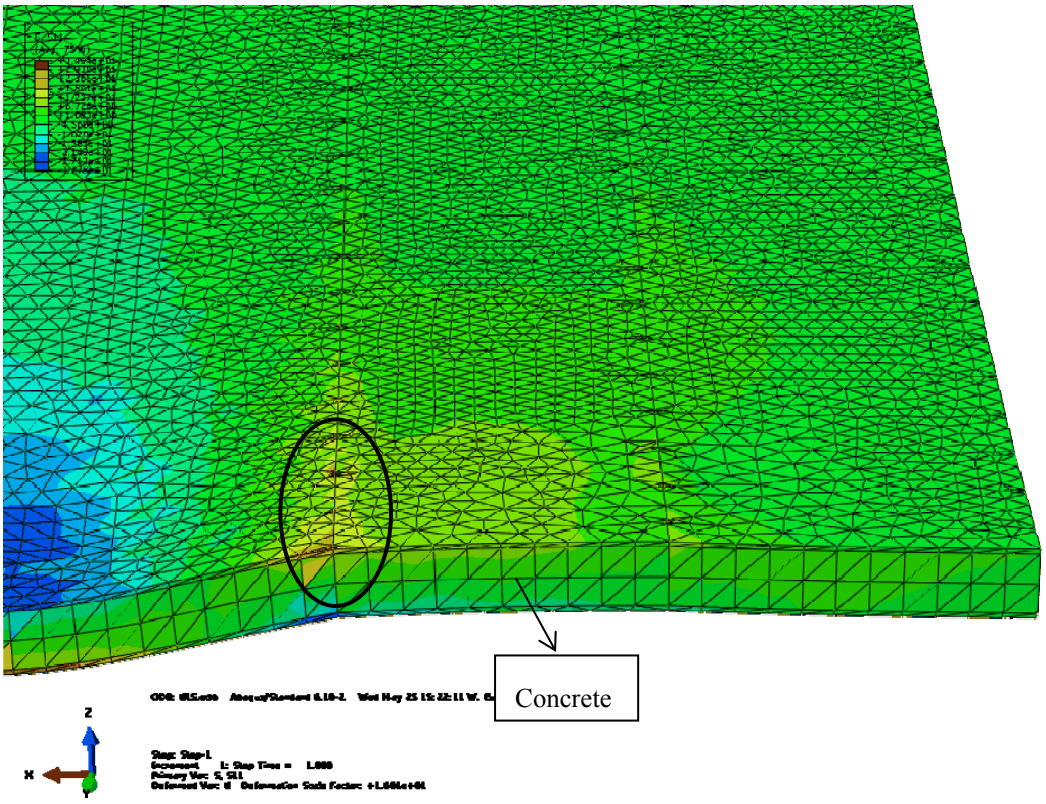


*Figure 3.55 Transverse stresses in concrete and FRP plates*

The difference in stresses in the interface between the concrete and FRP plates is approximately 1 MPa. This is a small difference because the elasticity modulus of concrete and FRP plates is 30MPa and 23 MPa respectively. However, in the longitudinal direction the difference of stresses in the interface is higher. The interfacial stresses between concrete and FRP plate in the longitudinal direction are approximately 10 MPa. These stresses have to be taken into account when the interfacial shear strength between the concrete and FRP plates are identified. In addition, maximum and principal stresses on the concrete were inspected. Maximum principal stresses were on the top surface with a value of approximately 10 MPa. In order to prevent cracking of the concrete tensile reinforcement can be provided. Minimum principal stresses were about -20 MPa, which is the same value as concrete design compression strength. Thus, concrete can carry the resulting load induced stresses.

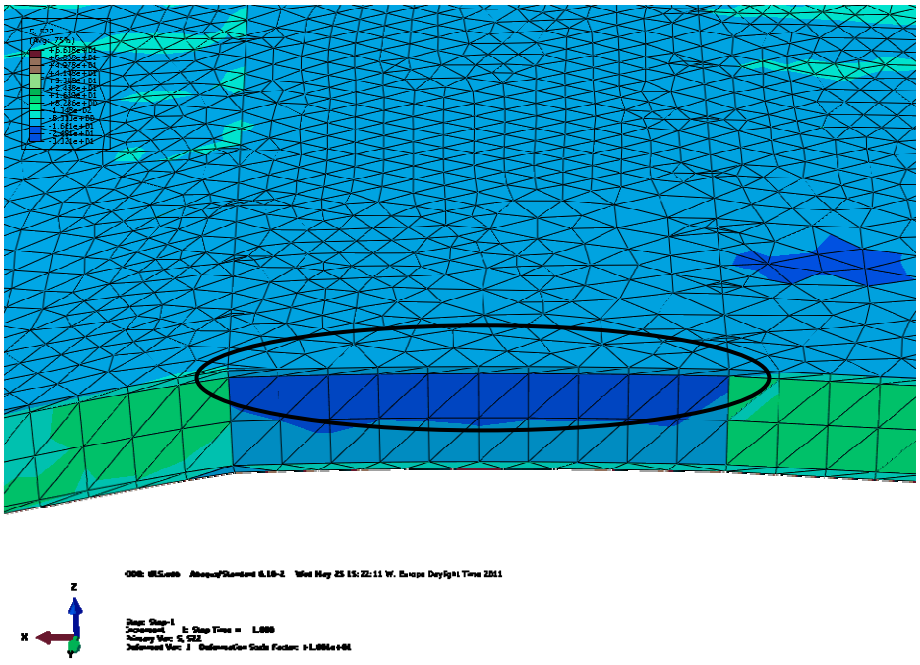

*Figure 3.56 Axial stresses in the deck*

Manufacturing of this deck is deemed to be off-site. The concrete will be casted off-site and holes for the shear studs will be prepared. The shear studs will be welded to the steel girder on-site. By prefabricating the concrete the effect of shrinkage and creep will be reduced due to controlled conditions during casting. After welding the shear studs the holes can be filled with non-shrink grouting and FRP plate is placed in the top. The configuration of the bridge with shear stud connections is shown in Figure 3.57.

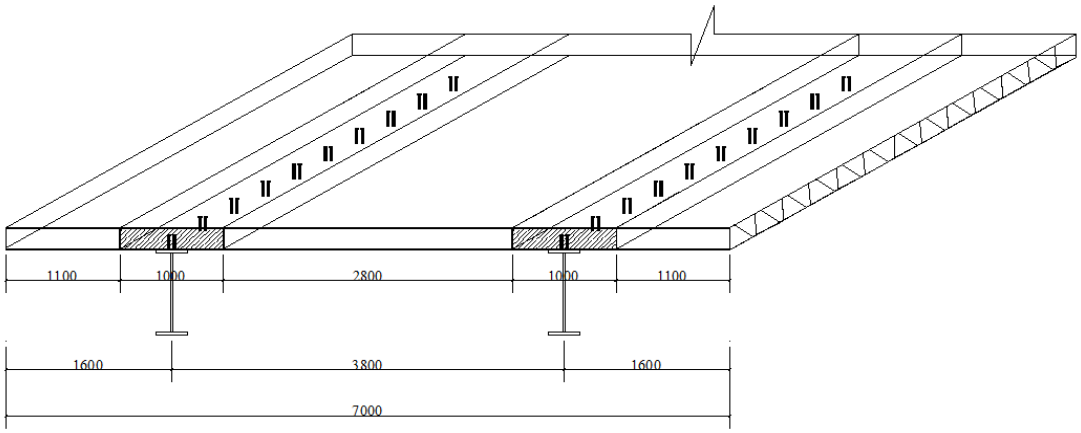


*Figure 3.57 Illustration of shear stud connections in the bridge*

# 4 Conclusions

A feasibility study was conducted on replacing and upgrading a concrete deck with an FRP deck. The aspects which were considered in this study are: girders working compositely and non-compositely with FRP deck, feasible types of connections between the deck and the girders and the behaviour of FRP deck. The following conclusions can be drawn from this study:

- A significant stress reduction 11.9% could be obtained by replacing the concrete deck with the lightweight FRP deck. This confirms the benefit of light-weight FRP decks which allows for increase in traffic loads.
- Bolted connection is a promising solution in connecting FRP decks to the steel girders when no composite action is intended. In this study a combination of adhesive bonding and bolts is proposed in order to avoid drilling holes in the FRP deck which might cause stress concentrations and rupture of the FRP. This connection which facilitates an easy on-site assembly has sufficient capacity to sustain load effects resulting from the interaction between the deck and the steel girders.
- In order to achieve higher stress reduction in the superstructure, the deck can be designed to act compositely with the underlying girders. Two different solutions were considered in this study; connecting the steel girder and FRP deck with adhesive bonding and shear studs connections in combination with concrete. The stress reductions achieved were 21.5% and 29.4 % respectively. The stress reduction when incorporating concrete in the connection is higher. The participation of the concrete will enhance the structural performance of the hybrid girder as a compressive flange. Thus; it is worth to attain composite action between the deck and the girders. This will lead to higher stress reductions, enhanced structural performance as well as lower costs.
- Adhesive bonding might be advantageous to the shear stud connections owing to easy installation process. However, the stresses induced in the interface might be higher than the capacity of FRP bonded to steel due to the failure of the FRP itself. The stresses in the case study considered in this thesis were higher than the capacity of FRP bonded coupon tests reported in the literature. It is worth mentioning that these stresses can be partially attributed to some simplifications made in the finite element modelling. Further research with more detailed model is needed on this problem.
- Shear stud connections have adequate capacity to bear the loads. In order to achieve rapid installation, the concrete can be incorporated during prefabrication of the deck. Further study has to be done to develop the proposed connections considering factors such as prefabrication, installation and local effects in the design.
- Configuration of the geometry of the deck is vital since it influences the performance of the deck. Asset deck exhibits a truss action while transferring the forces. Concentrated forces and stresses are obtained in the intersections between the webs and the girders, which might be critical for the bearing capacity of the deck.

# 5 Further research

In the feasibility study of this thesis Asset deck was investigated. Other FRP deck systems need to be studied as well, since the properties of FRP decks vary from system to system.

In an Asset deck the level component connection is a critical area (see Figure 5.1). In these areas peak peeling stresses and moments are observed. The strength of the FRP perpendicular to the fibres is significantly lower than the strength parallel to the fibres. These concentrated peeling stresses would cause rupture failure to the FRP deck component connection areas.

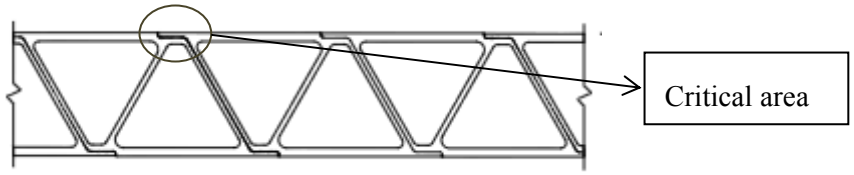


*Figure 5.1 Component level connection made of adhesive bonding of ASSET deck*

In order to reduce these concentrated stresses further investigation to optimize the deck for a better load transfer between the deck webs and flanges is necessary. Optimization can be done by considering factor such as geometry of the deck, constituent materials and fibre architecture.

When the deck is placed with the pultruded direction in the transverse direction of the bridge (as it is done today), concentrated stresses in the interface between the deck and the girders are obtained. If the deck is oriented in longitudinal direction of the bridge the problems of peak stresses will be avoided. In this case, however, the deflections of the deck will be higher, since the bi-directional behaviour of the deck is not very pronounced and the higher stiffness is required in the transverse direction of the bridge. In order to increase the transverse stiffness different solutions have to be developed.

Further research is needed in the design of the connections between the FRP deck and the steel girders. Once the conceptual designs of the connections especially bolt and shear stud connections are improved, testing of these connections is fundamental to verify the design. In addition, strength verification of bonded connections has to be researched by considering effects such as creep, moisture, temperature and fatigue.

Some other topics for further research that need to be investigated are:

- Proper modelling techniques
- Provide design models
- Vibration/damping ratios
- Long-term effects

# 6 References


(Cen), E. C. F. S. (2003) Eurocode 1: Actions on structures - part 2: Traffic loads on bridges. EN 1991-2:2003(

Alampalli, S. (2006) Field performance of an frp slab bridge. *Composite Structures,* 72(4)**,** 494-502.

Alampalli, S., O'connor, J. & Yannotti, A. P. (2002) Fiber reinforced polymer composites for the superstructure of a short-span rural bridge. *Composite Structures,* 58(1)**,** 21-27.

Alnahhal, W. & Aref, A. (2008) Structural performance of hybrid fiber reinforced polymer-concrete bridge superstructure systems. *Composite Structures,* 84(4)**,** 319-336.

Alnahhal, W., Aref, A. & Alampalli, S. (2008) Composite behavior of hybrid frp-concrete bridge decks on steel girders. *Composite Structures,* 84(1)**,** 29-43.

Alnahhal, W. I., Chiewanichakorn, M., Aref, A. J. & Alampalli, S. (2006) Temporal thermal behavior and damage simulations of frp deck. *Journal of Bridge Engineering,* 11(4)**,** 452-464.

Bai, Y., Vallée, T. & Keller, T. (2009) Delamination of pultruded glass fiber-reinforced polymer composites subjected to axial compression. *Composite Structures,* 91(1)**,** 66-73.

Berman, J. W. & Brown, D. L. (2010) Field monitoring and repair of a glass fiber-reinforced polymer bridge deck. *Journal of Performance of Constructed Facilities,* 24(3)**,** 215-222.

Brown, D. L. & Berman, J. W. (2010) Fatigue and strength evaluation of two glass fiber-reinforced polymer bridge decks. *Journal of Bridge Engineering,* 15(3)**,** 290-301.

Camata, G. & Shing, B. (2005) Evaluation of gfrp honeycomb beams for the o'fallon park bridge. *Journal of Composites for Construction,* 9(6)**,** 545-555.

Dutta, P. K., Kwon, S.-C. & Lopez-Anido, R. (2003) Fatigue performance evaluation of frp composite bridge deck protypes under high and low temperatures.

El-Qaleoby, W., El-Aela, A. G., Abou-Taleb, H. A. & El-Sheik, A. H. *Manufacturing 3-d braided composite trusses*. Available online).

Gurtler, H. W. (2004) Composite action of frp bridge decks adhesively bonded to steel main girders.

Harries, K. A. & J.Moses (2007) Replacing a composite rc bridge deck with an frp deck - the effect on superstructure stresses.

Hassan, T. K., Reis, E. M. & Rizkalla, S. H. Innovative 3-d frp sandwich panels for bridge decks.

Hong, T. & Hastak, M. (2006) Construction, inspection, and maintenance of frp deck panels. *Journal of Composites for Construction,* 10(6)**,** 561-572.

Jerome S. O'connor, J. M. H. U.S.A.'S experience using fibre reinforced polymer (frp) composite bridge decks to extend bridge service life.

Keelor, D. C., Asce, A. M., Luo, Y., Earls, C. J., M.Asce & Yulismana, W. (2004) Service load compression flange width in fiber reinforced polymer deck systems acting compositely with steel stringers.

Keller, T. & Gürtler, H. (2005a) Composite action and adhesive bond between fiber-reinforced polymer bridge decks and main girders. *Journal of Composites for Construction,* 9(4)**,** 360-368.

Keller, T. & Gürtler, H. (2005b) Quasi-static and fatigue performance of a cellular frp bridge deck adhesively bonded to steel girders. *Composite Structures,* 70(4)**,** 484-496.

Keller, T. & Gürtler, H. (2006) In-plane compression and shear performance of frp bridge decks acting as top chord of bridge girders. *Composite Structures,* 72(2)**,** 151-162.

Keller, T. & Schollmayer, M. (2004) Plate bending behavior of a pultruded gfrp bridge deck system. *Composite Structures,* 64(3-4)**,** 285-295.

Keller, T. & Schollmayer, M. (2006) In-plane tensile performance of a cellular frp bridge deck acting as top chord of continuous bridge girders. *Composite Structures,* 72(1)**,** 130-140.

Keller, T. & Schollmayer, M. (2009) Through-thickness performance of adhesive joints between frp bridge decks and steel girders. *Composite Structures,* 87(3)**,** 232-241.

Keller, T. & Vallée, T. (2005a) Adhesively bonded lap joints from pultruded gfrp profiles. Part i: Stress-strain analysis and failure modes. *Composites Part B: Engineering,* 36(4)**,** 331-340.

Keller, T. & Vallée, T. (2005b) Adhesively bonded lap joints from pultruded gfrp profiles. Part ii: Joint strength prediction. *Composites Part B: Engineering,* 36(4)**,** 341-350.

Kumar, P., Chandrashekhara, K. & Nanni, A. (2004) Structural performance of a frp bridge deck. *Construction and Building Materials,* 18(1)**,** 35-47.

Lombardi, N. J. & Liu, J. (2011) Glass fiber-reinforced polymer/steel hybrid honeycomb sandwich concept for bridge deck applications. *Composite Structures,* 93(4)**,** 1275-1283.

Majumdar, P. K., Liu, Z., Lesko, J. J. & Cousins, T. (2007) Analysis of cellular frp composite bridge deck utilizing conformable tire patch loading. *Composites and Polycon 2007*.

Majumdar, P. K., Liu, Z., Lesko, J. J. & Cousins, T. E. (2009) Performance evaluation of frp composite deck considering for local deformation effects. *Journal of Composites for Construction,* 13(4)**,** 332-338.

Moon, F. L., Eckel, D. A. & Gillespie, J. W. (2002) Shear stud connections for the development of composite action between steel girders and fiber-reinforced polymer bridge decks. *Journal of Structural Engineering,* 128(6)**,** 762-770.

Moses, J. P., Harries, K. A., Earls, C. J. & Yulismana, W. (2006) Evaluation of effective width and distribution factors for gfrp bridge decks supported on steel girders. *Journal of Bridge Engineering,* 11(4)**,** 401-409.

Motley, D. R., Castanos, S. A. & Klang, E. C. Effects of diagonal webs in frp bridge decks.

Nchrp Field inspection of in-service frp bridge decks.

Nilsson, M. (2002) Samverkansbroar ur ett samhällsekonomiskt perspektiv

Park, K.-T., Hwang, Y.-K., Lee, Y.-H. & Jung, J. (2007) Experimental study on durability comparison of the gfrp decks by resin types. *Journal of Civil Engineering,* 11(261-267.

Prachasaree, W. & Shekar, V. (2008) Experimental evaluation and field implementation of frp bridge deck modules. *Songklanakarin Journal of Science and Technology,* 30(4)**,** 501-508.

Reising, R. M. W., Shahrooz, B. M., Hunt, V. J., Neumann, A. R., Helmicki, A. J. & Hastak, M. (2004) Close look at construction issues and performance of four fiber-reinforced polymer composite bridge decks. *Journal of Composites for Construction,* 8(1)**,** 33-42.

Righman, J. (2002) Development of an innovative connection for frp bridge decks to steel girders.

Smith, C. (2001a) Environmental testing on pultruded structural shapes. *Composites 2001 Convention and Trade Show*.

Smith, C. (2001b) Environmental testing on pultruded structural shapes

Tuakta, C. (2005) *Use of fiber reinforced polymer composite in bridge structures.* Massachusetts Institute of Technology.

Turner, M. K., Harries, K. A., Petrou, M. F. & Rizos, D. (2004) In situ structural evaluation of a gfrp bridge deck system. *Composite Structures,* 65(2)**,** 157-165.

Zhou, A. & Keller, T. (2005) Joining techniques for fiber reinforced polymer composite bridge deck systems. *Composite Structures,* 69(3)**,** 336-345.

Zhou, A., Lesko, J. J., Coleman, J. T. & Cousins, T. E. Failure modes and failure mechanisms of fiber reinforced polymer composite bridge decks.

# APPENDIX

## Analytical Calculations

### 1. Old bridge data

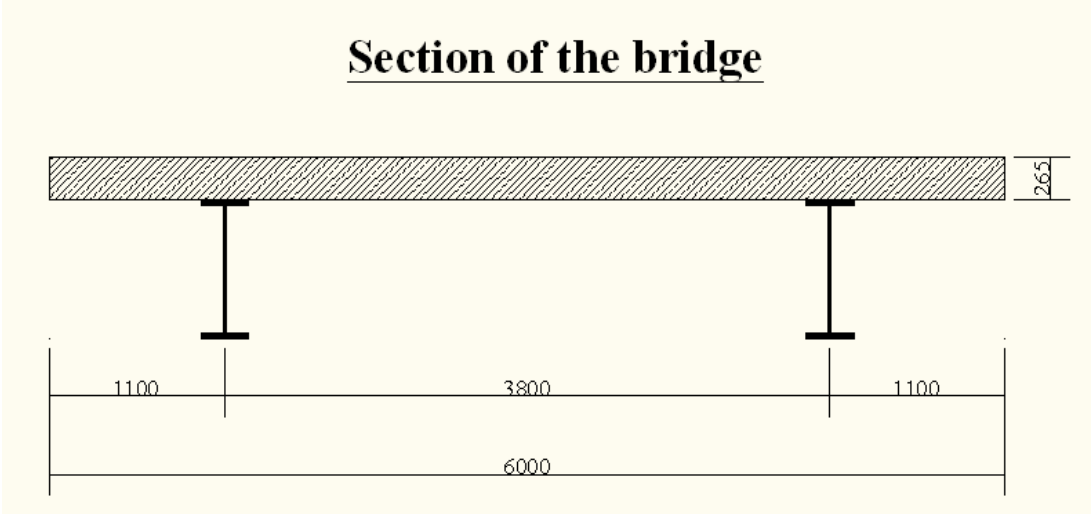


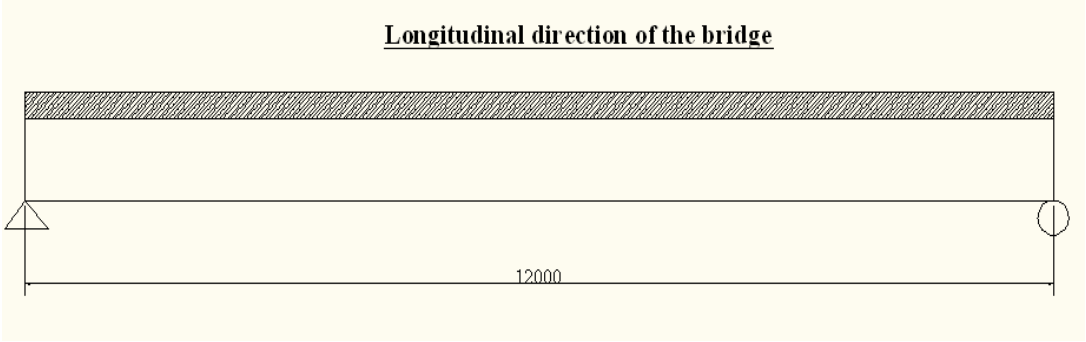


The measurements in the drawings are in mm.

### Bridge Data:

$L := 12m$ the span between the supports

$B_d := 6m$ the free span of the deck

$t_d := 265mm$ the average thickness of the concrete deck

**Steel girder dimensions:**

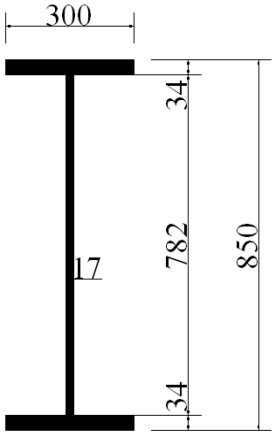


$H := 850mm$ height of the steel girder

$b_f := 300mm$ the width of the flange

$t_f := 34mm$ the thickness of the flange

$h_w := H - 2 \cdot t_f = 782 \cdot mm$ the height of the web

$t_w := 17mm$ the thickness of the web

$A_s := 2 \cdot t_f \cdot b_f + h_w \cdot t_w = 0.034\,m^2$

$$I_s := \frac{b_f \cdot H^3 - (b_f - t_w) \cdot h_w^3}{12} = 4.075 \times 10^{-3}\,m^4$$

**Material data**

Steel /ST44

$f_{yk} := 255MPa$ characteristic yielding strength

$f_u := 431.5MPa$ ultimate strength

$\gamma_s := 1$ partial factor for steel

$$f_{yd} := \frac{f_{yk}}{\gamma_s} = 255 \cdot MPa$$ design yield strength

$E_s := 210GPa$ the elastisity modulus of steel

$$\gamma_{steel} := 71.17 \frac{kN}{m^3}$$ density of steel

Concrete :

$$\gamma_c := 25 \frac{kN}{m^3}$$ density of concrete

## Load effects:

**Self weight**

**1. Concrete deck** **2. Steel girders**

$G_c := B_d \cdot t_d \cdot \gamma_c = 39.75 \cdot \frac{kN}{m}$ $G_s := A_s \cdot \gamma_{steel} = 2.398 \cdot \frac{kN}{m}$

**3. Asphalt layer**

$\gamma_{asphalt} := 23 \frac{kN}{m^3}$ $t_{as} := 10mm$

$G_{as} := B_d \cdot t_{as} \cdot \gamma_{asphalt} = 1.38 \cdot \frac{kN}{m}$

**4. Diaphragms**

The are three U-diaphragms used in the bridge.

$h_{dia} := 300mm$ $b_{dia} := 100mm$ $t_{dia} := 11mm$ $L_{dia} := 3741mm$

$V_{dia} := \left[h_{dia} \cdot t_{dia} + 2\left(b_{dia} - t_{dia}\right) \cdot t_{dia}\right] \cdot L_{dia} = 0.02 \cdot m^3$

$G_{dia} := \frac{3 V_{dia} \cdot \gamma_{steel}}{L} = 0.35 \cdot \frac{kN}{m}$

**4. Parapets**

$G_{par} := 250mm \cdot 320mm \cdot \gamma_c = 2 \cdot \frac{kN}{m}$

**Total characteristic self weight:**

$G_k := G_c + G_s + G_{as} + G_{dia} + G_{par} = 45.878 \cdot \frac{kN}{m}$

**The design self-weight for one girder**:

Ultimate Limit State $g_d := \frac{1.35 G_k}{2} = 30.968 \cdot \frac{kN}{m}$

Moment from the self-weight:

$M_{gc} := \frac{g_d \cdot L^2}{8} = 557.418 \cdot kN \cdot m$ $W_s := \frac{I_s}{\left(\frac{H}{2}\right)} = 9.589 \times 10^6 \cdot mm^3$

The maximum stress of the flange of the girder from the dead loads: $\sigma_{gc} := \frac{M_{gc}}{W_s} = 58.131 \cdot MPa$

## 2. New bridge data with FRP deck

The conrete deck is replaced with an FRP deck and it is widened one meter more.

$B_{FRP} := 7m$ the widened width of the FRP deck

$g_{FRP} := 925 \frac{N}{m^2}$ the weight of the FRP deck with reference to ASSET deck from Fiberline

The design self weight acting on one girder is:

$G_F := B_{FRP} \cdot g_{FRP} = 6.475 \cdot \frac{kN}{m}$

$G_{kF} := G_F + G_s + G_{as} + G_{dia} + G_{par} = 12.603 \cdot \frac{kN}{m}$

**The design self-weight for one girder**:

$G_{Fd} := \frac{G_{kF} \cdot 1.35}{2} = 8.507 \cdot \frac{kN}{m}$ Ultimate Limit State

$R_{Fd} := \frac{G_{Fd} \cdot L}{2} = 51.042 \cdot kN$

$M_{FRP} := \frac{G_{Fd} \cdot L^2}{8} = 153.126 \cdot kN \cdot m$

$\sigma_{gFRP} := \frac{M_{FRP}}{W_s} = 15.969 \cdot MPa$

## Traffic Loads :

The traffic loads are taken from the EN 1991-2 and load model 1 (LM1) is used for the calculations.

**1. OLD BRIDGE:**

Lane 1:

$L_L := 3m$ the width of the lane

$Q_{1k} := 300kN$ axle load

$q_{1k} := 9 \frac{kN}{m^2}$ uniformly distributed load

$\alpha_Q := 0.9$ $\alpha_{q1} := 0.7$ national adjustment factor

Lane 2:

$Q_{2k} := 200kN$ axle load

$q_{2k} := 2.5 \frac{kN}{m^2}$ uniformly distributed load

$\alpha_{q2} := 1$

In the figure below the characteristic values are shown.

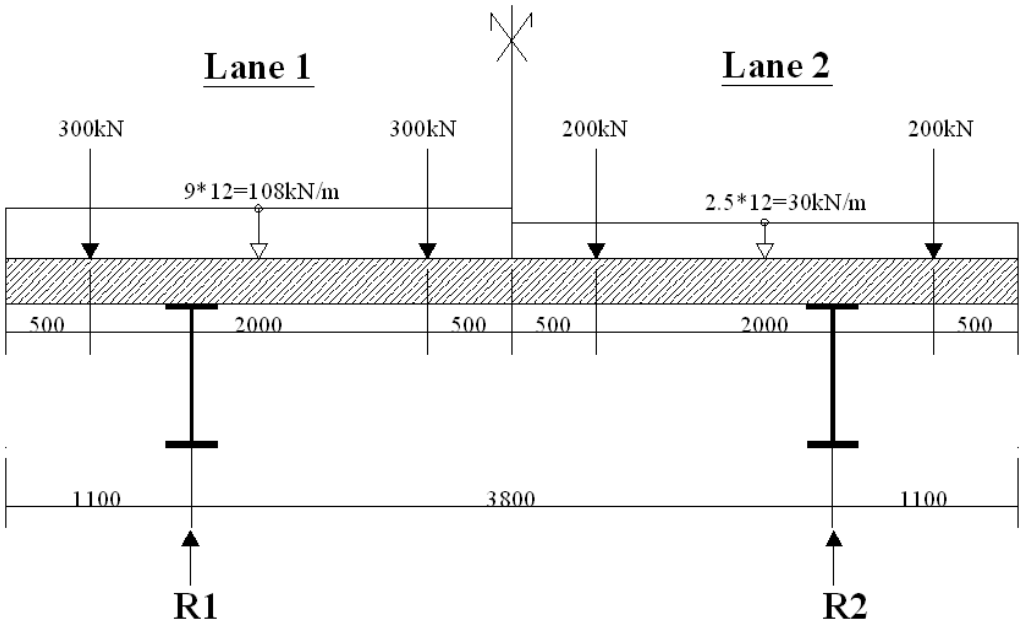

$C_c := 3.8m$ the distance between the main girders

$L_c := 1.1m$ the overhang distance

$S_1 := 2m$ the distance between wheel loads

$S_2 := 0.5m$ the distance between the end of the lane and the wheel load

$$Q_{1d} := 1.35\alpha_Q \cdot Q_{1k} = 364.5 \cdot kN \qquad q_{1d} := 1.35\alpha_{q1} \cdot q_{1k} \cdot L = 102.06 \cdot \frac{kN}{m}$$

$$Q_{2d} := 1.35\alpha_Q \cdot Q_{2k} = 243 \cdot kN \qquad q_{2d} := 1.35\alpha_{q2} \cdot q_{2k} \cdot L = 40.5 \cdot \frac{kN}{m}$$

$$M_1 := Q_{2d} \cdot \left(C_c + L_c - S_2\right) + Q_{2d} \cdot \left(\frac{C_c}{2} + S_2\right) + q_{2d} \cdot L_L \cdot \left(\frac{C_c}{2} + \frac{L_L}{2}\right) + Q_{1d} \cdot \left(\frac{C_c}{2} - S_2\right) \ldots$$
$$+ q_{1d} \cdot L_L \cdot \left(\frac{C_c}{2} - \frac{L_L}{2}\right) - Q_{1d} \cdot \left(L_c - S_2\right)$$

$$R_2 := \frac{M_1}{C_c} = 652.519 \cdot kN$$

$$R_1 := 2 \cdot Q_{1d} + 2 \cdot Q_{2d} + \left(q_{2d} + q_{1d}\right) \cdot L_L - R_2 = 990.161 \cdot kN$$

*Load distribution factors:*

$$\gamma_1 := \frac{R_1}{R_1 + R_2} = 0.603 \qquad \gamma_2 := 1 - \gamma_1 = 0.397$$

The total loads acting on the bridge when both lanes are loaded are shown in the picture below. The axle loads are applied to the middle in order to obtain the maximum moment:

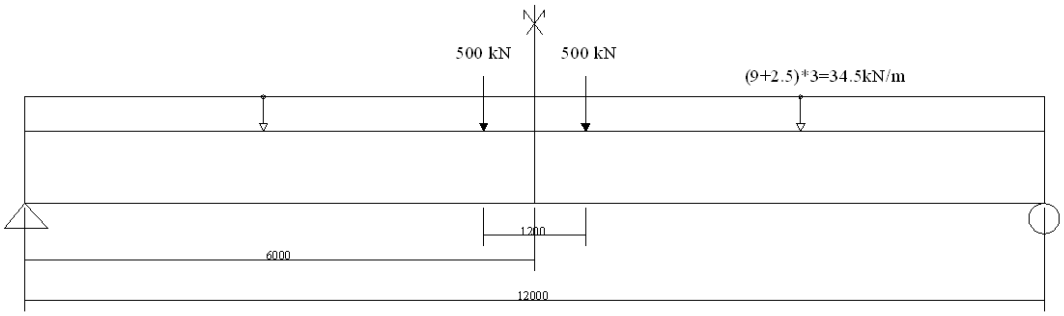


$$Q_d := Q_{1d} + Q_{2d} = 607.5 \cdot kN \qquad L_L = 3\,m$$

$$q_d := 1.35\alpha_{q1} \cdot q_{1k} \cdot L_L + 1.35\alpha_{q2} \cdot q_{2k} \cdot L_L = 35.64 \cdot \frac{kN}{m}$$

$C_w := 1.2m$ the distance between the wheels

$$R_d := q_d \cdot \frac{L}{2} + Q_d = 821.34 \cdot kN$$

$$M_{max} := R_d \cdot \frac{L}{2} - q_d \cdot \frac{\left(\frac{L}{2}\right)^2}{2} - Q_d \cdot \left(\frac{C_w}{2}\right) = 3.922 \times 10^3 \cdot kN \cdot m$$

The moment acting on the girder laying in the first lane:

$$M_{1m} := \gamma_1 \cdot M_{max} = 2.364 \times 10^3 \cdot kN \cdot m$$

$$\sigma_{m1} := \frac{M_{1m}}{W_s} = 246.543 \cdot MPa$$

Total Stress acting on the girder Self weight + Traffic loading:

$$\sigma_{Tc} := \sigma_{gc} + \sigma_{m1} = 304.674 \cdot MPa \qquad f_{yd} = 255 \cdot MPa \qquad \sigma_{Tc} \le f_{yd} = 0$$

## NEW BRIDGE WITH FRP DECK

The deck is widened by 0.5 meters on each side of the lanes

$L_{cn} := 1.6m$ the overhang distance

$S_{2n} := 1m$ the distance between the end of the lane and the wheel load

$L_{Ln} := 3.5m$

$$M_{1n} := Q_{2d} \cdot \left(C_c + L_{cn} - S_{2n}\right) + Q_{2d} \cdot \left(\frac{C_c}{2} + S_{2n}\right) + q_{2d} \cdot L_L \cdot \left(\frac{C_c}{2} + \frac{L_L}{2}\right) + Q_{1d} \cdot \left(\frac{C_c}{2} - S_{2n}\right) \ldots$$
$$+ q_{1d} \cdot L_L \cdot \left(\frac{C_c}{2} - \frac{L_L}{2}\right) - Q_{1d} \cdot \left(L_{cn} - S_{2n}\right)$$

$$R_{2n} := \frac{M_{1n}}{C_c} = 636.532 \cdot kN$$

$$R_{1n} := 2 \cdot Q_{1d} + 2 \cdot Q_{2d} + \left(q_{2d} + q_{1d}\right) \cdot L_{Ln} - R_2 = 1.061 \times 10^3 \cdot kN$$

Load distribution factors for the new bridge with FRP deck

$$\gamma_{1n} := \frac{R_{1n}}{R_{1n} + R_{2n}} = 0.625 \qquad \gamma_{2n} := 1 - \gamma_1 = 0.397$$

$$q_{dn} := 1.35\alpha_{q1} q_{1k} \cdot L_{Ln} + 1.35\alpha_{q2} q_{2k} \cdot L_{Ln} = 41.58 \cdot \frac{kN}{m}$$

$$R_{dn} := q_{dn} \cdot \frac{L}{2} + Q_d = 856.98 \cdot kN$$

$$M_{maxn} := R_{dn} \cdot \frac{L}{2} - q_{dn} \cdot \frac{\left(\frac{L}{2}\right)^2}{2} - Q_d \cdot \left(\frac{C_w}{2}\right) = 4.029 \times 10^3 \cdot kN \cdot m$$

The moment acting on the girder laying in the first lane:

$M_{1FRP} := \gamma_{1n} \cdot M_{maxn} = 2.519 \times 10^{3} \cdot kN \cdot m$

$$\sigma_{n1} := \frac{M_{1n}}{W_s} = 252.251 \cdot MPa$$

Total Stress acting on the girder Self weight + Traffic loading:

$\sigma_{TFRP} := \sigma_{gFRP} + \sigma_{n1} = 268.22 \cdot MPa \qquad f_{yd} = 255 \cdot MPa$

$\sigma_{TFRP} \le f_{yd} = 0$

## Hybrid Girder Design with concrete

If we want the stress reduction to be 20% more then composite action has to be provided between the girder and the deck. The amount of concrete needed for beff is calculated backwards in order to reduce the stress apart from the selfweight by 20 % more.

$\sigma_{rFRP} := 0.7 \cdot \sigma_{Tc} = 213.272 \cdot MPa$ reduced stress by 30%

$M_{tot} := M_{1FRP} + M_{FRP} = 2.672 \times 10^{3} \cdot kN \cdot m$ total moment acting on the girder

$$W_{new} := \frac{M_{tot}}{\sigma_{rFRP}} = 1.253 \times 10^{7} \cdot mm^{3}$$

Concrete C30/37 is used:

$E_c := 33GPa$

$\alpha := \frac{E_s}{E_c} = 6.364$ the tranformation coefficient

$h_c := 225mm$ the depth of the deck

$b_{effc} := 600mm$ the effective width of concrete

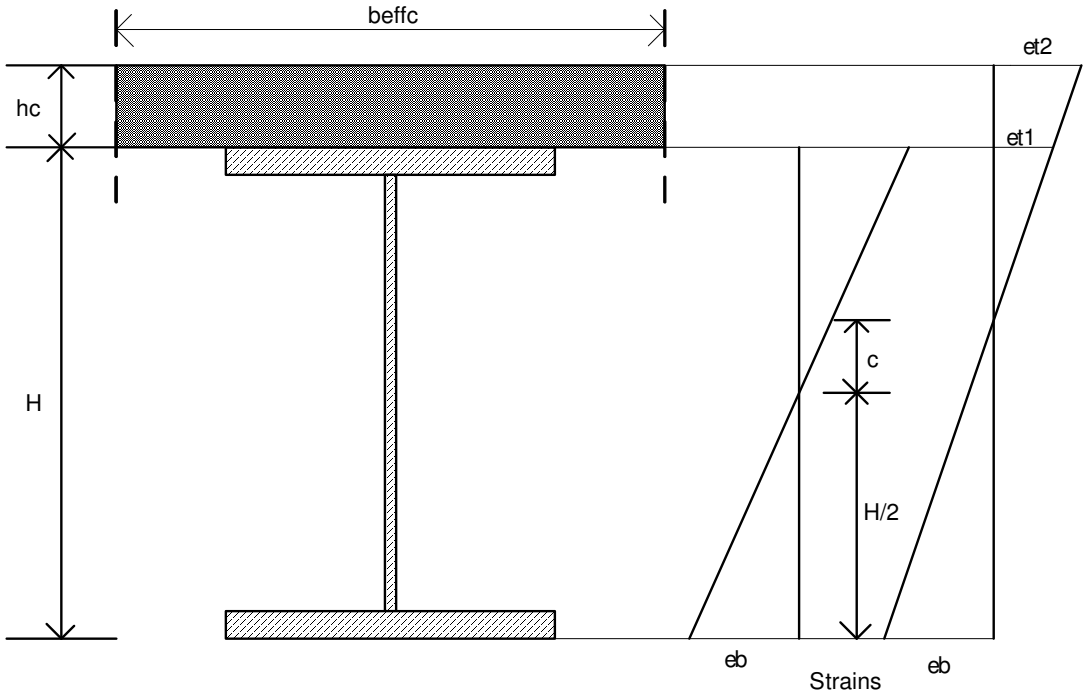


$$\varepsilon_{t1} := \frac{H - 2\cdot c}{H + 2\cdot c}\cdot\varepsilon_b \qquad \varepsilon_{t2} := \frac{H - 2\cdot c + 2\cdot h_c}{H + 2\cdot c}\cdot\varepsilon_b$$

$A_f := b_f\cdot t_f = 1.02\times 10^4\cdot mm^2$ flange area of the steel girder

$A_c := h_c\cdot b_{effc} = 1.35\times 10^5\cdot mm^2$

$$M_{R1} := 2\cdot\left[\left(A_f\cdot E_s\cdot\varepsilon_b\cdot\frac{H}{2}\right) + \left(\frac{H}{2}\cdot t_w\cdot\frac{1}{2}\cdot\varepsilon_b\cdot E_s\cdot\frac{H}{3}\right)\right]$$

$$M_{R2} := A_f\cdot E_s\cdot\varepsilon_b\cdot\left(\frac{H}{2} + c\right) + \varepsilon_{t1}\cdot A_f\cdot E_s\cdot\left(\frac{H}{2} - c\right) + \left(\frac{H}{2} + c\right)\cdot t_w\cdot\frac{1}{2}\cdot\varepsilon_b\cdot E_s\cdot\frac{2}{3}\cdot\left(\frac{H}{2} + c\right) \ldots$$
$$+\left(\frac{H}{2} - c\right)\cdot t_w\cdot\frac{1}{2}\cdot\varepsilon_{t1}\cdot E_s\cdot\frac{2}{3}\cdot\left(\frac{H}{2} - c\right) + \varepsilon_{t2}\cdot E_c\cdot A_c\cdot\left(\frac{H}{2} - c + \frac{h_c}{2}\right)$$

When M1=M2 the following equation is obtained:

$$A_f\cdot\alpha + \frac{t_w}{2}\cdot\left(\frac{H}{2} + c\right)\cdot\alpha = \left(\frac{H - 2\cdot c}{H + 2\cdot c}\right)\cdot A_f\cdot\alpha + \left(\frac{H - 2\cdot c}{H + 2\cdot c}\right)\cdot\frac{t_w}{2}\cdot\left(\frac{H}{2} - c\right)\cdot\alpha + \left(\frac{H - 2\cdot c + 2h_c}{H + 2\cdot c}\right)\cdot A_c$$

$$c := \frac{1}{2}\cdot A_c\cdot\frac{H + h_c}{2\cdot A_f\cdot\alpha + t_w\cdot\alpha\cdot H + A_c}$$

$c = 203.386\cdot mm$

$A_s := h_w\cdot t_w + 2\cdot b_f\cdot t_f = 3.369\times 10^4\cdot mm^2$

$I_s = 4.075 \times 10^{-3}\,m^4$ steel girder moment of inertia

$$I_{new} := I_s + A_s \cdot c^2 + \frac{1}{\alpha} \cdot \left[ \frac{b_{effc} \cdot h_c^{\,3}}{12} + b_{effc} \cdot h_c \cdot \left( \frac{H}{2} - c + \frac{h_c}{2} \right)^2 \right] = 7.927 \times 10^{-3}\,m^4$$

$$W_{bott} := \frac{I_{new}}{\left( \frac{H}{2} + c \right)} = 1.261 \times 10^{7} \cdot mm^3 \qquad W_{up} := \frac{I_{new}}{\left( \frac{H}{2} - c + h_c \right)} = 1.775 \times 10^{7} \cdot mm^3$$

$W_{bott} \geq W_{new} = 1$

In order to achieve a total stress reduction of 30 %, effective width of 600 mm of concrete is enough but when the creep and shrinkage effects are considered this effective width is lower. Thus in the following calcualtions an effective width of concrete of 1000 mm is considered.

## SHEAR STUD DESIGN

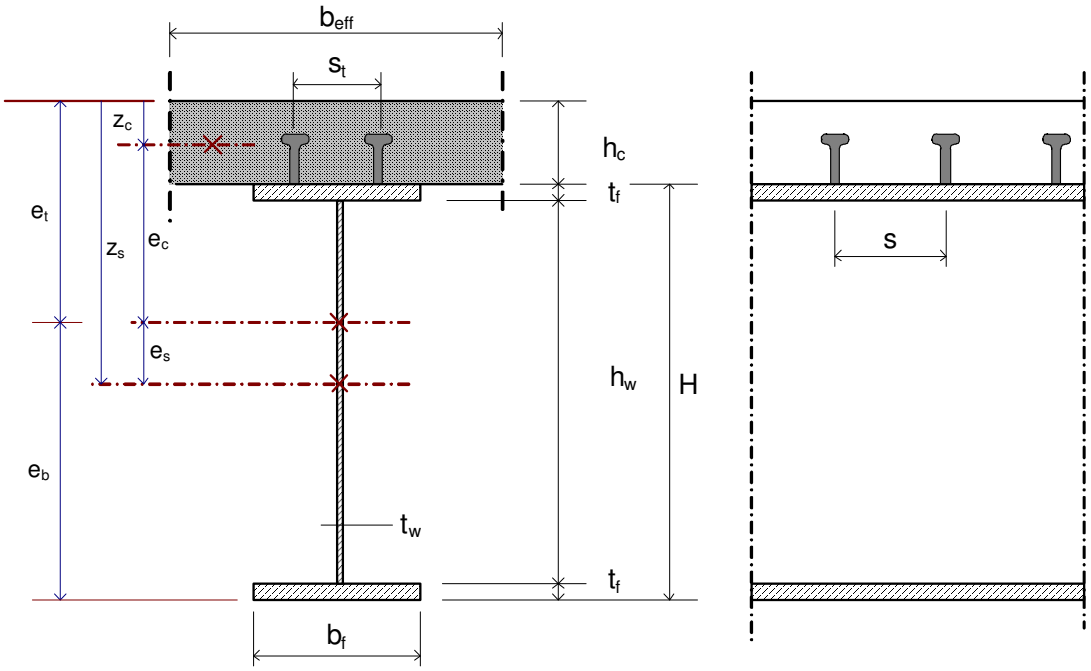


**Concrete (C30/37)**

$b_{eff} := 1000mm$

$h_{ov} := 225mm$

$f_{ck} := 30MPa$

$\gamma_{ov} := 1.5$

$f_{cd} := \frac{f_{ck}}{\gamma_c} = 20 \cdot MPa$

$\psi_L := 1.1$ creep multiplier

$\varphi_t := 1.5$ creep coefficient

$\xi := \sqrt{\frac{235MPa}{f_{yk}}} = 0.96$

**Shear studs**

$d := 22mm$ diameter of the shear stud

$d_h := 1.5 \cdot d = 33 \cdot mm$ diameter of the head

$h_h := 10mm$ the depth of the head

$h_h \geq 0.4 \cdot d = 1$ OK!

$s_t := 2.5 \cdot d = 55 \cdot mm$

$h_{sc} := 150mm$

$h_{sc} > 3 \cdot d = 1$ OK!

$d < 1.5 \cdot t_f = 1$

$s_{ov} := 2 \cdot h_{sc} + s_t = 355 \cdot mm$

$F_u := 450MPa$ ultimate steel strength of the shear studs

**Load effects**

$M_{Ed} := M_{tot} = 2.672 \times 10^{3} \cdot kN \cdot m$

$V_{Ed} := R_{Fd} + R_{dn} \cdot \gamma_{1n} = 586.759 \cdot kN$

*Modular ratio (Creep and shrinkage)*

$n_0 := \frac{E_s}{E_c} = 6.4$ modular ratio

$n_L := n_0 \cdot (1 + \psi_L \cdot \varphi_t) = 16.9$

*Calculation of cross-sectional constants for the transformed cross-section*

$A_s := h_w \cdot t_w + 2 \cdot b_f \cdot t_f = 3.369 \times 10^{4} \cdot mm^2$

$A_c := b_{eff} \cdot h_c = 0.225\,m^2$

$A_T := A_s + \frac{A_c}{n_L} = 0.047\,m^2$ transformed section area

$z_c := \frac{h_c}{2} = 0.113\,m$ $z_s := \frac{H}{2} + h_c = 0.65\,m$

$e_c := \frac{A_s \cdot z_s + \frac{A_c}{n_L} \cdot z_c}{A_T} - z_c = 0.385\,m$ $e_t := e_c + z_c = 0.498\,m$

$e_b := H + h_c - e_t = 0.577\,m$ $e_s := z_s - e_t = 0.152\,m$

$I_T := I_s + A_s \cdot e_s^{2} + \frac{1}{n_L} \cdot \left( \frac{b_{eff} \cdot h_c^{3}}{12} + b_{eff} \cdot h_c \cdot e_c^{2} \right) = 6.893 \times 10^{-3}\,m^4$

$W_{top} := \frac{I_T}{e_t} = 1.385 \times 10^{7} \cdot mm^3$ $W_{bot} := \frac{I_T}{e_b} = 1.194 \times 10^{7} \cdot mm^3$

$\sigma_{top} := \frac{M_{Ed}}{W_{top} \cdot n_L} = 11.436 \cdot MPa$ $\sigma_{top} \le f_{cd} = 1$

$\sigma_{bot} := \frac{M_{Ed}}{W_{bot}} = 223.83 \cdot MPa$ $\sigma_{bot} \le f_{yd} = 1$

***Check of shear studs***

1st moment of area of the concrete deck

$$S_c := \frac{A_c}{n_L}\cdot e_c = 5.137\times 10^6\cdot mm^3$$

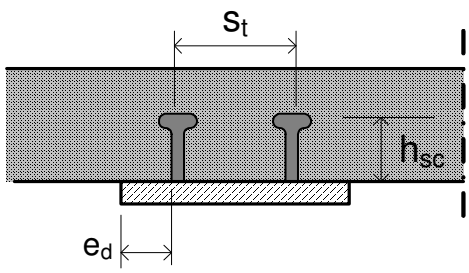


$e_{d\_min} := 25mm$ $\quad e_{d\_max} := 9\cdot\varepsilon\cdot t_f = 293.755\cdot mm$ $\quad \gamma_V := 1.25$

Use $e_d := \frac{b_f - s_t - d}{2} = 111.5\cdot mm$ it is within the limits

$s_t := b_f - 2\cdot\left(e_d + \frac{d}{2}\right) = 55\cdot mm$

$\frac{h_{sc}}{d} = 6.818$ $\quad \alpha := 1$

The design shear resistance of one headed shear stud (according to EC1994-2):

$$P_{Rd\_1} := \frac{0.8\cdot f_u\cdot\pi\cdot d^2}{4\cdot\gamma_V} = 104.977\cdot kN \qquad P_{Rd\_2} := \frac{0.29\cdot\alpha\cdot d^2\cdot\sqrt{f_{ck}\cdot E_c}}{\gamma_V} = 111.725\cdot kN$$

$P_{Rd} := \min\left(P_{Rd\_1}, P_{Rd\_2}\right) = 104.977\cdot kN$

The required c/c distance of the studs in the longitudinal direction is:

$s1 := \frac{2\cdot P_{Rd}\cdot I_T}{V_{Ed}\cdot S_c} = 0.48\,m$ $\quad s3 := 800mm$

$s2 := 22\cdot t_f\cdot\varepsilon = 0.718\,m$ $\quad s4 := 4\cdot h_c = 0.9\,m$

$s := \min(s1, s2, s3, s4) = 0.48\,m$

Use s = 350 mm $\quad s := 350mm$

Number of studs in the length of 12 meters is:

$L := 12m$

$N := \frac{L}{s} = 34.286$

$N_s := 35$ studs in one row

**Check of shear studs for fatigue**

$k_s := 0.75$

$V_{max} := k_s \cdot P_{Rd} = 78.733 \cdot kN$ maximum longitudinal shear force per connector

$\gamma_{Mf.s} := 1.25$ partial factor for headed shear studs for fatigue strength

$\gamma_{Ff} := 1$ partial factor for fatigue loading

$\Delta\tau_c := 90MPa$ reference fatigue strength for 2 million cycles

$\lambda_{v1} := 1.55$ $\lambda_{v2} := 1$

$t_{Ld} := 25$ the extended design life of the bridge

$\lambda_{v3} := \left(\frac{t_{Ld}}{100}\right)^{\left(\frac{1}{8}\right)} = 0.841$ $\lambda_{v4} := 1$

$\lambda_v := \lambda_{v1} \cdot \lambda_{v2} \cdot \lambda_{v3} \cdot \lambda_{v4} = 1.303$ damage equivalent factor

To calculate the shear stress range in the stud shank, fatigue load model 3 is used (single vehicle model) [EN1991-2:2003/ section 4.6.4] The minimum shear stress is zero and the maximum is calculated by placing the vehicle near the supports to obtain the maximum shear force.

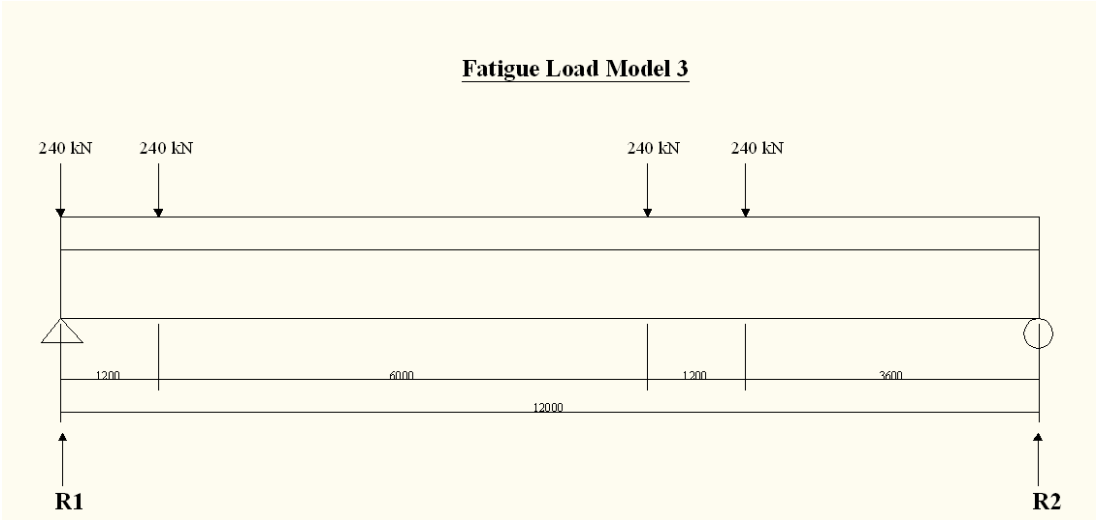

$P_f := 240kN$

$R_2 := \frac{P_f \cdot 8.4m + P_f \cdot 7.2m + P_f \cdot 1.2m}{12m} = 336 \cdot kN$ $R_1 := 4 \cdot P_f - R_2 = 307.481 \cdot kN$

$\gamma_{1n} = 0.625$ load distribution factor for one girder

$V_{Ed.L} := \gamma_1 \cdot R_1 = 185.341 \cdot kN$

$\Delta V_L := \frac{V_{Ed.L}}{2 \cdot N_s} = 2.648 \cdot kN$ longitudinal shear force acting on one connector

$A_{stud} := \frac{\pi \cdot d^2}{4} = 3.801 \times 10^{-4} m^2$

$\Delta\tau := \frac{\Delta V_L}{A_{stud}} = 6.965 \cdot MPa$ shear stress range on one shear stud

$\Delta\tau_{E.2} := \lambda_v \cdot \Delta\tau = 9.078 \cdot MPa$ $\gamma_{Ff} \cdot \Delta\tau_{E.2} \le \frac{\Delta\tau_c}{\gamma_{Mf.s}} = 1$ OK!

## Hybrid Girder Design with FRP deck

To calculate the effective width of the FRP deck just the flanges are taken into account. The level of assistance of the FRP flanges to the composite girder is calculated based on the upward shift of the neutral axis by back-calculating the effective FRP flange width using standard transformed section properties. The calculation is done for the middle of the span where maximum moment is acting.

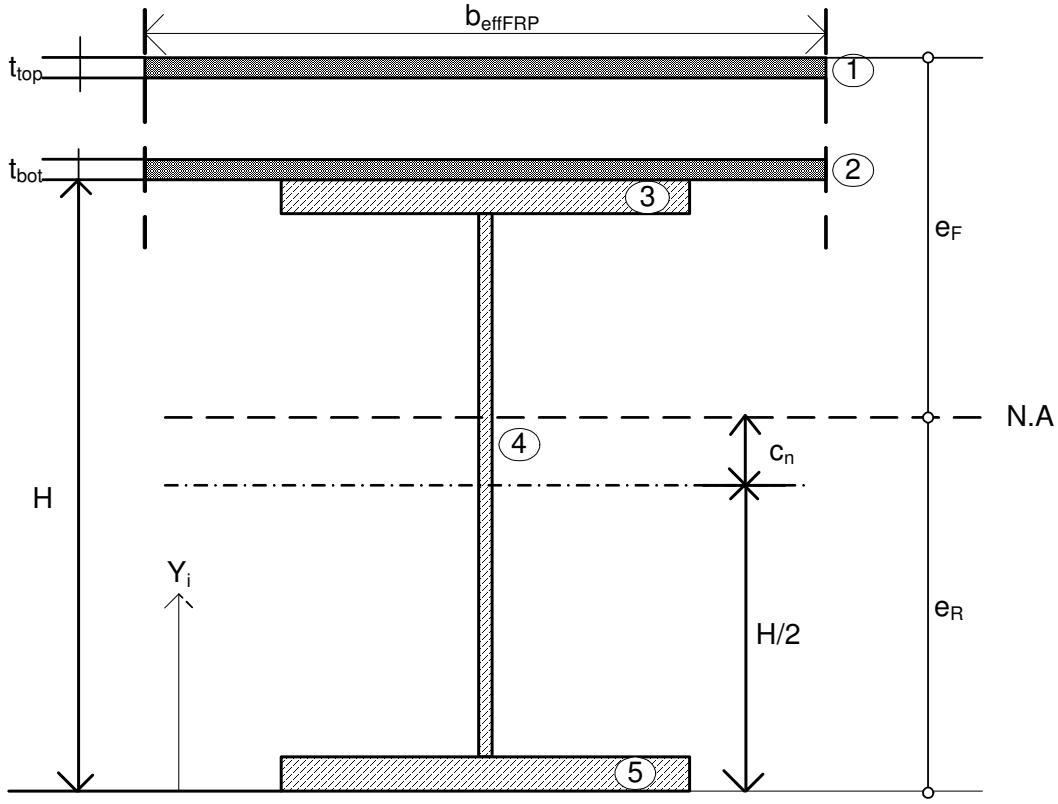


The increase of the neutral axis is picked by the finite element analysis.

$c_n := 85.34mm$

$\sigma_{botFRP} := 212MPa$

$E_{FRP} := 20GPa$ FRP flange x-direction(pultrusion) elasticity modulus

$\alpha_F := \frac{E_s}{E_{FRP}} = 10.5$ ratio of elasticity modulus of steel to elasticity modulus of FRP deck

$t_{Ftop} := 15mm$ the thickness of the top flange of FRP deck

$t_{Fbot} := 15mm$ the thickness of the bottom flange of FRP deck

$y_1 := H + h_c - \frac{t_{Ftop}}{2} = 1.067 \times 10^3 \cdot mm$ $A_1 := \frac{b_{effFRP} \cdot t_{Ftop}}{\alpha_F}$

$y_2 := H + \frac{t_{Fbot}}{2} = 857.5 \cdot mm$ $A_2 := \frac{b_{effFRP} \cdot t_{Fbot}}{\alpha_F}$

$y_3 := H - \frac{t_f}{2} = 833 \cdot mm$ $A_3 := A_f = 1.02 \times 10^4 \cdot mm^2$

$y_4 := \frac{H}{2} = 425 \cdot mm$ $A_4 := t_w \cdot h_w = 1.329 \times 10^4 \cdot mm^2$

$y_5 := \frac{t_f}{2} = 17 \cdot mm$ $A_5 := A_f = 1.02 \times 10^4 \cdot mm^2$

$Y_{NA} := \frac{H}{2} + c_n = 510.34 \cdot mm$

$$\frac{b_{effFRP} \cdot t_{Ftop}}{\alpha_F} \cdot y_1 + \frac{b_{effFRP} \cdot t_{Fbot}}{\alpha_F} \cdot y_2 \ldots = \left( \frac{b_{effFRP} \cdot t_{Fbot}}{\alpha_F} + \frac{b_{effFRP} \cdot t_{Fbot}}{\alpha_F} + \ldots \right) \cdot Y_{NA}$$
$$+ A_3 \cdot y_3 + A_4 \cdot y_4 + A_5 \cdot y_5 \qquad + A_3 + A_4 + A_5$$

$$b_{effFRP} := -\frac{A_3 \cdot y_3 - Y_{NA} \cdot (A_3 + A_4 + A_5) + A_4 \cdot y_4 + A_5 \cdot y_5}{\frac{t_{Fbot} \cdot y_2}{\alpha_F} - \frac{2 \cdot Y_{NA} \cdot t_{Fbot}}{\alpha_F} + \frac{t_{Ftop} \cdot y_1}{\alpha_F}} \qquad b_{effFRP} = 2.226\,m$$

The shear stresses acting on the flange of the beam:

$A_{eftop} := t_{Ftop} \cdot b_{effFRP} = 0.033\,m^2$ $A_{efbot} := t_{Fbot} \cdot b_{effFRP} = 0.033\,m^2$

1st moment of area of the effective deck

$$S_{FRP} := \frac{A_{eftop}}{\alpha_F} \cdot \left( \frac{H}{2} - c_n + h_c - \frac{t_{Ftop}}{2} \right) + \frac{A_{efbot}}{\alpha_F} \cdot \left( \frac{H}{2} - c_n + \frac{t_{Fbot}}{2} \right) = 2.875 \times 10^6 \cdot mm^3$$

$V_{Ed} := 403kN$

$d_1 := \frac{H}{2} - c_n + h_c - \frac{t_{Ftop}}{2}$ $d_2 := \frac{H}{2} - c_n + \frac{t_{Fbot}}{2}$

$$I_{TF} := I_s + A_s \cdot c_n^2 + \frac{1}{\alpha_F} \cdot \left( \frac{b_{effFRP} \cdot t_{Ftop}^3}{12} + A_{eftop} \cdot d_1^2 + \frac{b_{effFRP} \cdot t_{Fbot}^3}{12} + A_{efbot} \cdot d_2^2 \right)$$

$W_{trFRP} := \frac{I_{TF}}{Y_{NA}} = 1.115 \times 10^7 \cdot mm^3$ $M_{1FRP} = 2.519 \times 10^3 \cdot kN \cdot m$

$\sigma := \frac{M_{Ed}}{W_{trFRP}} = 239.582 \cdot MPa$ $\tau := \frac{V_{Ed} \cdot S_{FRP}}{I_{TF} \cdot b_f} = 0.679 \cdot MPa$

## Hybrid Girder Design with concrete and taking into account the effective width of the FRP panels

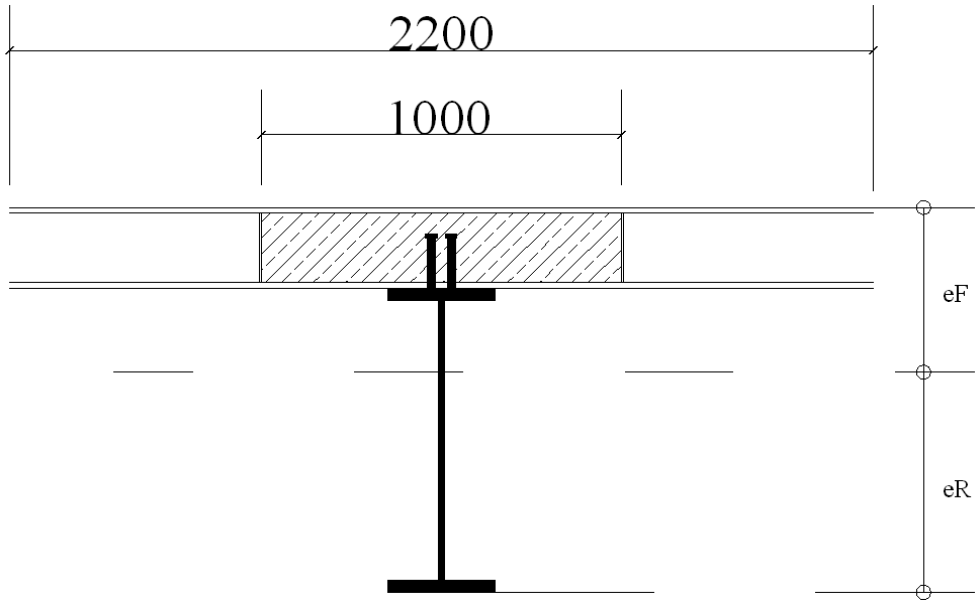


Modular ratios:

$n_L := n_0 \cdot (1 + \psi_L \cdot \varphi_t) = 16.9$

$\alpha_F := \frac{E_s}{E_{FRP}} = 10.5$

*Calculation of cross-sectional constants for the transformed cross-section*

Concrete FRP

$b_{eff} = 1\,m$ $b_{effF} := 2.22m$

$A_c := b_{eff} \cdot (h_c - t_{Ftop} - t_{Fbot}) = 0.195\,m^2$

$A_F := b_{effF} \cdot t_{Ftop} + b_{effF} \cdot t_{Fbot} = 0.067\,m^2$

$$A_{Tr} := A_s + \frac{A_c}{n_L} + \frac{A_F}{\alpha_F} = 0.052\,m^2$$

tranformed section to steel

$z_c := \frac{h_c}{2} = 0.113\,m$ $z_s := \frac{H}{2} + h_c = 0.65\,m$

$$z_{Ftop} := \frac{t_{Ftop}}{2} = 7.5 \times 10^{-3}\,m$$

$$z_{Fbot} := h_c - \frac{t_{Fbot}}{2} = 0.217\,m$$

$$e_F := \frac{A_s \cdot z_s + \frac{A_c}{n_L} \cdot z_c + \frac{b_{effF} \cdot t_{Ftop}}{\alpha_F} \cdot z_{Ftop} + \frac{b_{effF} \cdot t_{Fbot}}{\alpha_F} \cdot z_{Fbot}}{A_{Tr}} = 0.463\,m$$

$$e_R := H + h_c - e_F = 0.612\,m$$

$$I_{TFr} := I_s + A_s \cdot \left(\frac{H}{2} - e_R\right)^2 + \frac{1}{n_L} \cdot \left[\frac{b_{eff} \cdot \left(h_c - t_{Ftop} - t_{Fbot}\right)^3}{12} + A_c \cdot \left(e_F - z_c\right)^2\right] \ldots + \frac{1}{\alpha_F} \cdot \left[\begin{array}{l} \frac{b_{effF} \cdot t_{Ftop}^{\,3}}{12} + b_{effF} \cdot t_{Ftop} \cdot \left(e_F - \frac{t_{Ftop}}{2}\right)^2 \ldots \\ + \frac{b_{effF} \cdot t_{Fbot}^{\,3}}{12} + b_{effF} \cdot t_{Fbot} \cdot \left(e_F - h_c + \frac{t_{Fbot}}{2}\right)^2 \end{array}\right]$$

$$W_{topF} := \frac{I_{TFr}}{e_F} = 1.631 \times 10^7 \cdot mm^3 \qquad W_{botF} := \frac{I_{TFr}}{e_R} = 1.236 \times 10^7 \cdot mm^3$$

$$\sigma_{topF} := \frac{M_{Ed}}{W_{topF} \cdot n_L} = 9.713 \cdot MPa \qquad \sigma_{top} \le f_{cd} = 1$$

$$\sigma_{botF} := \frac{M_{Ed}}{W_{botF}} = 216.112 \cdot MPa \qquad \sigma_{bot} \le f_{yd} = 1$$

## Horizontal Loads

$\alpha_Q = 0.9$ $\alpha_{q1} = 0.7$

$Q_{1k} = 300 \cdot kN$ $q_{1k} = 9 \cdot \frac{kN}{m^2}$

$w_1 := 3m$ the width of one lane

$L_h := 12m$

$Q_{hk1} := 0.6 \cdot \alpha_Q \cdot \left(2 \cdot Q_{1k}\right) + 0.1 \cdot \alpha_{q1} \cdot q_{1k} \cdot w_1 \cdot L_h = 346.68 \cdot kN$ horizontal braking force

$Q_{trk} := 0.25 \cdot Q_{hk1} = 86.67 \cdot kN$ transverse braking force

# Bolted connection design

Adhesive material Properties / SikaDur 330:

$f_{ts} := 30MPa$ tensile stress

$E_{s330} := 3300MPa$ elasticity modulus

$\gamma_{ad} := 2$ partial safety factor of the adhesive

$f_{tsd} := \frac{f_{ts}}{\gamma_{ad}} = 15 \cdot MPa$ design stress

Bolts Class 8.8

Nominal diameter of the bolt: $d_b := 14mm$

Diameter of the head: $d_0 := 25mm$

Nominal area of the bolt: $A_n := 154mm^2$

Resistant area of the bolt: $A_b := 115mm^2$

Yield strength: $f_{yb} := 640MPa$

Ultimate strength: $f_{ub} := 800MPa$

Steel plate /S355 :

$f_{yp} := 355MPa$ $f_{up} := 510MPa$

1) Tension Resistance of one bolt:

$k_2 := 0.63$ Countersunk bolt

$\gamma_{M2} := 1.25$ Partial factor

$F_{t.Rd} := \frac{k_2 \cdot f_{ub} \cdot A_b}{\gamma_{M2}} = 46.368 \cdot kN$ [EN 1993-1-8 / Table 3.4]

2) Shear Resistance of one bolt:

$\alpha_v := 0.5$ $F_{v.Rd} := \frac{\alpha_v \cdot f_{ub} \cdot A_b}{\gamma_{M2}} = 36.8 \cdot kN$

The horizontal braking force will be transferred to the bolds through the adhesive:

The worst case is assumed when the lateral force is carried by two bolted connections.

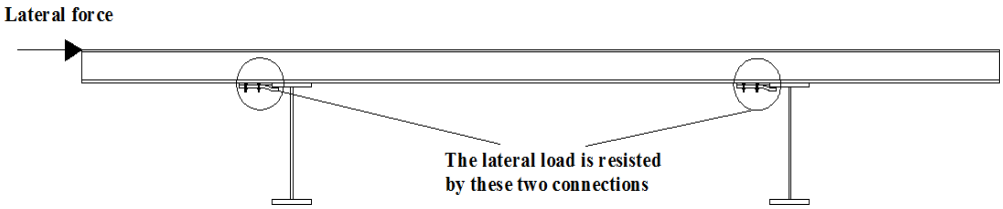


Force carried by one bolted connection is:

$Q_b := \frac{1.35Q_{trk}}{2} = 58.502 \cdot kN$ design action force

The area of the steel plate to resist this force is: $A_p := \frac{Q_b}{f_{tsd}} = 3.9 \times 10^3 \cdot mm^2$

Select the length of the plate as 200 mm.

$l_p := 200mm$ $b_p := \frac{A_p}{l_p} = 19.501 \cdot mm$

The dimensions of the steel plate are selected as:

$l_p = 200 \cdot mm$ and $b_p := 80mm$ $t_p := 10mm$ thickness of the plate

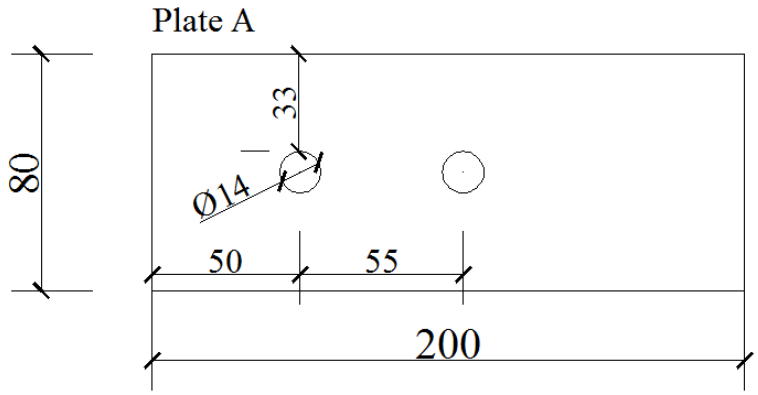


Check of minimum and maximum spacing of the bolts:

End distance: $e_{1min} := 1.2 \cdot d_0 = 30 \cdot mm$ $e_{1max} := 4.t_p + 40mm = 80 \cdot mm$

$e_1 := 33mm$ within limits OK!

Edge distance: $e_{2min} := 1.2 \cdot d_0 = 30 \cdot mm$ $e_{2max} := 4.t_p + 40mm = 80 \cdot mm$

$e_2 := 50mm$ within limits OK!

Spacing : $p_{1min} := 2.2 \cdot d_0 = 55 \cdot mm$ $p_{1max} := \min(14 \cdot t_p, 200mm) = 140 \cdot mm$

$p_1 := 55mm$ within limits OK!

Bearing resistance:

$$\alpha_d := \frac{e_1}{3 \cdot d_0} = 0.44 \qquad \alpha_b := \min\left(\alpha_d, \frac{f_{ub}}{f_{up}}, 1\right) = 0.44$$

$$k_1 := \min\left(\frac{2.8 \cdot e_2}{d_0} - 1.7, 2.5\right) = 2.5$$

$$F_{b.Rd} := \frac{k_1 \cdot \alpha_b \cdot f_{up} \cdot d_0 \cdot t_p}{\gamma_{M2}} = 112.2 \cdot kN$$

$$Q_b \le F_{b.Rd} = 1 \qquad \text{OK!}$$

Tensile design ultimate strength capacity of the net cross-section of the plate:

$$A_{net} := b_p \cdot t_p - t_p \cdot d_0 = 550 \cdot mm^2$$

$$N_{u.Rd} := \frac{0.9 \cdot A_{net} \cdot f_{up}}{\gamma_{M2}} = 201.96 \cdot kN \qquad [\ \text{EN1993 -1-1 / (6.7)}\ ]$$

$$Q_b \le N_{u.Rd} = 1 \qquad \text{OK!}$$

Shear force acting on one bolt is: $F_{v.Ed} := \frac{Q_b}{2} = 29.251 \cdot kN$

$$F_{v.Ed} \le F_{v.Rd} = 1 \qquad \text{OK!}$$

The design of the bolts when uplift load is acting:

The uplift forces are attained from finite element analysis.

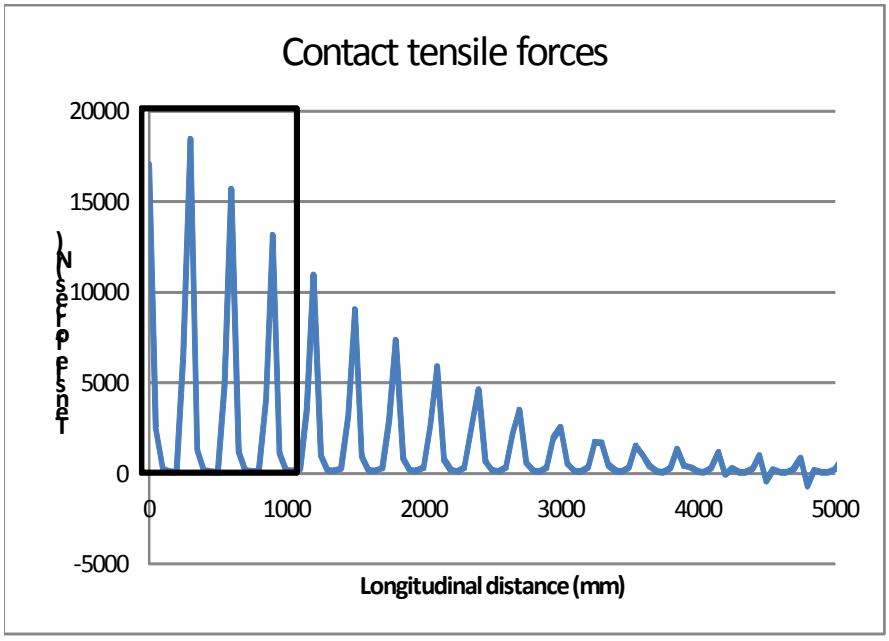

The tesile force that can be carried by one connection is:

$F_{td} := 2 \cdot F_{t.Rd} = 92.736 \cdot kN$ it is multiplied by two because one connection has two bolts

The total tensile force for 1 meter is computed by adding the maximum tensile forces:

$F_{Ed} := 87.3kN$ for 1 m

$F_{Ed} \leq F_{td} = 1$

Thus the bolted connection is decided to be placed each 1.0 meter.

Check the capacity of the adhesive bond:

$A_{ad} := b_p \cdot l_p = 1.6 \times 10^4 \cdot mm^2$

$\sigma_{tad} := \frac{F_{Ed}}{A_{ad}} = 5.456 \cdot MPa$

These stresses are less than the resistance of 8MPa which was determined by Keller et. al. for adhesively bonded FRP plate to steel plate.